TEMPERATURE-INDEX MODELING OF MASS BALANCE AND RUNOFF IN THE VALDEZ

GLACIER CATCHMENT IN 2012 AND 2013

by

Jennifer L. Davis
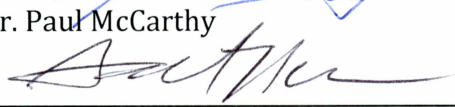
RECOMMENDED: _____
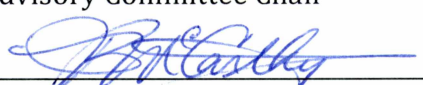
Dr. Anna Liljedahl

_____

Dr. Paul McCarthy

_____

Dr. Gabriel Wolken
Advisory Committee Co-Chair

_____

Dr. Anthony Arendt
Advisory Committee Chair

_____

Dr. Paul McCarthy
Chair, Department of Geosciences

APPROVED: _____

Dr. Paul Layer
Dean, College of Natural Science and Mathematics

_____

Dr. John Eichelberger
Dean of the Graduate School

28 April 2015
_____

Date

TEMPERATURE-INDEX MODELING OF MASS BALANCE AND RUNOFF IN THE

VALDEZ GLACIER CATCHMENT IN 2012 AND 2013

A

THESIS

Presented to the Faculty

of the University of Alaska Fairbanks

in Partial Fulfillment of the Requirements

for the Degree of

MASTER OF SCIENCE

By

Jennifer L. Davis, A.S., B.S.

Fairbanks, Alaska

May 2015

Abstract

Glaciers play an important role in both storage and generation of runoff within individual watersheds. The Valdez Glacier catchment (342 km^2), located in southern Alaska in the Chugach mountains off of Prince William Sound, is characterized by large annual volumes of rain- and snowfall. As Valdez Glacier and other glaciers within the catchment (comprising 58% of the catchment area) continue to melt in a warming climate, it is unclear how the runoff will be affected. Temperature-index modeling is one method used to estimate glacier mass balance and runoff in highly glacierized catchments, and may be suitable for predicting future runoff regimes. In this study, we used a combination of field measurements (air temperature, glacier mass balance, streamflow, and ground-penetrating radar (GPR)-derived snow water equivalent (SWE) from a parallel study) and modeled climate data (PRISM) to a) calibrate a temperature-index model to glacier mass balance in 2012; b) validate the model to laser altimetry; and c) calibrate a temperature-index model to runoff measurements in fall of 2012 and in spring, summer and fall of 2013.

We calibrated the snow-radiation coefficient (r_{snow}), ice-radiation coefficient (r_{ice}), and melt factor (MF) of the temperature-index model to glacier mass balance measurements from 2012. Using the calibrated- r_{snow}, r_{ice}, and MF (i.e. r_{snow}, r_{ice}, and MF = 0.20, 0.50 and 4.0, respectively), we calculated 2012 annual glacier mass balance (B$_a$) at 0.05 ± 0.49 meters water equivalent (m w.eq.) We next validated the model to 2012 laser altimetry annual glacier mass balance estimates (B$_a$ = 0.20 ± 0.6 m w.eq.). We then modeled glacier mass balance in 2013 using r_{snow}, r_{ice}, and MF from the 2012 calibration. The model underestimated summer glacier mass balance in 2013, resulting in annual glacier mass balance (B$_a$ = 0.55 m w.eq.) that did not fall within the 2013 laser altimetry annual balance estimate (B$_a$ = -1.15 +0.29/-0.30 m w.eq.). We therefore re-calibrated MF to 2013 laser altimetry measurements, resulting in an annual glacier mass balance (B$_a$) of -1.10 ± 0.49 m w. eq. We next calibrated the storage constants of the runoff model to hydrographs from mid-September until mid-October 2012, and from May until October 2013, with r_{snow}, r_{ice}, and MF set to values from the 2012 glacier mass balance calibration. Total modeled runoff in mid- September until mid-October 2012 was within 3% of measured runoff (*E*- and *lnE*- were 0.54 and 0.76, respectively). Modeled runoff in 2013 was calculated to within 5% of 2013 runoff measurements (*E*- and *lnE*-values of 0.79 and 0.70, respectively). We next modeled runoff in 2013 using MF from the 2013 glacier mass balance

calibration to laser altimetry (i.e. MF = 7.0). The fit of 2013 modeled to measured runoff was reduced (*E*- and *lnE*- values of 0.44 and 0.54, respectively), suggesting that additional glacier mass balance measurements are necessary in 2013 in order to properly calibrate the model. Results indicate that glacier melt parameters likely vary inter-annually. Therefore, the temperature-index model is capable of modeling both glacier melt and runoff in a maritime catchment, provided that ablation stake, air temperature, precipitation, and streamflow measurements are available for the simulation period.

Table of Contents

List of Figures

List of Tables

Acknowledgments

First and foremost, I would like to thank my main advisor, Dr. Anthony Arendt (University of Alaska Fairbanks, Geophysical Institute), and my co-advisor, Dr. Gabriel Wolken (Alaska Division of Geological & Geophysical Surveys), for allowing me the opportunity to pursue my dream of living in Alaska, studying at the University of Alaska Fairbanks (UAF), and ultimately changing the direction of my life in the most exciting of ways! Not only have you offered a consistently open door for research questions and advice, but you each have been an inspiration through your unwavering patience and understanding, devotion to science and teaching, sense of humor and adventure, and steady approach to life.

I would also like to thank my committee members, Dr. Anna Liljedahl (Water & Environmental Research Center) and Dr. Paul McCarthy (Chair of the Department of Geosciences). Thank you, Dr. Liljedahl, for supporting this project both by finding funds for the project and by sharing your expertise in the realm of hydrologic modeling and streamflow measurement. Dr. McCarthy, thank you for being so responsive and available to answer questions, review reports, provide feedback, and motivate discussion and a new perspective of the project. I cannot thank you enough for the time you have invested in this project.

To my committee as a whole, Drs. Arendt, Wolken, Liljedahl, and McCarthy – I cannot think of a better group of people to mentor a graduate student. I feel incredibly lucky to have had each of you as member of my committee. I know I am a better person just by having worked alongside each of you.

Thank you to Ed Neal for all the time and effort you invested in helping me measure streamflow. I cannot thank you enough for everything! You were an integral part of the stream gauging component to this project and I learned an incredible amount from you.

Thank you to all of the organizations that provided funding, equipment, and support to this

On a final note, I would like to extend my sincerest gratitude to friends and family, who have been a constant source of strength, encouragement, love and support throughout this process. To my mother and father – Thank you from the bottom of my heart for unselfishly encouraging me to chase my dream, even if that meant going thousands of miles away from you. You have taught me to work hard and invest in myself today so that I can feel incredible tomorrow. Absolutely none of this would have been possible without you. Thank you for coming to visit me in Alaska, and in essence, bringing home to me. You will never know how much that has meant to me. I love you both immensely!

To Seth –Thank you for loving me and supporting me day to day, and for wading with me through turbulent waters and calm, gentle seas. Thank you for continually pushing me to go get what I want and to seize the day, for talking reason into me when I've reached breaking-point after breaking-point, for teaching me to snowboard, for going on so many adventures with me, and for always lending an ear and a heart to every deep conversation we've ever shared. Thank you for your sense of humor; you have kept me laughing throughout this whole process, and that has made a world of difference. I love you infinitely!

To friends, both near and far, who I have not named explicitly – You know who you are! Thank you for supporting me and for making this journey so enjoyable.

Chapter 1

Introduction

Glaciers occupy and regulate runoff events in many alpine catchments throughout Alaska, by acting as a storage unit for precipitation and meltwater, while providing stream flow during dry periods (Fountain & Tangborn, 1985). Recent mass balance studies on Alaska glaciers have shown that most have been decreasing in volume over the past 60 years in response to climate change (Gardner et al., 2013). The focus of investigations of Alaska glaciers has primarily been to determine sea level rise contributions. However, changing storage capacities of glaciers also have an impact on catchment hydrology (O'Neel et al., 2014), contributing to both diurnal and seasonal variations of stage and discharge in glacially-fed streams, influencing ecological and geomorphological characteristics of the entire downstream watershed (Dorava & Milner, 2000; O'Neel et al., 2014). On short time scales, glaciers thin and retreat as climate warms, resulting in elevated inputs of glacier melt to the hydrologic system and decreasing storage of runoff from precipitation (Hock, 2005; Hock et al., 2005). Over time, however, melt runoff volume decreases as the glacier loses area, which decreases melt inputs to the system while simultaneously decreasing response times to precipitation events of receiving rivers and streams that transport glacier runoff (Stahl et al., 2008).

In addition to altering watershed hydrology, thinning and retreating glaciers often result in modification of the proglacial landscape, where lake development is common. In glacial and proglacial settings, lakes will form wherever glacial ice or topography, for example, terminal moraines associated with a previous glacial advance, impedes the local or regional drainage (Clague and Evans, 1994; Clague and Evans, 2000). Increased meltwater generation associated with climate changes can cause instability and even catastrophic failure of marginally moraine- or ice-dammed lakes, resulting in outburst flooding (Clague and Evans, 2000). On the other hand, in the absence of instability, moraine- and ice-dammed lakes that capture glacier meltwater act as a damper to the hydrologic system by reducing the amplitude of high flow events and supplementing low flow (Dorava & Milner, 2000).

In Alaska, there are numerous moraine- and ice-dammed lakes that have formed over the past 50 years due to rapid changes in volume of alpine glaciers (Post & Mayo, 1971). In south and southeast Alaska, where steep mountains with highly glaciated valleys are frequently exposed to heavy precipitation events and to high rates of summer glacier melt, proglacial lakes may

become even more important as hydrologic buffering units. Even though glaciated hydrologic systems containing lakes are prevalent in Alaska, few studies have explored how these systems balance additional inputs of precipitation, snow, and glacier melt in a changing climate. The Valdez Glacier catchment, in southern Alaska, is one such catchment that contains both a proglacial, moraine-dammed lake as well as a rapidly retreating and thinning glacier. Due to its close proximity to the Valdez community, roadways and infrastructure, there is a pressing need to examine the relationship between Valdez Glacier, the proglacial lake, and the proglacial stream that transports water from the lake in order to mitigate damages that could result from increases in runoff volume.

Modeling has proven effective for investigating changes in glacier volume and the resulting impacts on runoff in many regions (Juen et al., 2007; Stahl et al., 2008; Zhang et al., 2008; Bliss et al., 2014), using many different modeling approaches. One approach is the temperature-index model, which uses air temperature from stations near the glacier of interest as a proxy for the melt energetics at the glacier surface (Radic & Hock, 2006). Another approach is with hydrologic models coupled to a glacier sub-model, which have been successfully employed to estimate glacier melt rates and glacier runoff (Stahl et al., 2008). A third melt modeling approach is the energy glacier mass balance approach, which requires a more extensive set of meteorological observations to calculate surface energy fluxes (Oerlemans et al., 1998; Hock, 2003; Mernild et al., 2007). The type of model used often depends on availability of forcing data within the catchment of interest.

Temperature-index models are computationally inexpensive, and therefore well suited to large-scale, multiannual modeling studies (e.g. Radic & Hock, 2006; Radic et. al., 2014). A recent global temperature-index modeling study suggests that runoff from 36.2% of glaciers in Alaska will increase over the next two decades, while total runoff from all glaciated catchments throughout Alaska will gradually decline by a total of 29% by the end of the 21st century (Bliss et al., 2014). The model in this study is calibrated to the Alaska region based on data from two glaciers only, and while errors in glacier mass balance and runoff estimates on individual glaciers can be large, integrating the modeling results over several glaciers greatly reduces this error. However, by coupling glacier mass balance modeling with streamflow measurements within an individual catchment, more detailed, site-specific information regarding the sensitivity of an individual catchment to changes in glacier volume can be obtained, which can reduce modeling error.

While temperature-index modeling has been applied to individual glacier catchments globally (Braithwaite & Zhang, 2000; Pellicciotti, et al., 2005; Huss et al., 2008; Carenzo et al., 2009), few such studies have been conducted in the Alaska region. Young (2013) applied a temperature-index model to a large glacier in the Alaska Range, where detailed meteorological data were previously unavailable. The study, which included a relatively detailed network of local temperature observations, saw significant differences between simulated glacier mass balances and those observed using independent airborne altimetry data over long timescales, while over short timescales, simulated glacier mass balance agreed with altimetry studies. The study had no way to validate runoff estimates due to a lack of streamflow observations. With ablation data from 2012 and streamflow data from 2012 and 2013, we aimed to use a temperature-index model to assess glacier mass balance and runoff in the Valdez Glacier catchment in 2012 and 2013. We calibrated modeled-melt and runoff using data collected during our field investigations, thereby contributing to on-going modeling efforts that focus on individual glaciated catchments in Alaska.

1.1 Research Objectives

The objective of this study was to calibrate a temperature-index model to measured glacier ablation during the 2012 field season, and streamflow during the 2012 and 2013 field seasons. Results provided information on the relationship between meltwater runoff, rainfall runoff and streamflow. The calibration exercise sets the foundation for modeling glacier mass balance and runoff in the Valdez Glacier catchment using future climate scenarios. Results will be used to refine assessments regarding the potential for glacier-related hazards in Valdez, Alaska. The project will contribute to on-going glacier hazard assessments being conducted through the Climate & Cryosphere Hazards Program at the Alaska Division of Geological & Geophysical Surveys.

Specific components of the overall project include:

- collection of field measurements to characterize the present-day hydrological regime of the watershed, including glacier mass balance and streamflow;
- calibration of a physically-based glacier melt model; and,
- comparison of simulated runoff to measured streamflow.

1.2 Site Description

This project focuses on the Valdez Glacier and nearby glaciers within the Valdez Glacier catchment, which is approximately 10 miles outside of Valdez, in southern maritime Alaska. The Valdez Glacier catchment drains a total area of 342 km^2. The glaciated portion of the catchment includes Valdez Glacier and several smaller glaciers, which together comprise a total area of 199 km^2 (58% of the land cover within the catchment). As of 2012, Valdez Glacier covers a total area of 147 km^2 (Figure 1.1).
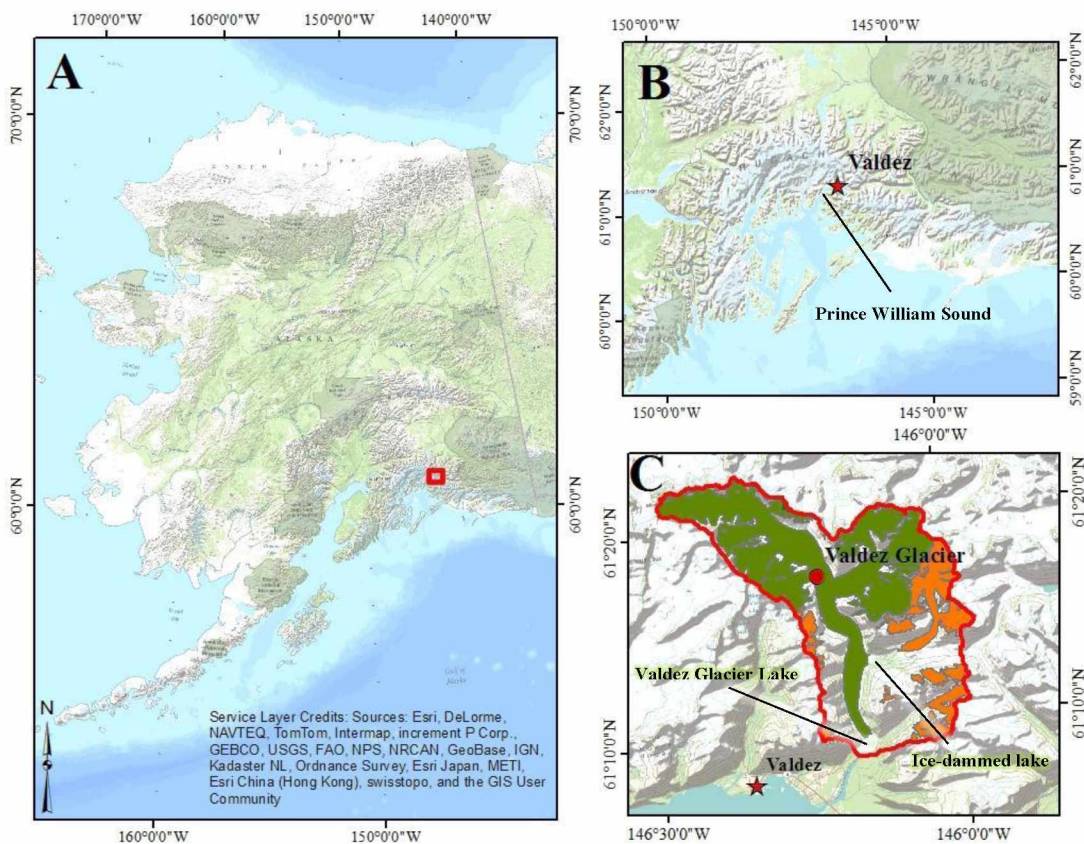
Figure 1.1: Location map. A&B) The Valdez Glacier watershed is located in southern Alaska, in the Chugach Mountains on the shores of Prince William Sound. C) The City of Valdez is located within 10 miles of the glacier and its catchment (outlined in red), which is comprised of Valdez Glacier (in green; labeled with red point) and several smaller unnamed glaciers (in orange). The catchment contains an ice-dammed lake at the margin of the main trunk of Valdez Glacier.

With the exception of one small advance from 1905 to 1908, Valdez Glacier has been retreating since it was first observed in 1898 by thousands of geologists and gold prospectors who used the glacier as a highway to the Copper River and Yukon basins (Grant and Higgins, 1910;

Martin, 1913;). Valdez Glacier retreated an estimated total length of 642 m (an average of 18 m per year) and the ablation area thinned by 5 to 6 m per year, from 1901 to 1935 (Field, 1937). The rapid changes in the glacier resulted in the abandonment of a mining camp that, at one time, was situated just above the ice surface (Field, 1932). Increased meltwater runoff caused the stream to shift, resulting in flooding and overthrowing of many cabins at the old Valdez townsite, in 1905 (Martin, 1913). Airborne altimetry observations show that the glacier decreased in volume at an average rate of 1.37 km^3 yr^{-1}, from 1950 to 2004 (Arendt et al., 2006). The retreat and thinning of Valdez Glacier resulted in the formation of Valdez Glacier Lake in the 1950s (Keinholz, 2010). The lake captures all glacier melt before the water is transferred to Valdez Glacier Stream, and ultimately to Prince William Sound (PWS). The thinning of the glacier also resulted in separation of a glacier tributary from the main branch of the Valdez Glacier. Runoff from the tributary's sub-basin is therefore dammed by the main trunk of the glacier, creating an ice-dammed lake (Figure 1.1). The marginal ice-dammed lake has been observed to drain seasonally to Valdez Glacier Lake (Keinholz, 2010). Therefore, the ice-dammed lake presents potential for outburst floods in the area.

The Valdez townsite was relocated out of the proglacial valley after the major earthquake and tsunami in 1964, but infrastructure still exists within this glacial valley. At present, the Haul Road embankment separates several housing and business units, recreational areas, the Valdez landfill, and the Pioneer Field Airport from the Valdez Glacier Stream floodplain (Figure 1.2).

6
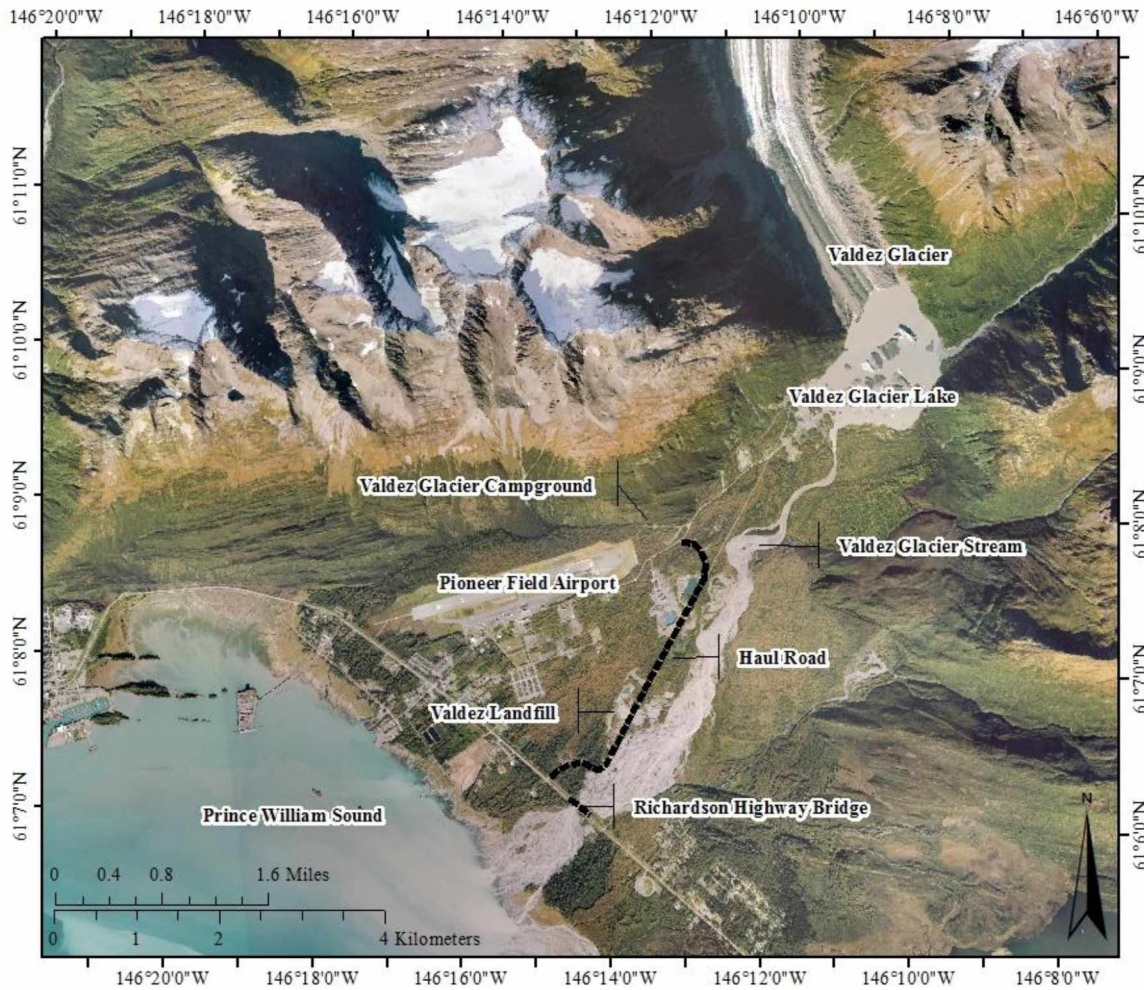
Figure 1.2: Map of proglacial area showing locations of infrastructure that may be susceptible to future flooding.

Perhaps most importantly, Valdez Glacier Stream flows immediately under a bridge at the Richardson Highway, the only road into and out of downtown Valdez, before connecting to Prince William Sound. From 2001 to 2006, four storm events resulted in a flooding of Valdez Glacier Stream, causing erosion, shifting of the stream channel, and in at least two cases, breaching of the Haul Road, flooding of nearby gravel pits located west of the stream channel, and floodwater encroaching on the city landfill (U.S. Army Corps of Engineers, 2007). Flooding hazards associated with ice jams, outbursts due to lake margin instability, and heavy rainfall events coupled with glacial meltwater runoff will be continued cause for concern as Valdez Glacier continues to change. It is because of these concerns that monitoring volume changes of

Valdez Glacier and the associated runoff is so important. Understanding the relationship between changes in Valdez Glacier mass balance and total runoff in the watershed can aid in predicting future flow regimes in Valdez Glacier Stream.

Located in a maritime climate, Valdez is known for receiving heavy precipitation throughout the year (Shulski and Wendler, 2007). The heaviest rainfall events occur in September and October, while the heaviest snowfall events typically occur in December and January, based on 30-year average weather station data from the National Oceanic and Atmospheric Administration (NOAA). Valdez receives an average annual total precipitation of 829 cm water equivalent (w. eq.) of snow and 178 cm of rain per year, based on NOAA weather station data (1950 to 2010). The added volume of runoff from non-glacier derived snow melt and rainfall contributes to the many flooding events reported by the community (U.S. Army Corps of Engineers, 2007).

1.3 Modeling and Field Study Design

We designed our modeling and field observation strategies for the Valdez Glacier catchment based on availability of pre-existing datasets. Previous glaciological investigations include laser altimetry mass balance measurements of Valdez Glacier, which provide a measure of annual balance on the glacier, but not detailed information on seasonal variations that are necessary for model calibration. Meteorological data include daily air temperature and precipitation observations from two National Oceanic and Atmospheric Administration (NOAA) Weather Service Offices (WSOs) located at the town of Valdez and Pioneer Field Airport. These data are located at low elevation sites (11 m and 29 m asl, respectively) and therefore do not provide information on the spatial distribution of air temperature and precipitation across the catchment.

Given the lack of detailed meteorological observations throughout the Valdez Glacier catchment, we chose a temperature-index model for our simulations. We utilized the Distributed Enhanced Temperature Index Model (DETIM) (Hock and Tijm-Reijmer, 2012) due to its application in several recent and ongoing studies throughout Alaska (the model is described in detail in Chapter 3). We designed a field program that was optimized for our temperature-index modeling. Our field efforts focused on instrumenting the glacier with temperature and precipitation sensors, which allowed us to calculate a more representative basin-wide temperature and precipitation lapse rate to force model simulations. In addition, we installed an ablation stake

network to provide data necessary for calibration of glacier melt. Finally, we initiated stage and discharge observations at the previously un-gauged Valdez Glacier Stream. Streamflow measurements are essential for calibration and validation of the DETIM runoff model. We investigated the stability of the Valdez Glacier Lake outlet to Valdez Glacier Stream, because morphological changes at the lake outlet could cause a change in the established rating curve. We then calculated mean daily discharge using the established rating curve and continuous stage data.

DETIM is primarily used here to determine summer glacier mass balance on Valdez Glacier, which, coupled with winter glacier balance, can provide a measure of annual glacier mass balance in 2012 and 2013. A parallel study on Valdez Glacier, conducted by McGrath et al. (in preparation), used GPR to measure snow depth on Valdez Glacier. The study is important to our project as it allowed us to formulate an initialization snow grid for the model, and also to estimate winter balance of Valdez Glacier. We determined annual balance of the glacier in 2012 and 2013 using our winter glacier balance estimate from the GPR data, along with modeled summer glacier balance. Finally, we validated the simulations by comparing our modeled annual glacier mass balance to laser altimetry measurements. Field methods used to obtain glacier mass balance information, meteorology, and streamflow are described in Chapter 2, while our glacier melt and runoff modeling techniques are described in Chapter 3. In Chapter 4, we present potential error associated with our field and modeling methods by exploring model sensitivity to various input parameters.

We investigated how well the temperature-index model is able to depict runoff from a large glacier in maritime Alaska by coupling glacier mass balance and runoff measurements with temperature-index modeling over two consecutive years. We also investigated the limitations associated with calibrating the melt model to a single year of ablation data, which represent a relatively small network of ablation stakes and air temperature sensors on Valdez Glacier. Finally, we investigate the main drivers of glacier melt and runoff on Valdez Glacier and discuss what this means for the future glacier melt and runoff regime.

Chapter 2

Meteorology, Glacier Mass Balance, & Discharge Observations

Introduction

A field program was initiated in spring 2012 to measure mass balance on Valdez Glacier, collect meteorological data describing conditions on and off the ice surface, and measure discharge from the Valdez Glacier watershed. The observations provided input and calibration data for the temperature-index simulations described in Chapter 3.

2.1 Meteorology

We installed a total of thirteen ablation stakes on Valdez Glacier and equipped four of the thirteen with air temperature and relative humidity (T/RH) sensors (HOBO Pro v2 U23-001; Table 2.1; labelled S-G01 through S-G04 in Figure 2.1). The air temperature sensors were launched at a 15-minute sampling interval in order to determine variability of near surface air temperatures as a function of elevation along the length of the glacier (Figure 2.1).

Table 2.1: Air temperature sensors throughout Valdez Glacier catchment in 2012. [Column 1: air temperature sensor ID; Column 2: air temperature sensor elevation; Column 3: start date of measurement period; Column 4: end date for the 2012 measurement period.]

Sensor ID	Elevation (m asl)	Start Date	End Date
S-G01	278	4/20/2012	9/16/2012
S-G02	821	4/19/2012	9/16/2012
S-G03	1248	4/19/2012	9/16/2012
S-G04	1494	4/19/2012	-*
VGL	77	7/4/2012	10/10/2012
Prospector	486	4/21/2012	8/8/2012
Schrader	1465	5/24/2012	10/11/2012

*Air temperature sensor, S-G04, was buried by snow by the end of the measurement period.
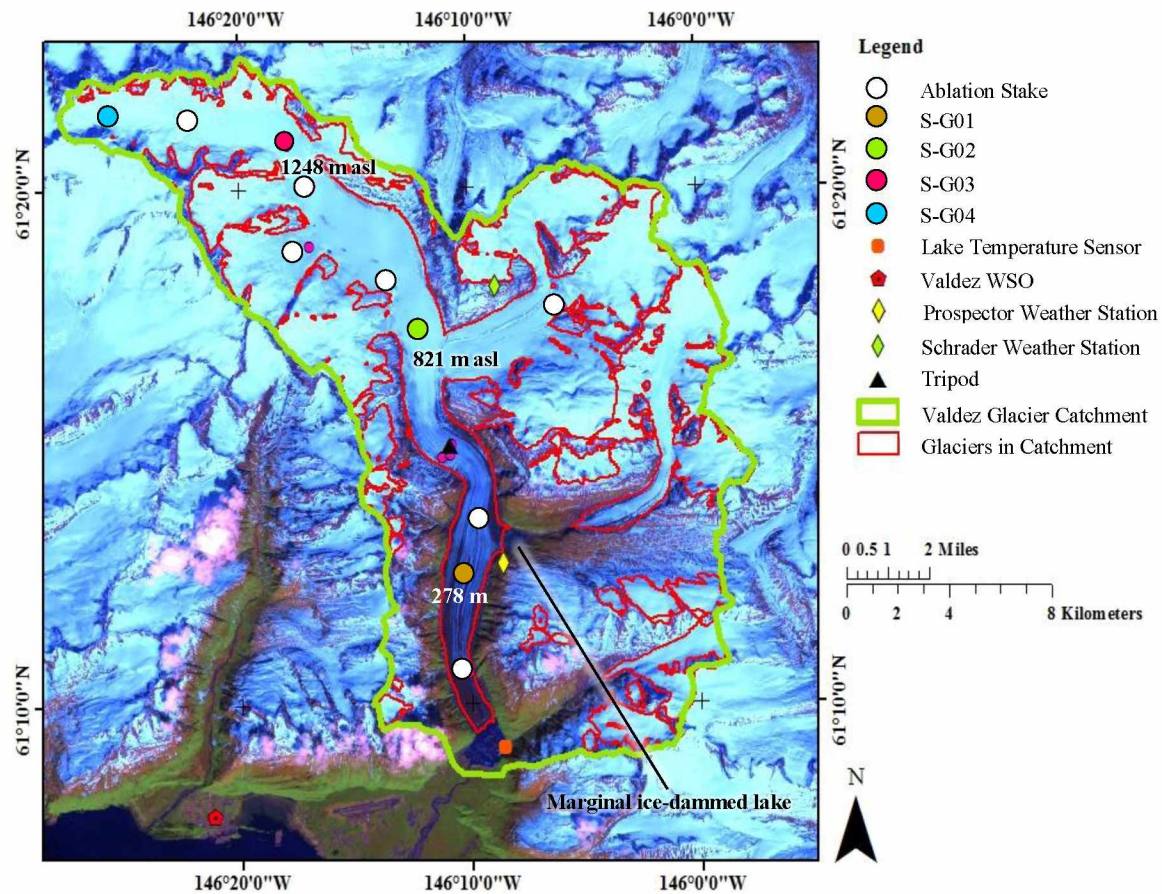
Figure 2.1: Ablation stake network placed on Valdez Glacier during the 2012 melt season. Of the 12 stakes, 4 were equipped with floating air temperature sensors (S-G01 – S-G04). Air temperature and precipitation data from the NOAA Weather Service Office (WSO) were also evaluated for the 2012 and 2013 seasons. Elevations of on-ice air temperature sensors are labeled on map. The marginal ice-dammed lake was equipped with a camera in attempt to capture seasonal draining.

The air temperature sensors were installed using a floating air temperature stand designed to maintain the height of the sensor at 2 m above the glacier surface throughout the melt season (Young, 2013). One on-glacier tetrahedron (Hulth, 2010) was installed on Valdez Glacier at 586 m asl. The tetrahedron was equipped with an air temperature and relative humidity sensor (HOBO Pro v2 U23-001 T/RH). By the end of the melt season, the tetrahedron had fallen partway into a crevasse, allowing for salvage of air temperature data only; the floating air temperature stand at S-G01 was bent 90° down-glacier with the air temperature sensor located approximately 0.40 m above the glacier surface; the floating air temperature stand at S-G06 was stuck on the ablation stake at an angle of 40° to the glacier surface, placing the air temperature

sensor approximately 1.5 m above the ice; and, the ablation stake at S-G04 had been buried by snow and could not be found.

Two off-glacier weather stations (Prospector and Schrader) were constructed near the Prospector and Schrader ridge tops adjacent to Valdez Glacier, at elevations of 486 m and 1465 m asl respectively (Figure 2.1; Table 2.1). Each weather station was equipped with an air temperature sensor (Campbell Scientific 107-L), a radiation shield (41303-5A 6-gill radiation shield), and a tipping bucket rain gauge (Campbell Scientific TE525WS-L). These instruments recorded at 15-minute intervals to match the sampling rate of the on-glacier sensors. An additional air temperature sensor (HOBO Pro v2 U23-001) was installed on the southeast side of Valdez Glacier Lake (VGL; Figure 2.1; Table 2.1) at a 15-minute sampling interval. Equipment failures, wildlife disturbance, and offsets in sensor deployment resulted in data gaps amongst sensors installed throughout the catchment (Table 2.1).

2.1.1 On-Glacier & Ridgetop Air Temperatures & Lapse Rates

We calculated daily temperature at all sensors using 15-minute air temperature data (Figure 2.2).
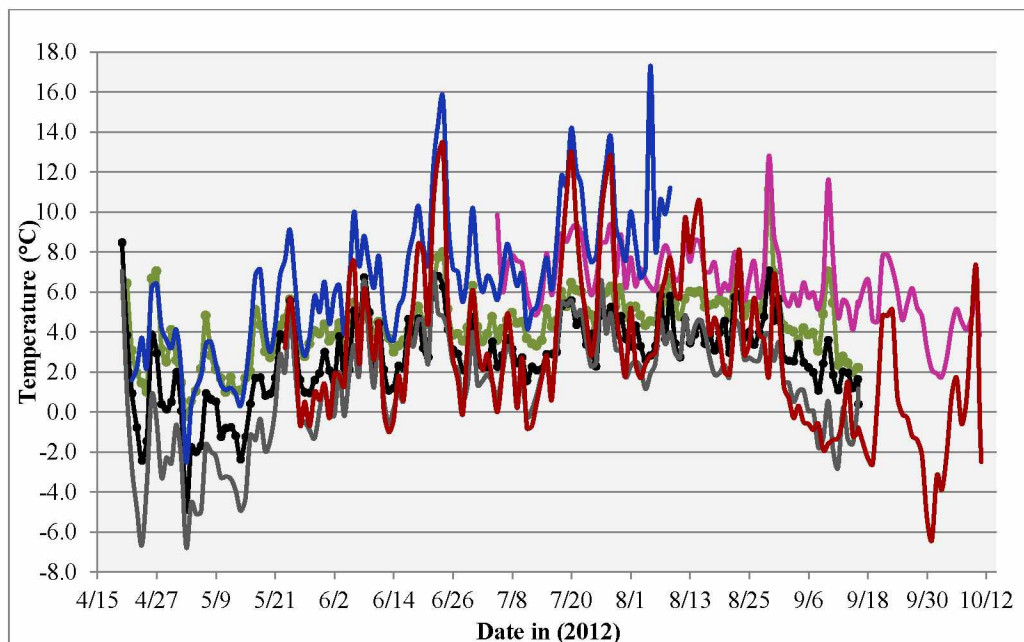
Figure 2.2: Mean daily air temperatures measured at weather stations located throughout Valdez Glacier catchment in 2012. [Prospector (486 m asl; blue line), Schrader (1465 m asl; red line), VGL (77 m asl; pink line), S-G01 (278 m asl; green line), S-G02 (821 m asl; black line), and S-G03 (1248 m asl; gray line)]

The air temperature data from stakes located at elevations 278 m (S-G01), 821 m (S-G02), and 1248 m (S-G03) were used to calculate average daily and monthly lapse rates across the glacier surface. Air temperature data for the months of April and September covered only part of each month, and thus average lapse rates for these months were based on only the portion of the month for which temperature data were available. For the month of April, lapse rates were based on data from April 19 to April 30, 2012, while lapse rates for September were based on data from September 1 through September 16, 2012. In addition, since ablation stakes were measured on October 11, 2012, we also lack air temperature lapse rate for the month of October. We corrected for data gaps by supplementing our air temperature observations with gridded temperature data (section 2.1.2). We calculated monthly lapse rates from 278 m asl (S-G01) to 821 m asl (S-G02), from 821 m asl (S-G02) to 1248 m asl (S-G03), and from 278 m asl (S-G01) to 1248 m asl (S-G03) (Table 2.2).

Table 2.2: Average monthly air temperature lapse rates calculated from air temperature sensors on the Valdez Glacier during summer 2012. [Column 1: month; Column 2: lapse rate from S-G01(278 m asl) to S-G02 (821 m asl); Column 3: lapse rate from S-G01 (278 m asl) to S-G03 (1248 m asl); Column 4: lapse rate from S-G02 (821 m asl) to S-G03 (1248 m asl); Column 4: lapse rates derived from PRISM temperature data (64 to 2154 m asl).]

Month	On-Glacier Lapse Rate, 278 to 821 m asl (°C/100m)	On-Glacier Lapse Rate, 278 to 1248 m asl (°C/100m)	On-Glacier Lapse Rate, 821 to 1248 m asl (°C/100m)	PRISM Lapse Rate (°C/100m)
April	-0.530	-0.781	-1.00	-0.320
May	-0.420	-0.578	-0.699	-0.370
June	-0.202	-0.263	-0.301	-0.320
July	-0.258	-0.273	-0.233	-0.260
August	-0.305	-0.348	-0.337	-0.290
Sept	-0.311	-0.512	-0.717	-0.370
October	--	--	--	-0.340
Average	-0.338	-0.459	-0.548	-0.324

In general, the average monthly air temperature lapse rates from S-G01 to S-G02 were less negative than the lapse rates from S-G02 to S-G03, while lapse rates from S-G01 to S-G03 fell between those calculated in the other lapse rate datasets. As a result, we focused on the lapse rate dataset from S-G01 to S-G03. Monthly averages ranged from -0.263 °C/100 m in June, to -0.781 °C/100 m in April. Daily lapse rates ranged from -0.859, on April 23, 2012, to +0.185 °C/100 m, on September 15, 2012 (Figure 2.3). The average lapse rate for Valdez Glacier

throughout the 2012 study period was calculated at -0.441°C/100 m. We used daily lapse rates for model simulations.
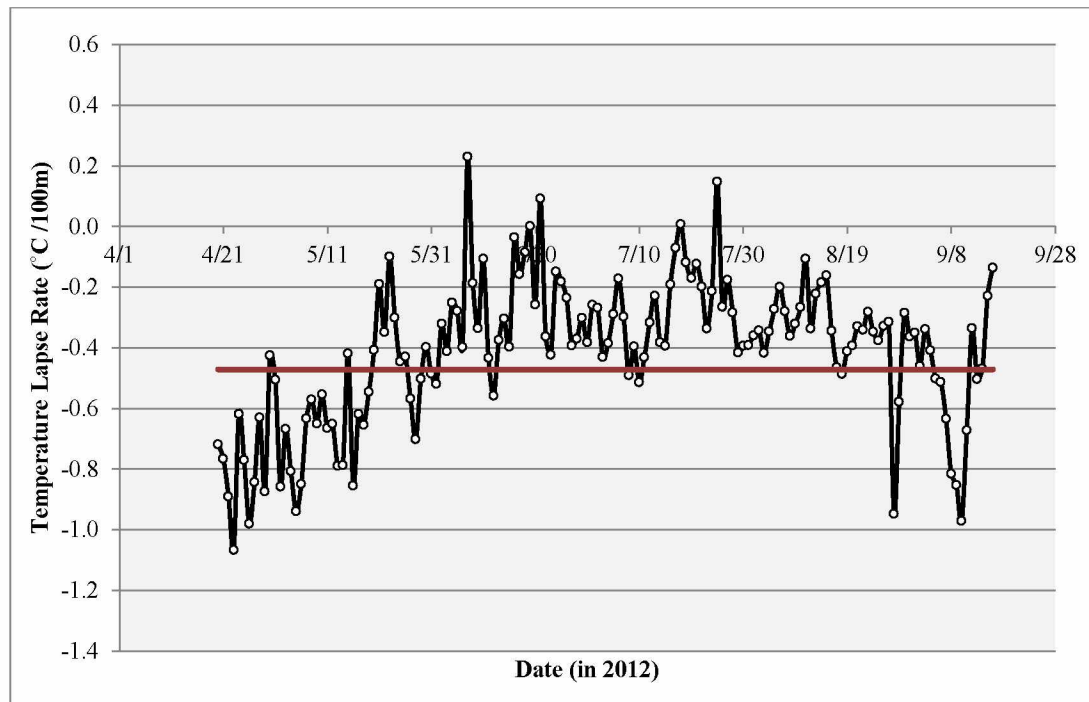
Figure 2.3: Daily air temperature lapse rates between air temperature sensors placed at 278 and 1248 m asl (S-G01 and S-G03) on Valdez Glacier during summer 2012. Red line shows the average daily lapse rate (-0.441°C/100 m) during summer 2012.

The difference between air temperature observations at similar elevations at on- and off-glacier surfaces varied according to elevation (Figure 2.2). Recorded air temperatures at 486 m asl (Prospector) were, on average, 2.5°C above those recorded at 278 m asl on Valdez Glacier (S-G01). Similarly, air temperatures at 1465 m asl (Schrader) were, on average, 1.4°C above those recorded at 1248 m asl on the glacier (S-G03). Air temperatures observed at Schrader were comparable to those observed at 1248 m asl (S-G03), but indicate higher maximum daily air temperatures at Schrader and lower daily minimum air temperatures at S-G03. Our observations indicate that air temperature and lapse rates vary throughout the catchment according to elevation and surface conditions (i.e. glacier or non-glacier). We expect the glacier to be the largest contributor to runoff in the catchment; therefore, we use on-glacier air temperature lapse rates calculated from 278 m asl (S-G01) to 1278 m asl (S-G03) to drive glacier melt model simulations.

2.1.2 PRISM Air Temperature Lapse Rates

PRISM (Precipitation-elevation Regressions on Independent Slopes Model) is a statistical and climatological model that uses digital elevation models (DEMs) to group grid cells in a given region into topographic facets, and predicts air temperature and precipitation within each grid cell based on linear regression analysis of air temperature or precipitation in each facet with elevation (Daly, 1994). Because our model simulations for 2012 spanned from March 29 to October 11, whereas air temperature data collection started in April and ended in September 2012, PRISM climatological normals from 1971-2000 (800-m^2 resolution) were used to calculate lapse rates. We used the PRISM lapse rates to fill gaps in air temperature sensor data. This includes the period extending from March 29 to April 19, as well as from September 16 to October 11. We first compare our calculated lapse rates from on-glacier sensors to PRISM lapse rates.

For the period spanning from March to October, monthly normals were extracted from the PRISM dataset for the entire Valdez Glacier catchment. Monthly temperature lapse rates were then calculated using the extracted normals in order to establish a point of comparison to lapse rates calculated from on-glacier temperature sensors. The seasonally averaged lapse rate from PRISM was -0.324 °C/100 m, which was 27% greater than those measured on the glacier (-0.441°C/100 m). Although relatively close in comparison, because the PRISM average lapse rate is derived from temperatures throughout the entire watershed, whereas the on-glacier lapse rate describes lapse rate within the glacier extent only. The differences between the two lapse rates suggest the possibility of error associated with using only on-glacier lapse rates in runoff model simulations (section 4.1.1), which incorporate snow melt and rainfall from un-glaciated portions of the catchment. Even so, we utilized our daily temperature lapse rates determined from on-glacier air temperature sensors S-G01 and S-G03, filling in data gaps with monthly normal temperature lapse rates derived from PRISM. For 2013, with no daily air temperature lapse rate information from the glacier, we used lapse rates derived from PRISM monthly normals.

2.1.3 Precipitation & Precipitation Gradient

Weather stations on the ridgetops at 486 m asl (Prospector) and 1465 m asl (Schrader), (Table 2.1; Figure 2.1) were instrumented with rain gauges to capture rainfall at different elevations. Capturing variations of rainfall with elevation is important given the drastic

topography changes in the catchment. Elevations in the catchment range from sea level to approximately 2600 m asl. Precipitation is controlled in part by air temperature that determines if it will fall as snow versus rain. We compared rainfall measurements from the Schrader (1465 m asl), Prospector (486 m asl), and NOAA WSO (11 m asl) stations to PRISM monthly normals calculated at 1705 m asl during the period of sensor measurement overlap (May 24 to August 8, 2012) in order to assess how precipitation varies with elevation (Figure 2.4).
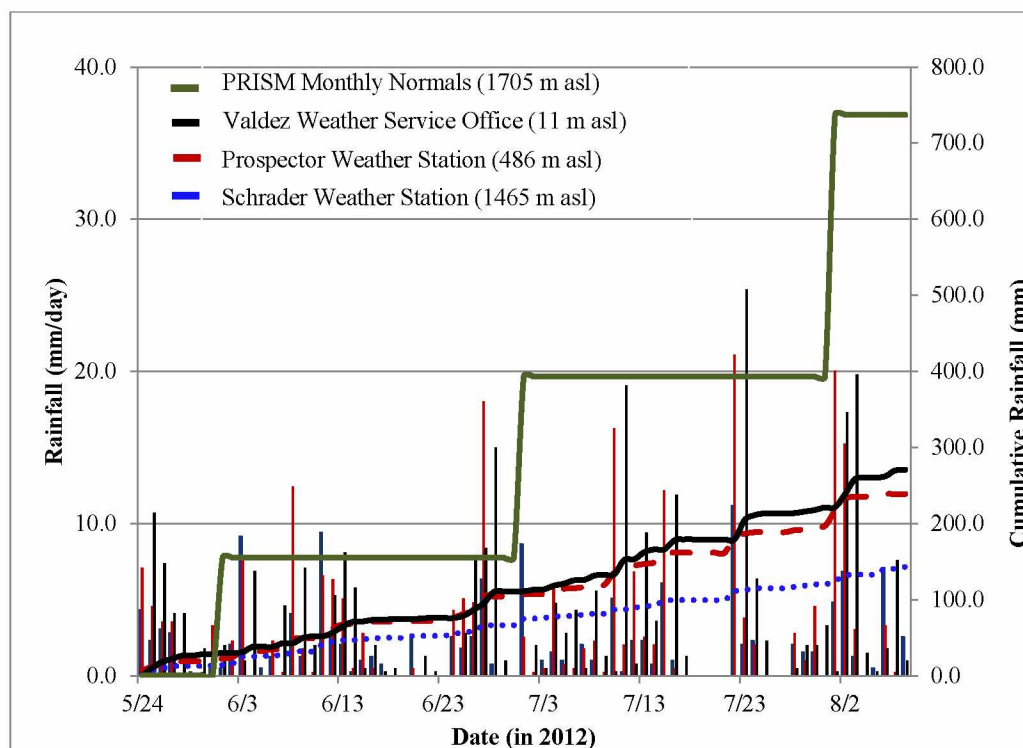
Figure 2.4: Rainfall (mm/day; colored bars, left axis) and cumulative rainfall (mm; colored lines, right axis) at the Prospector ridgetop weather station (red bars for daily and red dotted line for cumulative rainfall), the Schrader ridgetop weather station (blue bars for daily and blue dotted line for cumulative rainfall), the weather service office (black bars for daily and solid black line for cumulative rainfall), and the PRISM monthly cumulative rainfall from monthly averages at 1705 m asl (solid green line).

The data show decreasing quantities of cumulative rainfall with elevation during the period of measurement overlap. Cumulative rainfall totals over the measurement period at the WSO (11 m asl), Prospector (486 m asl) and Schrader (1465 m asl) were 27 cm, 24 cm, and 14 cm, respectively. The total rainfall at 1705 m asl according to PRISM monthly normals was 74 cm. The PRISM results suggest that increasing quantities of rainfall should be observed with increasing elevation, which is contrary to what we observed from our field measurements. We

observed a reduction of signal by 11% from 11 m asl (WSO) to 486 m asl (Prospector), and a reduction of 48% from 11 m asl (WSO) to 1465 m asl (Schrader). The reduction in signal with elevation is most likely a result of wind turbulence at the rain gauge sensor orifice causing undercatch (Groisman and Legates, 1994; Yang et al., 1998), which can account for up to 40% error in precipitation measurements (Groisman and Legates, 1994). Another possible source of error in rainfall measurements at our sensors could result from temperature lapse rates, which cause precipitation to fall as snow at higher elevations where temperature is lower. The tipping bucket rain gauges used in this study are not designed to measure snowfall. Thus, a portion of the reduction in precipitation signal may be a result of the gauges' inability to measure snowfall.

Precipitation gradient, defined as change in total precipitation with increasing elevation, is an important input to glacier mass balance modeling. Precipitation gradient along with air temperature lapse rate informs the model about rainfall and snowfall variation according to elevation. Because we experienced undercatch when attempting to measure rainfall at the ridgetop sensors, we turned to PRISM rainfall and snowfall data to calculate precipitation lapse rate over the course of the model simulation periods. In addition, the rain gauge data only applies to the elevation range from 11 m to 1465 m asl; therefore, PRISM monthly normals allowed us to calculate a precipitation lapse rate that is more representative of the entire Valdez Glacier catchment. We extracted monthly rainfall and snowfall normals (1971-2000) from PRISM covering the Valdez Glacier catchment for each month of our model simulation period (March to October, 2012), covering the elevation range of 64 m asl to 2154 m asl. We calculated the linear regression equation for each month, taking the average gradient observed over the entire period for model simulations (Table 2.3).

Table 2.3: PRISM-derived precipitation gradients for Valdez Glacier catchment, from 64 -2154 m asl. [Column 1: month; Column 2: total precipitation gradient; Column 3: rainfall gradient; Column 4: snowfall gradient.]

Month	Total Precipitation Gradient (mm/100 m)	Rainfall Gradient (mm/100 m)	Snowfall Gradient (mm/100m)
March	14	--	14
April	5.7	-0. 085	6.3
May	3.9	2.2	3.5
June	2.9	2.9	--
July	5.5	5.5	--
August	7.0	7.0	--
September	9.4	6.5	7.5
October	24	-0.20	26
Average	8.4	3.4	11

The most complete record of rainfall for the 2012 hydrologic year (October 1, 2011 – September 30, 2012) & 2013 hydrologic year (October 1, 2012 - September 30, 2013) is from the NOAA WSO. Total cumulative precipitation was calculated to 2.79 m for the 2012 hydrologic year (Figure 2.5) and 2.40 m for the 2013 hydrologic year (Figure 2.6). We used snowfall and rainfall data from Valdez WSO (11 m asl) to determine the percent of total precipitation that fell as snow or rain. Of the total precipitation measured at the WSO in the 2012 hydrologic year, 84% of this fell as rainfall at the station, whereas 16% fell as snow. In 2013, 83% of the total precipitation fell as rain, whereas 17% fell as snow.
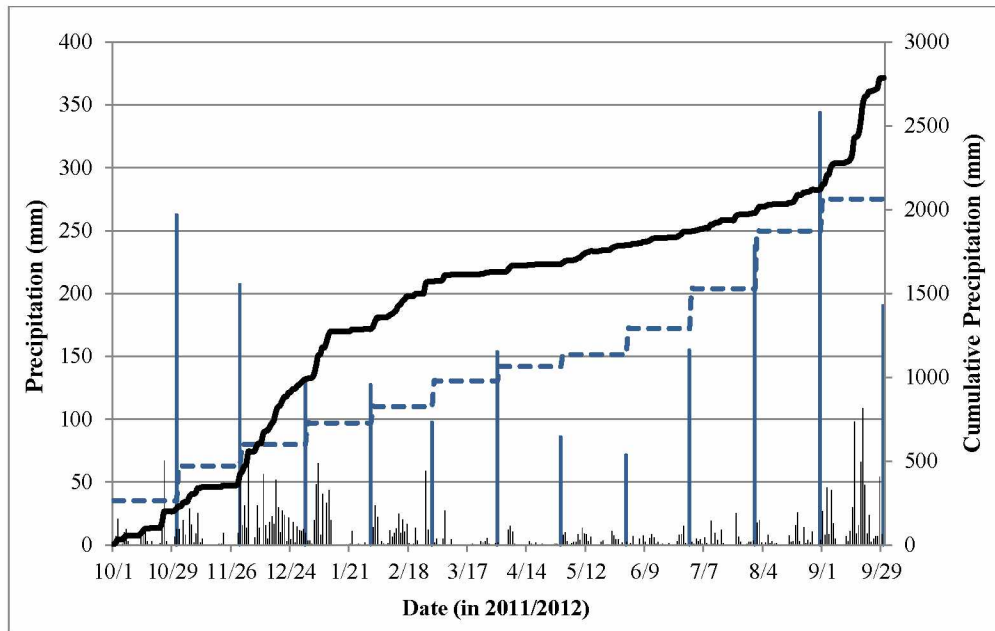
Figure 2.5: Precipitation (mm/day) and cumulative precipitation (mm) from Valdez WSO (11 m asl; black columns and black line) and PRISM monthly normals (1705 m asl; blue columns and dashed blue line) for the 2012 hydrologic year (October 1, 2011-September 30, 2012).
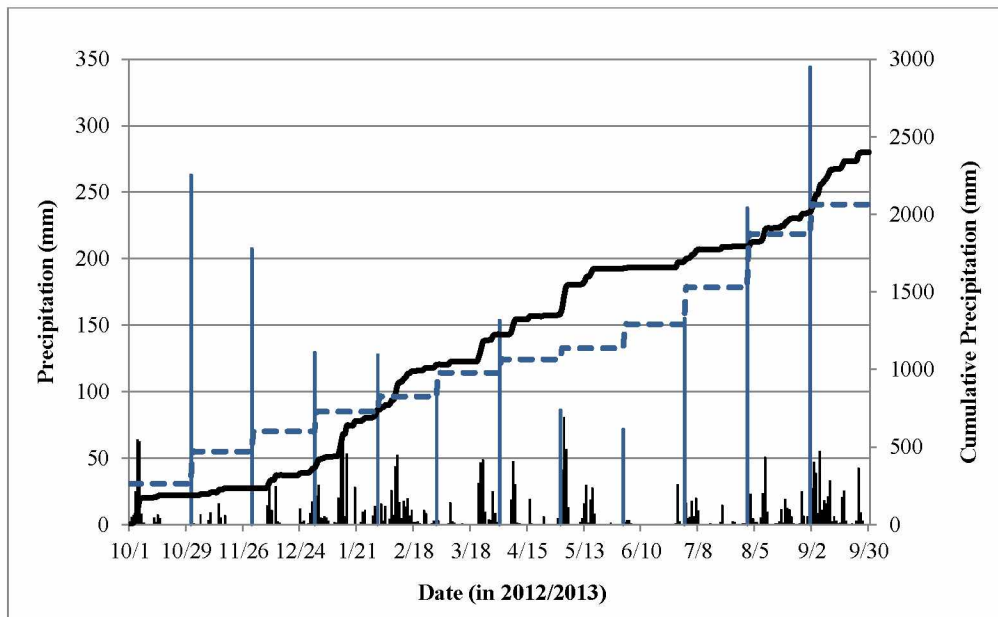
Figure 2.6: Precipitation (mm/day) and cumulative precipitation (mm) from Valdez WSO (11 m asl; black columns and black line) and PRISM monthly normals (1705 m asl; blue columns and dashed blue line) for the 2013 hydrologic year (October 1, 2012-September 30, 2013).

The PRISM cumulative precipitation, derived from monthly normals at 1705 m asl, are very similar to the precipitation data captured by the Valdez WSO (11 m asl). PRISM-based cumulative precipitation over one hydrologic year was calculated at 2.06 m (Figures 2.5 and 2.6), with 36% falling as rainfall and 64% falling as snow. The PRISM precipitation data suggests that the ratio of precipitation falling as snow versus rainfall is variable with elevation. We obtained a precipitation gradient that is more representative of the elevations throughout the entire catchment by using PRISM snowfall and rainfall data to calculate an average gradient for model simulations (Table 2.3).

2.2 Glacier Mass Balance

Mass balance on Valdez Glacier was calculated for both winter (statistical approach) and summer (DETIM model), for 2012 and 2013. Although efforts were made to target observations to the end of the winter and summer balance seasons, the exact dates varied according to conditions in a particular year (i.e. floating-date system; Cogley et al., 2011). Laser altimetry measurements use a fixed-date system. We used a fixed-date system for model validation and comparison with laser altimetry measurements. In both cases, we calculated a linear relationship between snow depth and elevation from measurements acquired using ground-penetrating radar (GPR). We assumed a constant snow density, based on snow pit measurements (0.36 g /cm; Gusmeroli et al., in preparation), throughout both time and space. We then calculated balance at a particular location within the glacier extent using the snow depth to elevation relationship determined by the linear regression. We calculated summer balance using DETIM, by extrapolating ablation at stake locations on the glacier to all areas within the glacier outline based on elevation. Together, the winter and summer glacier mass balances allowed us to calculate an annual glacier mass balance for both 2012 and 2013. The glacier mass balances cover the period ranging from peak snow accumulation to the end of our measurement period for the given year. Annual glacier mass balance estimates did not consider refreezing of water that infiltrates the glacier surface, nor did they account for internal ablation resulting from frictional heating from englacial flows. We also did not consider glacier mass loss due to calving or subaqueous melting. Methods for determining winter balance and acquiring summer calibration data are herein described.

2.2.1 Winter Glacier Mass Balance

GPR measurements of snow depth were acquired as part of a parallel study on Valdez Glacier from March 25 to March 29, 2012 (Alaska DGGS, unpublished raw data, in press). Results of the GPR data indicated snow depths ranging from 0.21 m w. eq. at the glacier terminus, to 2.19 m w. eq. at the head of the glacier. The equilibrium line altitude (ELA), as determined by locating the transition from glacier ice to firn layers in the GPR traces (A. Gusmeroli, personal communication), was located between 1300 and 1400 m asl at the end of the 2012 winter season. In 2013, repeat GPR measurements along the main trunk and smaller branches adjacent to the main trunk of Valdez Glacier reveal the complexity of spatial variability of snow accumulation on Valdez Glacier. Snow depth, or snow water equivalent (SWE), gradient with elevation ranged from 0.0 m m^{-1} to upwards of 0.0045 m m^{-1} (Gusmeroli et al., 2014, in preparation).

Several approaches can be used to extrapolate glacier-centerline snow depth measurements for the purpose of glacier-wide winter balance calculations. In the parallel study conducted by Gusmeroli et al., SWE was measured using GPR along the main trunk of Valdez Glacier and upper tributaries of the glacier. They extrapolated GPR-derived SWE over the glacier by establishing bins, each with a linear function of SWE with elevation. Over the main trunk of the glacier overall R^2 for SWE with elevation relationship in 2012 was 0.86 (Gusmeroli et al., in preparation). McGrath et al. (in preparation) performed a multivariate analysis comparing snow depth distribution on several Alaska glaciers to topographic parameters including surface elevation, aspect and a parameter that quantifies the degree to which a surface is affected by wind (S$_x$). Their calculations for Valdez Glacier showed that surface elevation and S$_x$ accounted for 77% and 12% of the variability in snow depth respectively, with the overall multivariate regression model having an R^2 of 0.68. McGrath et al. (in preparation) calculated independent R^2 for elevation and wind at 0.66, and 0.036, respectively (D. McGrath, personal communication). They also calculated residuals associated with their estimated versus observed SWE measurements, and used a nearest-neighbor approach to determine residuals in unmeasured areas on the glacier. By adding the residuals to the estimated SWE, the multivariate regression produces an R^2 of 0.88 (McGrath et al., in preparation).

The Valdez Glacier catchment contains several smaller glaciers for which there is no snow depth information. Therefore, we concluded that incorporating a more complex regression model based on topographical characteristics (i.e. wind redistribution) into our winter balance

calculations may introduce error in SWE estimations for portions of the catchment located outside the Valdez Glacier footprint. We used a simple linear regression of snow depth with elevation, for both 2012 and 2013. For 2012, our linear equation was

$$SWE = 0.0012(elevation) + 0.323, \qquad (2.1)$$

where SWE is in m. w. eq., and elevation is in m asl. We defined the 2011-2012 winter season as the onset of winter in 2011 to the end of winter in 2012. We observed an R^2 of 0.86 and a SWE gradient of 0.0012 m m^{-1} for 2012. The GPR data used to calculate the winter balance is from the main trunk of Valdez Glacier, extending from 137-1551 m asl (Figure 2.7).
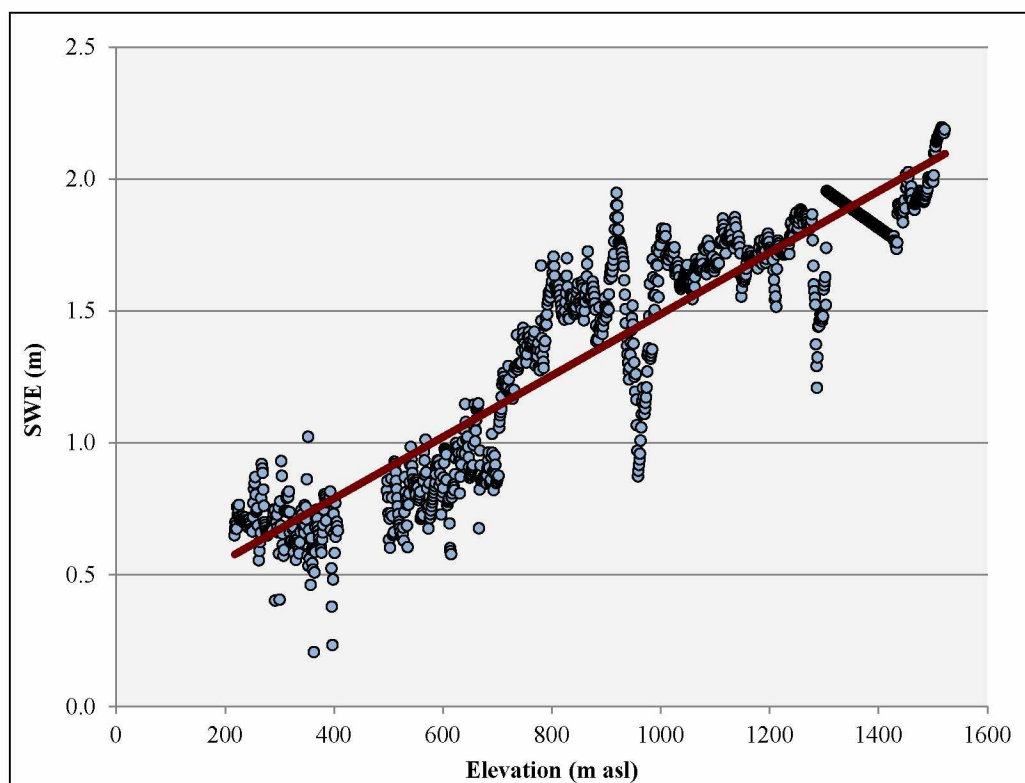
Figure 2.7: Distribution of SWE with elevation on Valdez glacier on March 29, 2012. Red line shows a linear regression between snow accumulation and elevation used to calculate the 2012 winter balance. $R^2 = 0.86$.

The linear regression analysis of SWE with elevation was used to extrapolate SWE over the entire Valdez Glacier catchment using elevation data from a SPOT 2007 DEM (Korona et al., 2009; Figure 2.8).
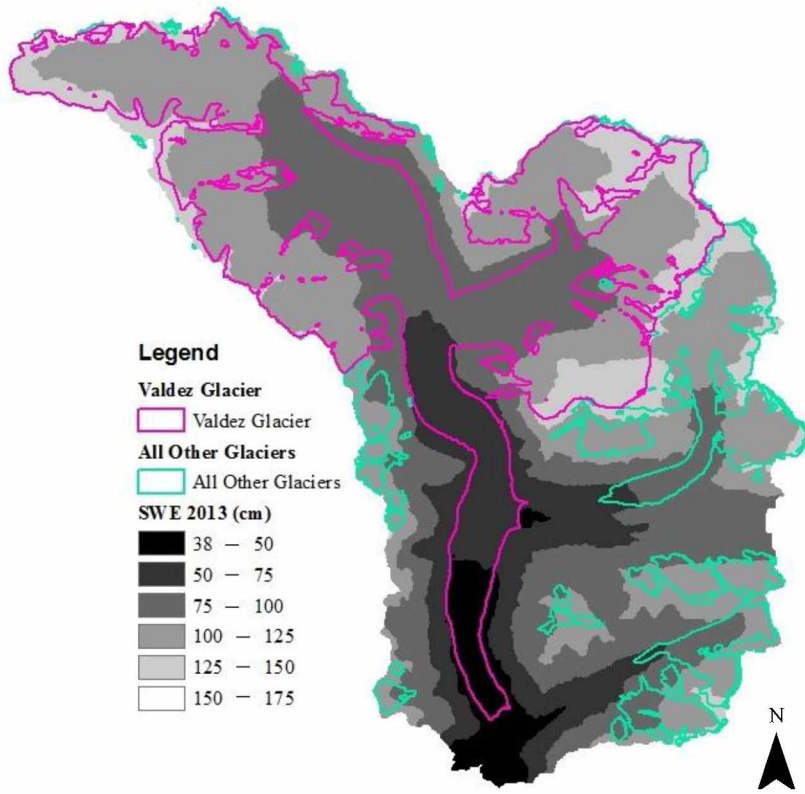
Figure 2.8: Spatial variability of estimated snow water equivalent (SWE) throughout the Valdez Glacier watershed, in 2012 and 2013, based on a linear regression analysis of GPR-derived SWE.
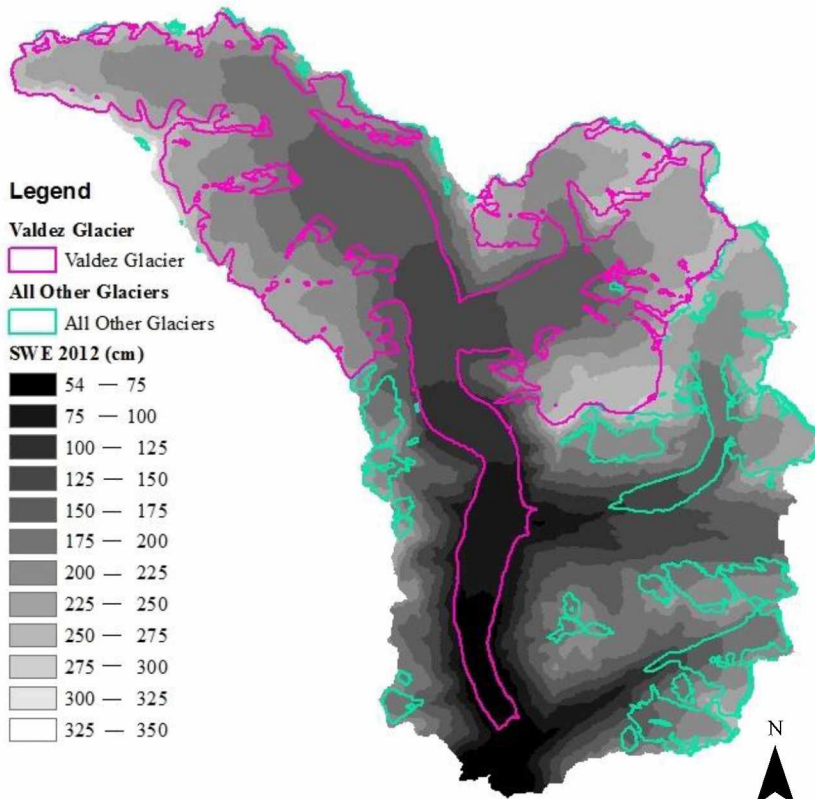
By summing the SWE observed in every grid cell located within the glacier extent and dividing by the total area within the glacier boundary, we calculated winter balance on Valdez Glacier to 1.90 m w.eq. (Table 2.4).

Table 2.4: Glacier-wide winter mass balance in 2012 and 2013. [Column 1: year; Column 2: date of year at which the end-of-season maximum snow depth was calculated; Column 3: Glacier-wide winter mass balance (B_w)].

Year	Date of Snow Depth Maximum	Glacier-Wide Winter Mass Balance (B_w; m w. eq.)
2012	March 29	1.90
2013	April	1.62

Winter balance on Valdez Glacier during winter 2012-2013 was calculated using GPR data, collected on March 14, 2013, in a similar fashion to calculations of 2011-2012 winter balance (Figure 2.9). The equation for 2013 SWE with elevation was

$$SWE = 0.0005(elevation) + 0.356, \qquad (2.2)$$

where SWE is in m.w.eq. and elevation is in m asl. We defined the 2012-2013 winter season as the period spanning from October 11, 2012 to April 9, 2013. We observed an R^2 of 0.67 (similar to McGrath et al., in preparation) and a SWE gradient of 0.0005 m m^{-1}, for 2013 (Figure 2.9).
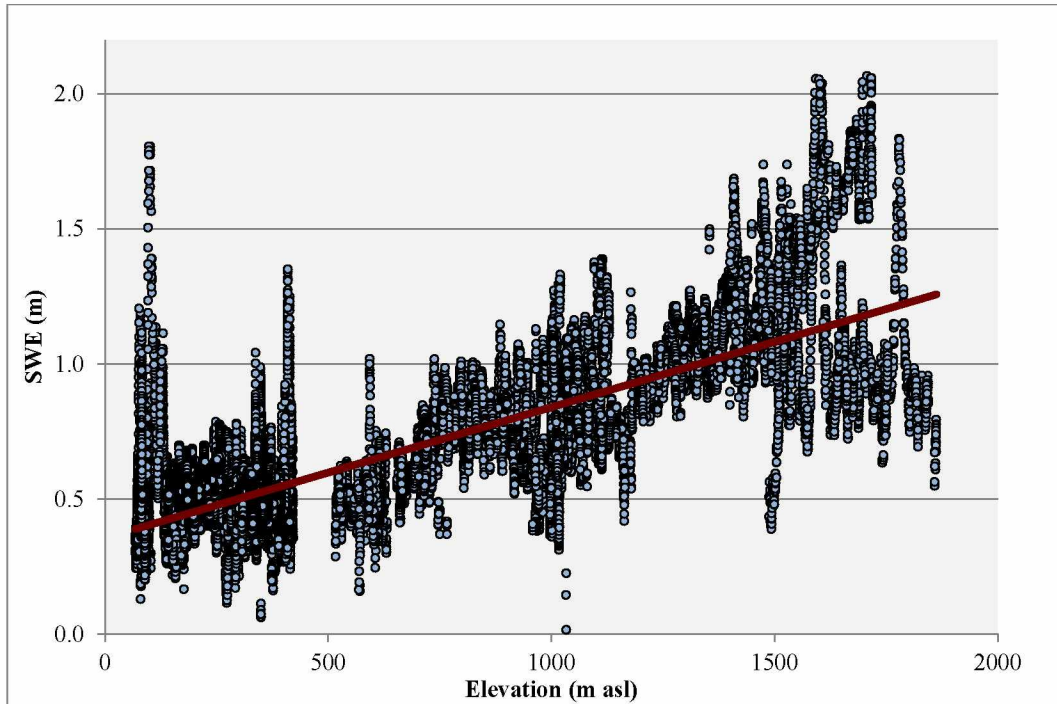
Figure 2.9: Distribution of SWE with elevation on Valdez glacier on March 14, 2013. Red line shows a linear regression between snow accumulation and elevation used to calculate the 2013 winter balance. $R^2 = 0.67$.

Two late-season snowfall events meant that the GPR measurement performed in 2013 did not capture maximum snow accumulation on the glacier and needed to be adjusted accordingly. We determined the date of maximum snow depth of the Valdez snowpack by analyzing WSO snow depth and air temperature data. We selected the date after which air temperatures became consistently above freezing and snow depth was consistently decreasing. We determined the date of maximum snow depth to be April 9, 2013, which is 26 days after the date of the GPR measurement. We adjusted the extrapolated GPR-derived SWE estimates to what they would have been on the date of maximum snow depth using snow accumulation data from the Alaska Department of Transportation's (DOT's) Thompson Pass weather station and the Valdez WSO. We calculated the ratio of GPR-derived SWE (from March 14, 2013) at the elevation of each weather station to maximum SWE at each weather station on April 9, 2013 (Table 2.5). The average of each ratio was used to re-calculate snow within the catchment (Figure 2.8) based on elevation according to the following equation:

$$SWE_{corr} = SWE_{GPR} \times CF, \qquad (2.3)$$

where SWE_{corr} is corrected SWE, SWE_{GPR} is GPR-derived SWE, and CF is the average ratio of maximum SWE to GPR-derived SWE (Table 2.5). We calculated winter balance for 2013 at 1.62 m w.eq. (Table 2.4).

Table 2.5: GPR-derived SWE at the elevation of Thompson Pass and Valdez WSO weather stations and maximum SWE observed at each weather station at the end of the winter season (April 9, 2013). The correction factor was used to adjust snow depth calculations on the glacier. [Column 1: weather station ID; Column 2: elevation of weather station; Column 3: GPR-derived SWE at each elevation; Column 4: maximum SWE observed on April 9, 2013; and Column 6: ratio of maximum SWE to GPR-derived SWE.]

Weather Station	Elevation (m asl)	SWE from GPR (m w.eq.)	Maximum SWE (m w.eq.)	SWE Correction Factor
Thompson Pass	885	2.62	3.95	1.51
Valdez WSO	11	1.14	1.95	1.71
AVERAGE				1.61

In parallel GPR-derived winter glacier mass balance studies, the winter balance for Valdez Glacier was calculated as 0.11 ± 0.04 km^3, or 2.23 ± 0.78 m. w. eq., for the 2011-2012 winter season (A. Gusmeroli, personal communication), and as 0.88 km^3, or 2.60 m w. eq., for the 2012-2013 winter season (McGrath et al., in preparation). Our estimates of winter balance for the 2011-2012 and 2012-2013 winter seasons, being 1.90 and 1.62 m w.eq. (Table 2.4), respectively, each fall within the margin of error determined by the more complex methods described in the parallel GPR studies. Differences observed between our 2013 winter balance estimate and the McGrath et al. (in preparation) estimate can be explained by differences in resolutions of DEMs used in each study (IFSAR 2013 at 5 m resolution versus SPOT 2007 at 30 m resolution), by a single versus multi-regression approach, and by methods used to correct GPR SWE measurements to maximum end-of-season SWE. McGrath et al. (in preparation) use temperature and precipitation data from a nearby SNOWTEL station located southwest of the Valdez Glacier catchment near Sugarloaf Mountain (168 m asl). They adopt a snow density of 0.33 g cm^{-3} as determined from GPR investigations to convert snow to SWE. They also apply a moist adiabatic lapse rate to project the data to elevations on the glacier and determine the end-of-season maximum at each glacier elevation. In contrast, we used precipitation data from two weather stations (Valdez WSO and ADOT at Thompson Pass) in order to better constrain the snow

distribution with elevation and we adopted a snow density of 0.36 g cm^{-3}, as determined from 2012 snow pit data from Valdez Glacier (A. Gusmeroli, personal communication) to convert snow depth to SWE. Methods presented by McGrath et al. produced an overall correction factor of 32%, while our methods produce a correction factor of 61%. The higher correction factor used in our SWE adjustment calculations accounts for our higher estimation of glacier-wide winter balance on the glacier.

2.2.2 Summer Glacier Mass Balance

A field campaign to Valdez Glacier was conducted in October 2012, to measure snow and ice melt during the melt season. Ablation stakes were positioned in 13 locations along the length of the Valdez Glacier, at intervals that ranged between 2 and 7 km laterally along the glacier flow line (Figure 2.3). Stakes were comprised of ¾-inch PVC pipe, cut into 2-meter sections and connected via an internal cord (in a similar fashion to camp tent poles), in order to allow exposed sections to drop onto the ice surface. Each stake was steam-drilled into the ice. Three stakes were installed within the 580-m asl elevation band in order to estimate melt variability within a single elevation band.

Measurements of ablation stake height above the ice and snow surface before and after the 2012 melt season (April 19, 2012 and October 11, 2012) produced point values for melt at each ablation stake (Table 2.6; Figure 2.10). The data show a linear relationship between melt and elevation.

Table 2.6: Mass balance at ablation stakes on Valdez Glacier, October 11, 2012.
[Column 1: ablation stake ID; Column 2: latitude of ablation stake; Column 3: longitude
of ablation stake; Column 4: elevation of ablation stake; and Column 5: glacier mass
balance measured on October 11, 2012.]

Stake ID	Latitude (°)	Longitude (°)	Elevation (m asl)	Mass Balance (m w.eq.)
STK01	61.177	-146.2	77	-5.97
STK02	61.208	-146.2	278	-5.52
STK03	61.227	-146.2	380	-5.43
STKTRI	61.247	-146.2	584	-3.91
STK04	61.251	-146.2	586	-4.29
STK05	61.247	-146.2	590	-4.88
STK06	61.288	-146.2	821	-2.57
STK07	61.334	-146.3	1141	-1.48
STK08	61.348	-146.3	1249	-1.12
STK11	61.295	-146.1	1122	-2.16
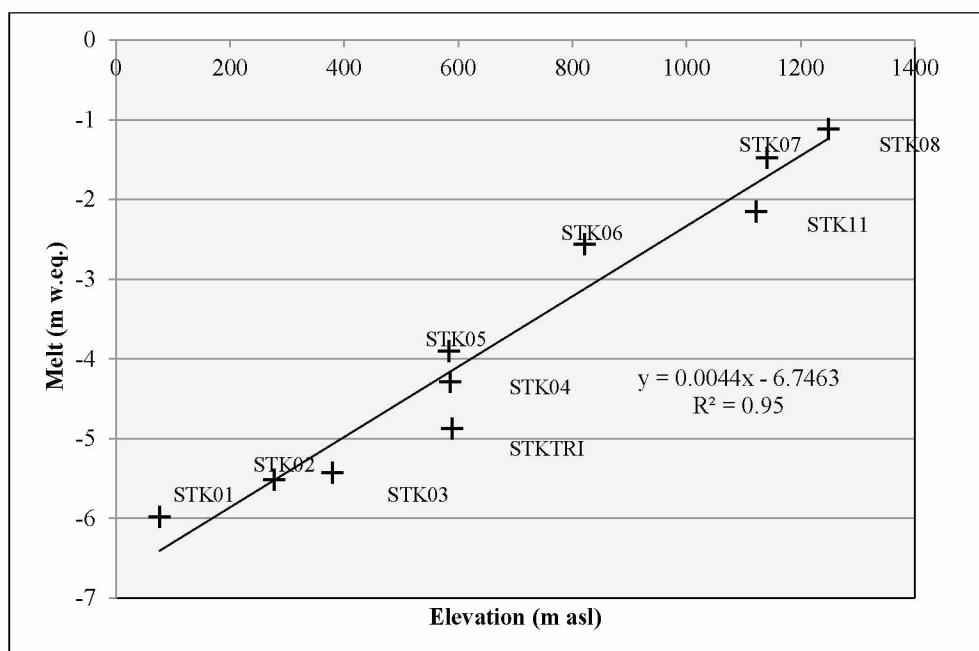
Figure 2.10: Melt measured at ablation stake locations on Valdez Glacier (April 19 –
October 11, 2012) (plus signs). Black line is the linear regression of melt against
elevation.

2.3 Lake Outlet Stability

Water surface elevation of the Valdez Glacier Lake was assessed using a dGPS in October of 2012. The lake elevation was also assessed with the dGPS in September 2013. Field observations conclude that the periglacial landscape near Valdez Glacier, and specifically within the Valdez Glacier Stream floodplain, is comprised of poorly sorted pebbly sands and silts, intermixed with large cobbles and boulders, signifying that at some point in history, these sediments were transported by water. The environment in and around Valdez Glacier Stream has changed significantly over the last 100 years. Most notably, Valdez Glacier has retreated greater than 2.5 km and Valdez Glacier Lake formed sometime after 1950, as Valdez Glacier retreated after carving out the basin (Keinholz, 2010). The lake dampens meltwater runoff variations in the stream, and possibly even glacial lake outbursts, from higher elevations in the Valdez Glacier catchment. If larger sediment is able to move from the outlet of Valdez Glacier Lake, changes to the geometry of the outlet could occur, which could mean that the stage-discharge relationship changed over the course of the study period. In order to gain a sense of the stability of the lake outlet and build confidence in the rating curve established for Valdez Glacier Stream a stability analysis was conducted.

To begin the process of outlet stability assessment, rock diameters were measured at 30 cm increments across one 8.9 m transect and one 17.8 m transect across the lake sill, or channel outlet from the lake. The rock diameter survey determined an average diameter of 21.0 cm, with diameters ranging between 2.3 and 61.5 cm. The Shields Equation was used to calculate critical shear stress necessary to entrain the bed particles characterized by rock diameter observations. The Shields equation relates shear stress necessary to entrain particles at the stream bed to average diameter of sediment, maximum diameter of sediment, sediment density, coarseness of the sediment at the stream bed, and gradient of the surface water:

$$\tau_{crit} = \theta_{crit}(s - 1)\rho g D \qquad (2.4)$$

where τ_{crit} is the shear stress necessary to move bed particles, θ_{crit} is the Shields entrainment function, s is the ratio of specific weight of sediment to be entrained to specific weight of water, ρ is the density of water, g is acceleration due to gravity, and D is the diameter of sediment for a given percentile. θ_{crit} is a nondimensional constant based on distribution of particle size, shape and packing at the streambed (Lorang & Hauer, 2003). Typical values of θ_{crit} for streambeds composed primarily of cobbles and boulders range from 0.052 to 0.054 (Berenbrock & Tramner, 2008). The calculation for critical shear stress is often performed using a value for D that

represents the 50th, 74th or 84th percentiles (Lorang & Hauer, 2003). Rock diameters in each percentile were calculated using data from the diameter surveys across the lake sill (Table 2.7).

Table 2.7: Rock diameters for the 50th, 74th, and 84th percentiles for rocks across the Valdez Glacier Lake sill were calculated for lake outlet stability assessment. [Column 1: percentile; Column 2: average rock diameter within the corresponding percentile.]

Percentile	Rock Diameter (cm)
D_{50}	16.75
D_{74}	30.74
D_{84}	33.89

Because the overall stability of the lake outlet is being assessed, the most conservative measure of shear stress is used in further calculations to determine a channel depth at which we can expect bed material to be transported, causing significant alteration to the channel and altering the rating curve. Thus, the diameter representing the 50th percentile is used in this investigation. Rock density used to calculate the ratio of specific weight of water to specific weight of rock, or *s*, were obtained from Case et al. (1966) who measured densities of various rock units in the Prince William Sound region (Table 2.8).

Table 2.8: Densities of rock units commonly found in the Prince William Sound region (Case et al., 1966). The total average density is used to assess the Valdez Glacier Lake outlet stability.

Rock Unit	No. of Specimens	Densities (g cm^{-3})		
		Minimum	Maximum	Average
Granite	8	2.58	2.69	2.62
Sedimentary (Orca Group)	16	2.63	2.75	2.69
Volcanic (Orca Group)	8	2.78	2.96	2.87
Sedimentary (Valdez Group)	10	2.64	2.74	2.69
			Total Average:	2.72

The average of all rock unit densities, calculated at 2.72 g cm^{-3}, is used in our calculation of critical shear stress. With D set to 16.75 cm, or the diameter of rocks in the 50th percentile, critical shear stress was calculated at 152.24 N m^{-2}.

In the next phase of lake outlet stability assessment, critical shear stress necessary to entrain bed particles at the lake outlet is used to determine a channel depth, given observable water surface slope, necessary to move bed particles:

$$\tau_b = \rho g h S , \quad (2.5)$$

where τ_b is the shear stress at the stream bed, ρ is the density of water, g is gravitational acceleration, h is the stream channel depth, and S is the average water surface slope across the lake sill.

Average surface slope of water in Valdez Glacier Stream across the lake sill was evaluated using a digital terrain model (DTM) obtained from a 2007 Light Detection and Ranging (LiDAR) dataset collected by Aero-Metric, in September 2007, which were processed and distributed by the United States Geological Survey (USGS) (Aero-Metric, 2009). As elevations of streams and lakes are difficult to measure using LiDAR, USGS interpolates elevations from bank to bank across each lake or stream feature, perpendicular to stream flow, such that each transect is flat from bank to bank and gradient downstream reflects that of the terrain immediately surrounding the channel (Heidemann, 2012). The 2007 LiDAR DTM indicates that elevations within the Valdez Glacier Lake and outlet to Valdez Glacier Stream do not change significantly (Figure 2.11), implying that the terrain immediately surrounding the lake outlet does not have much gradient.
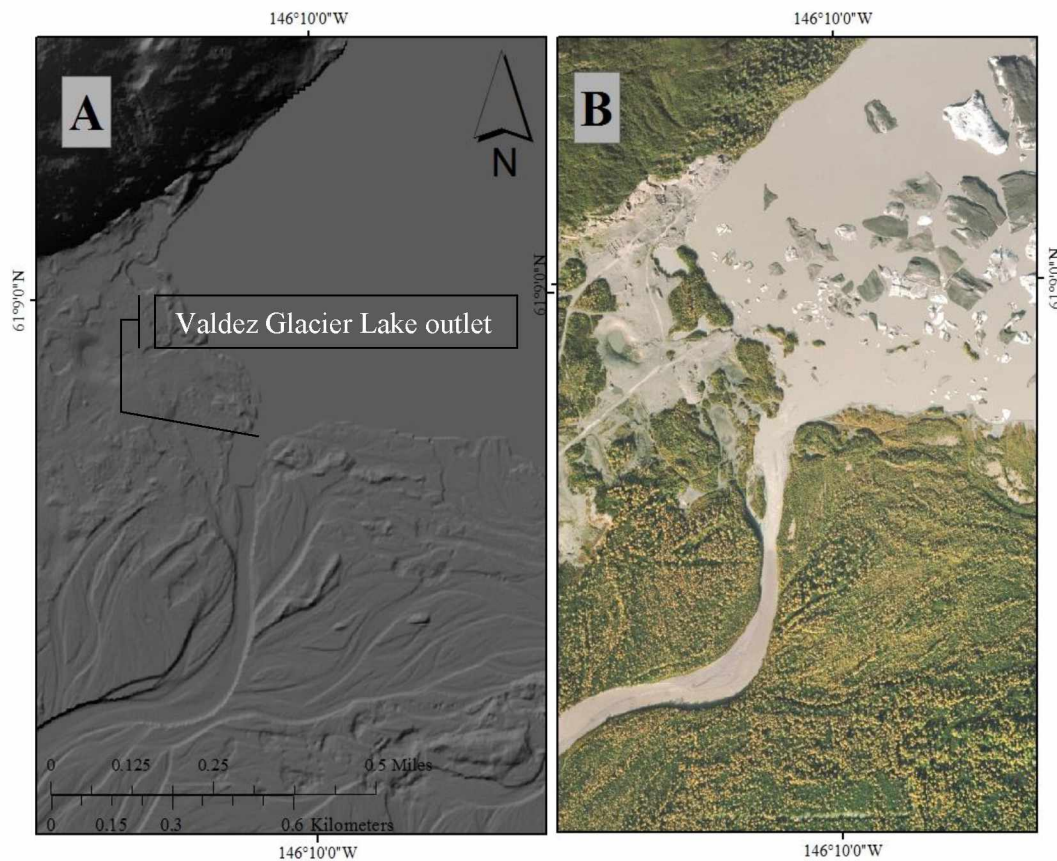
Figure 2.11: LiDAR DTM from 2007 showing Valdez Glacier Lake outlet. A) Hillshade created using 2007 LiDAR DTM at 2-meter resolution shows existence of abandoned stream channels and implies a flat lake and lake outlet at the start of Valdez Glacier Stream; B) Orthoimagery of Valdez Glacier Lake and its outlet to Valdez Glacier Stream shows existence of icebergs not observed in the LiDAR DTM. This implies that values across the lake and stream have been interpolated to reflect slope of adjacent banks as stated in Chapter 4 of the USGS National Geospatial Program standard for LiDAR data collection and evaluation.

The observed flatness in the LiDAR hillshade is a reflection of this interpolation process known as "hydro-flattening" (Heidemann, 2012). A slope analysis of the 2007 LiDAR DTM (Figure 2.12), confirms flat water surfaces at the outlet of Valdez Glacier Lake, with the exception of slopes at the stream banks.
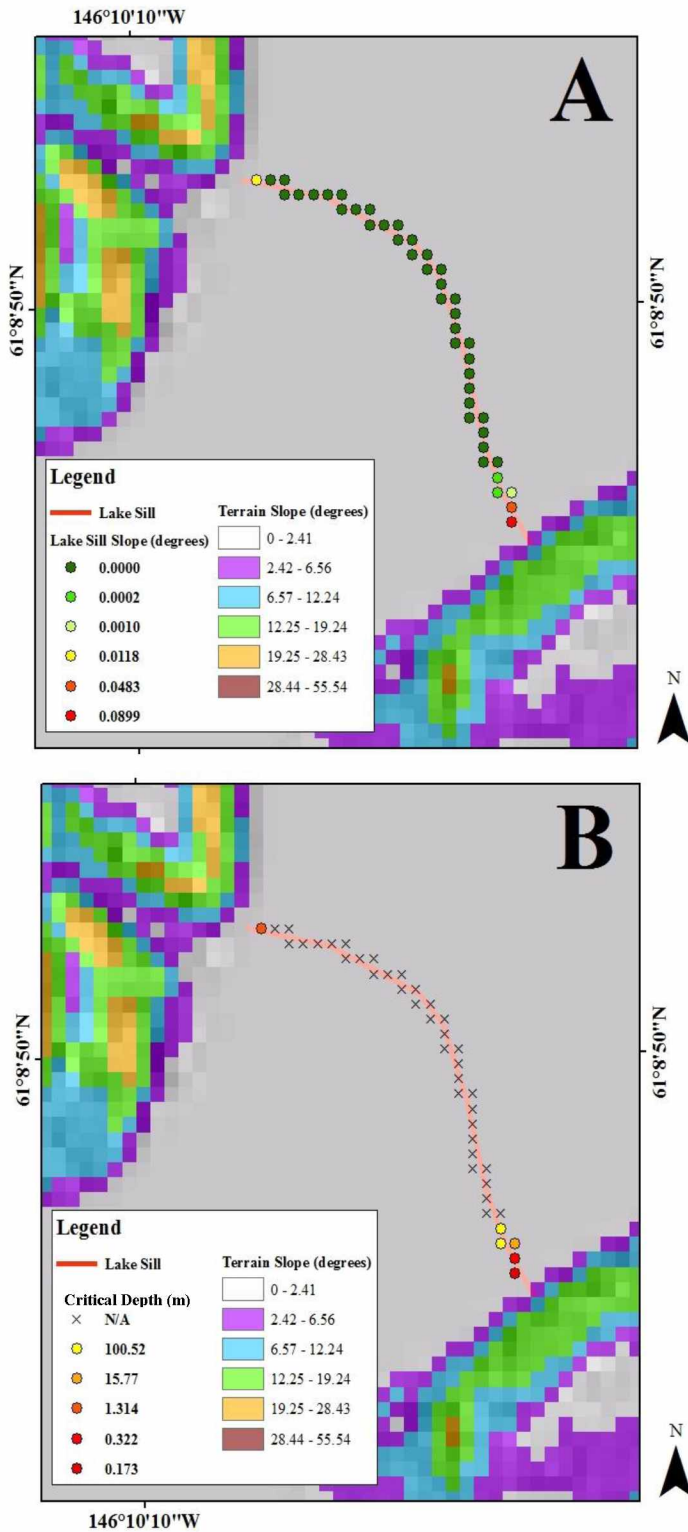
Figure 2.12: Slope of lake sill (degrees; colored dots in map A) and critical depths (m; colored dots in map B) at Valdez Glacier Lake outlet. Pixel coloration in both maps represents degree slope of surrounding terrain. A) The degree slope across the Valdez Glacier Lake outlet to Valdez Glacier Stream based on LiDAR 2007 DEM at a 2-meter resolution shows 0° gradient near the center of stream channel with higher gradients at the banks. Gradients were used to determine critical depths of the stream channel at which particle entrainment occurs. B) Critical depths necessary to entrain bed material and cause alteration of the rating curve for Valdez Glacier Stream indicate that movement of bed material throughout the central portion of the sill is unlikely.

The average water surface slope at the lake outlet was calculated at 0.0018 m m^{-1}, with slopes across the entire sill transect ranging between 0 to 1.69 m m^{-1}, again reflecting the flat terrain that exists in the area immediately surrounding the outlet of Valdez Glacier Lake. The lack of gradient in the central section of the lake sill indicates that these points are unlikely to experience particle entrainment. However, at points along the bank of the stream channel at the lake outlet, where the greatest slopes are observed, particle entrainment and channel alteration could still be possible during peak flows.

Setting τ_b to 152.24 Nm^{-2} (from page 27) in equation 2.4, the depth of water necessary to entrain bed materials with diameters in the 50th percentile was calculated across the range of slopes derived from the LiDAR analysis. These depths, here-forth referred to as critical depth, range from 0.17 m to a maximum of 100.52 m (Figure 2.12). Only three locations along the banks of the lake sill transect require depths less than 15 m to allow particle entrainment.

The maximum depth of water achievable in Valdez Glacier Stream at the lake outlet during peak flow determines the overall stability of the sill, and hence how confident we can be that the rating curve established for Valdez Glacier Stream is applicable to the entire study period. The maximum depth of the stream channel at the lake outlet was not measured during the highest flow. However, we can deduce from topography and past behavior of the lake and stream system that depths above 15 m are unlikely at the lake outlet. The topographic variability observed in the Valdez Glacier foreland is relatively low. In addition, Valdez Glacier Lake has a tendency to increase spatial extent with heavy influxes of water, which allows water to re-occupy the many abandoned channels in the foreland (Figure 2.11). Therefore, it is more likely that the lake margins will expand and water will be diverted into older stream channels before depth in Valdez Glacier Stream can reach the critical depth (15 m). However, significant outburst events or calving events could potentially cause bed particle movement at the Valdez Glacier Lake outlet. Thus, over longer timescales and if future studies are to be conducted at this study site, lake sill stability is an important consideration and should be investigated.

2.4 Discharge Measurements in Valdez Glacier Stream

No discharge data existed from Valdez Glacier Stream prior to our study. Our measurement strategy was based on continuous measurements of lake and stream water elevation (stage), which we related to synoptic stream discharge measurements. Development of an accurate rating curve requires that the channel morphology is stable.

2.4.1 Stream Gauging

In May of 2012, four pressure transducers (HOBO U20-001-01) were deployed in the proglacial area to measure stream and lake stage. One was installed in Valdez Glacier Stream at Richardson Highway bridge, one in the Valdez Glacier Lake, and two in the air to collect continuous barometric pressure in order to correct data recorded by the non-vented sensors (Figure 2.13). Each sensor was set to record at 15-minute intervals, which we used to calculate hourly lake stage (Figure 2.14).
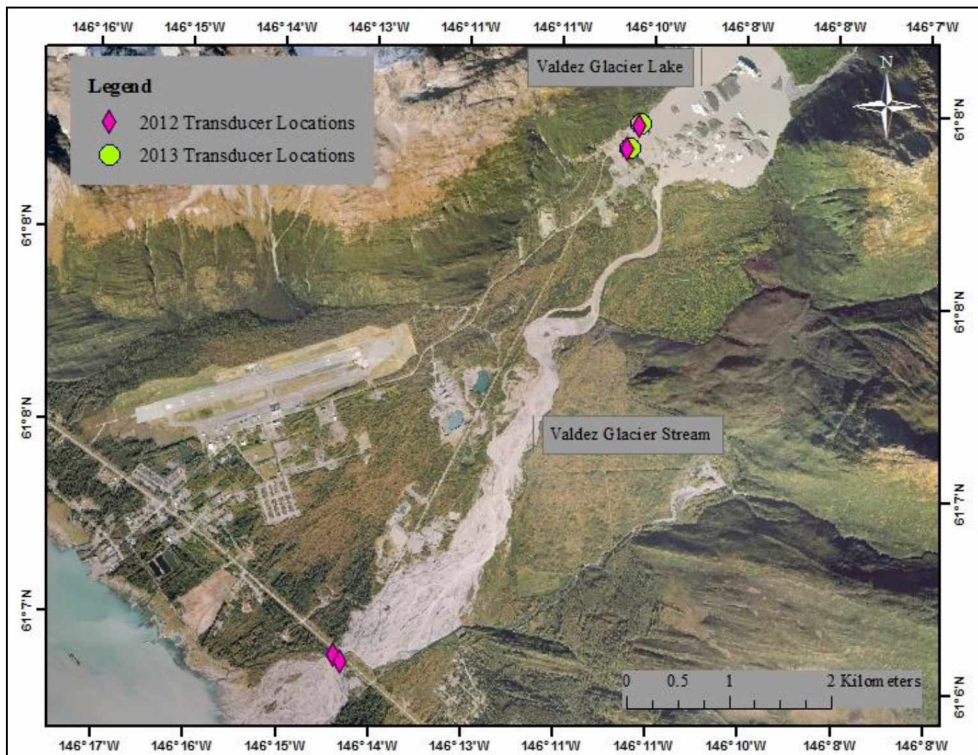
Figure 2.13: Locations of HOBO pressure transducers used to measure lake and stream stage during the 2012 and 2013 field seasons.
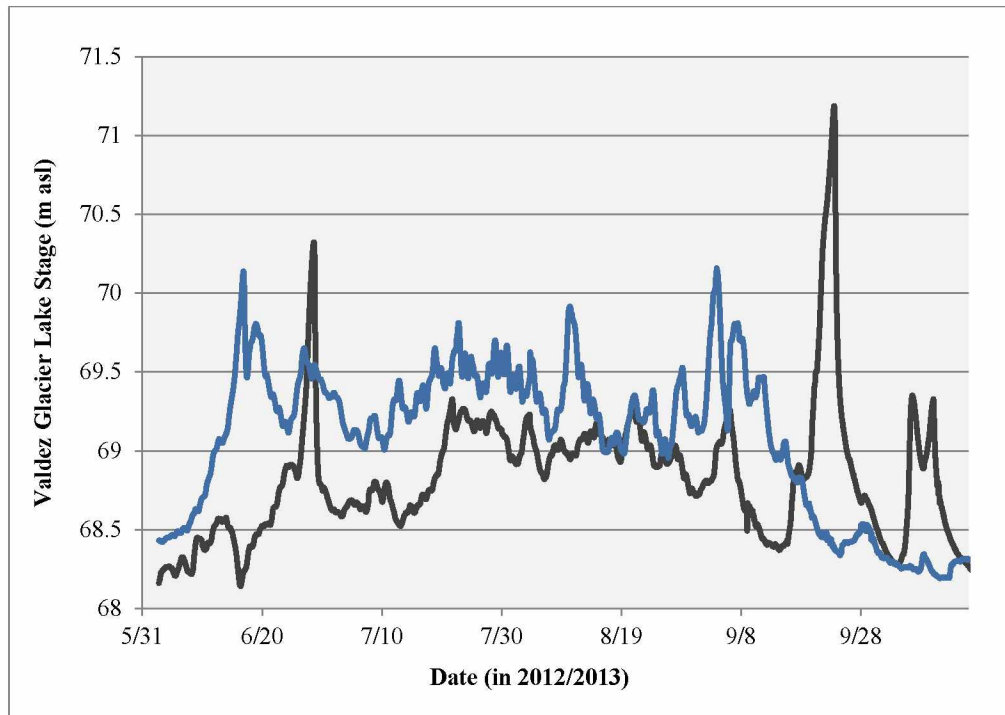
Figure 2.14: Hourly stage data from Valdez Glacier Lake during the 2012 (gray line) and 2013 (blue line) field seasons. Measurements prior to September 13, 2012 were not used for further investigation in this study.

Upon reviewing data from the 2012 field season, it became apparent that scouring of the channel was occurring at Richardson Highway bridge. Visits to the site in May 2013, when the channel was dry, confirmed that down-cutting had indeed occurred at the bridge sensor location. Thus, it was determined that the best location to collect stream stage data was in Valdez Glacier Lake. During the 2013 field season, one pressure transducer (HOBO U20-001-01) was installed in the Valdez Glacier Lake, and one was deployed in the air for barometric pressure correction purposes (Figure 2.13). Both sensors deployed in 2013 sampled at 15-minute intervals, which we used to calculate hourly lake stage (Figure 2.14). Lake surface elevations measured using a dGPS on October 9, 2012 and October 24, 2013 were used to correct lake stage measurements to a known elevation. The 2012 lake transducer was relocated on September 13, 2012 before measuring its exact location. Therefore, stage measurements recorded prior to September 13, 2012 were excluded from further analyses.

Discharge was measured using the StreamPro Acoustic Doppler Current Profiler (ADCP) and the River Ray ADCP. An ADCP is a device designed to float across a water body while reflecting ultrasonic signals off of particles that are suspended in the water. The ADCP then uses

the Doppler relationship to determine velocity in a water column from backscatter (Mueller & Wagner, 2009). The WinRiver II software is used to communicate with the ADCP, and is able to calculate total discharge based on the measured velocities in sections of water columns, or bins, across a transect. Discharge was measured on a periodic basis to capture the flow during a range of stages in the 2012 and 2013 seasons. Streamflow measurements with the ADCP were collected at a site downstream of Richardson Highway bridge during the 2012 field season. Each measurement was conducted using ropes to manually pull the ADCP across the stream transect. Streamflow measurements in 2013 were conducted at the outlet of Valdez Glacier Lake using a raft and motor (Figure 2.15). The number of measurement transects conducted for each discharge value ranged between four and eight.
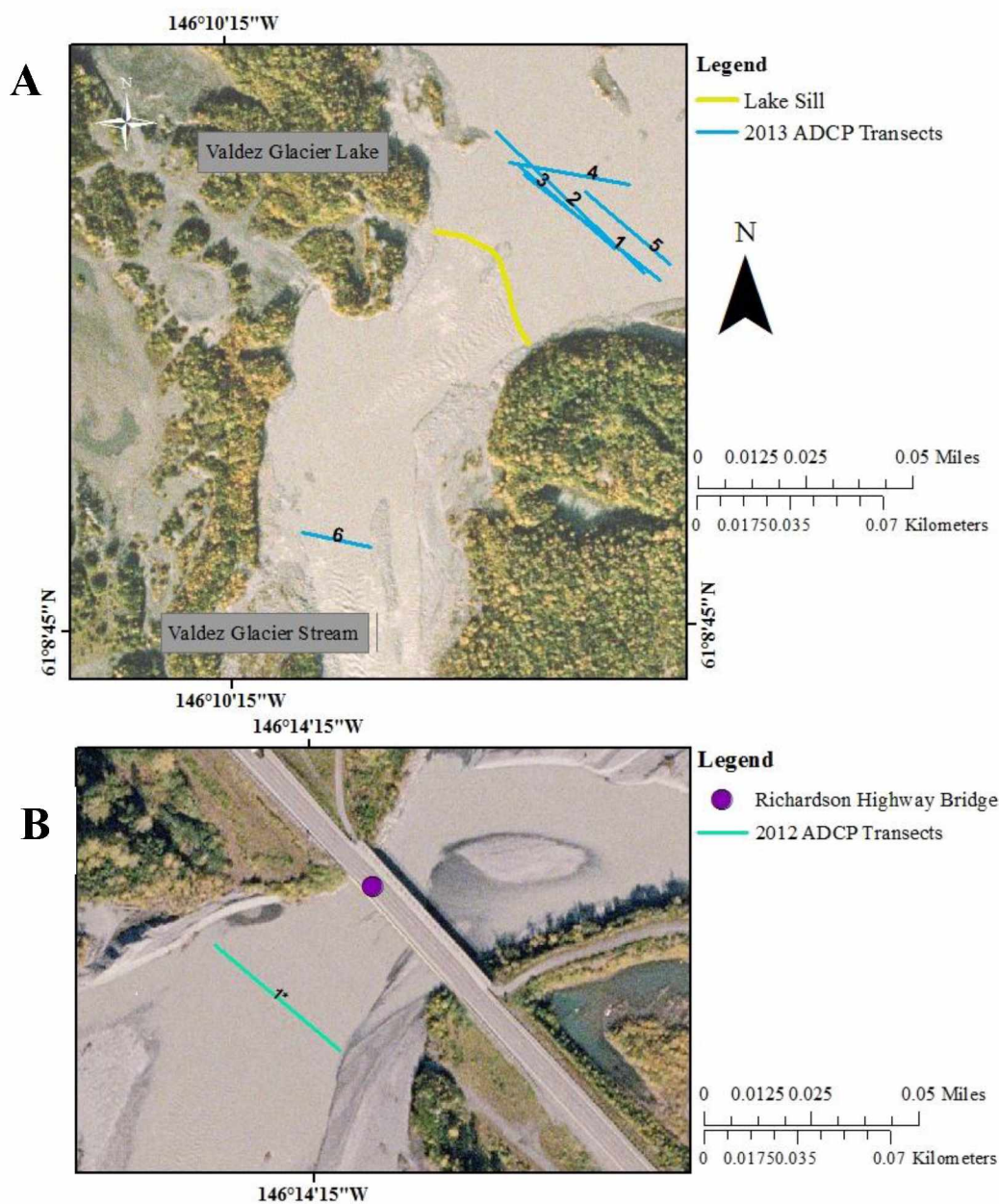
Figure 2.15: (A) LiDAR 2007 image showing ADCP transect locations in 2013 (A) and 2012 (B). (A) Transects were conducted near just above or below the lake sill during 2013. (B) The transect conducted during 2012 was measured at Richardson Highway bridge. Results of the transect measurements can be seen in Table 2.9. Transects are numbered according to ID number in Table 2.9.

Streamflow measured in 2012 included drainage from the overall Valdez Glacier stream watershed (398 km^2), while 2013 measurements represent the sub-basin draining into the lake (342 km^2). In order to make the 2012 discharge measurements useful for runoff model

calibration, we adjusted the discharge measurement by eliminating flow inputs downstream of the lake outlet. The percentage flow increase from the lake outlet to the bridge was determined from discharge measurements conducted on October 23, 2013, which were taken both at the lake outlet and at the bridge. The measurements were conducted at approximately 11:53AM and 12:44PM AK time, respectively. Lake stage and discharge were dropping during the entire site visit on this date. The measurement at the bridge lagged the measurement at the lake outlet by approximately 51 minutes, and correspondingly, the lake stage had dropped by approximately 8 mm, according to lake sensor data. The percent difference in the runoff measurements at these two locations on October 23, 2013 was 9.8%. All measurements collected in 2012 at Richardson Highway bridge were thus corrected for the change in drainage area by subtracting 9.8% from the measured discharge.

Ten measurements were conducted in 2012, and six were conducted in 2013 (Table 2.9). We did not use discharge measurements pre-dating the transducer relocation (September 13, 2012) for further analysis. Measurements that are excluded from analysis are not assigned a number in Table 2.9 and are not displayed in Figure 2.15. Each measurement used for further streamflow analysis is numbered in Table 2.9, which summarizes the measurement date and time, stage, and corresponding discharge.

Table 2.9: ADCP measurements collected during the 2012 and 2013 field seasons. [Column 1: transect ID (see Figure 2.15); Column 2: date and military time of measurement; Column 3: gage height; Column 4: discharge at gage height.]

Transect ID Number	Date, Time	Gage Height (m asl)	Discharge (m^3 s^{-1})
--	5/31/2012, 1130	68.279[†]	14.8 ± 2.47
--	5/31/2012, 1530	68.230[†]	16.4 ± 2.47
--	5/31/2012, 1940	68.322[†]	19.2 ± 2.47
--	6/1/2012, 1000	68.308[†]	11.1 ± 2.47
--	7/13/2012, 2245	68.783[†]	35.3 ± 2.47
--	7/14/2012, 1000	68.792[†]	34.5 ± 2.47
--	7/14/2012, 1400	68.811[†]	45.6 ± 2.47
--	7/14/2012, 1800	68.833[†]	50.7 ± 2.47
--	7/15/2012, 1800	68.844[†]	52.5 ± 2.47
1*	9/15/2012, 1330	68.359	22.5 ± 1.4
1	9/11/2013, 1315	69.406	156.5 ± 2.9
2	9/12/2013, 1045	69.391	148.9 ± 7.4
3	9/13/2013, 1022	69.004	92.8 ± 0.6
4	9/14/2013, 1126	68.863	74.8 ± 1.8
5	9/15/2013, 1655	68.960	85.4 ± 2.6
6	10/23/2013, 1130	68.191	13.2 ± 0.6

†Note: Listed gage heights were calculated using the 2013 rating curve. The transducer was relocated on September 13, 2012. Measurements conducted prior to September 13, 2012 were not used for modeling exercises. Error for these measurements was calculated using the average standard deviation observed in the 2013 measurements.

2.4.2 Valdez Glacier Stream Rating Curve

A rating curve is typically established based on stage data collected in a stable portion of the stream that is measured for discharge (Kennedy, 1984). In glacier-fed streams, when large portions of the stream are not stable due to active erosion and deposition, it becomes challenging to establish a rating curve based on stream stage. Thus, it is common for rating curves in glacier-fed streams to be developed using stage data from proglacial lakes, which has proven successful for Mendenhall River, in Juneau, AK, for example (Neal & Host, 1999). We employed the lake stage approach, using Valdez Glacier Lake stage data to establish the Valdez Glacier Stream rating curve. We plotted discharge against stage to begin the process of rating curve establishment. We next fit an equation to the data points. The best-fitting equation was then used to calculate discharge from continuous stage data. We found that the Valdez Glacier Stream

discharge and Valdez Glacier Lake stage data was best represented by a linear relationship (R^2 = 0.97; Figure 2.16).
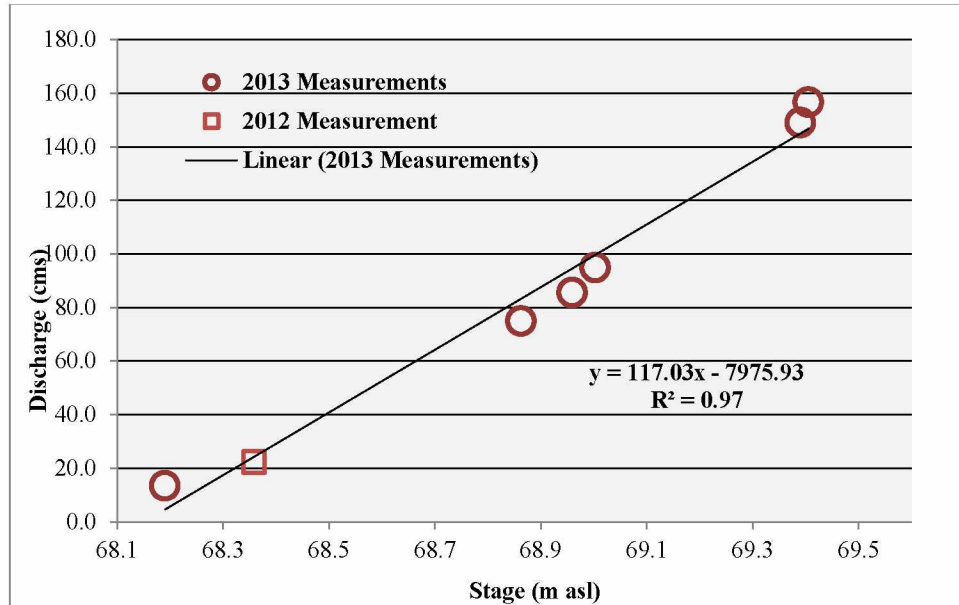
Figure 2.16: Discharge in Valdez Glacier Stream versus stage of Valdez Glacier Lake on September 15, 2012 (red square) and in 2013 (red circles). Black line is a linear least squares fit to the stage/discharge data. [Note: Stage data was evaluated at different datum for 2012 and 2013. The discharge measurement from 2012 has a corresponding stage that was corrected using the stage-discharge relationship developed from 2013.]

The rating curve calculated using 2013 stage and discharge data was re-calculated in a separate study that used 2014 stage and discharge data (E. Neal, personal communication). Therefore, we concluded that the rating curve did not change over the course of the study period, which supports the idea of a stable lake outlet (Section 2.3). We used the rating curve to correct lake stages from 2012 to the 2013 datum, assuming stable morphology of the channel and lake outlet. We adjusted the 2012 lake stage measurements to the 2013 datum by first calculating lake stage during the September 15, 2012 discharge measurement (corrected to the lake outlet), using the 2013 rating curve (Figure 2.16). Next we subtracted the calculated stage from the original measured stage, indicating that the 2012 datum was offset by 0.710 m in elevation from the 2013 datum. The offset was then used to re-calculate 2012 lake stage measurements (Figure 2.14).

2.4.3 Runoff Characterization in 2012 & 2013

Hydrographs for the 2012 and 2013 field seasons, spanned from May 31, 2012 to October 18, 2012 (Figure 2.17), and from May 26 to October 24, 2013 (Figure 2.18), respectively. Daily peak discharge is estimated at ~320 $m^3 s^{-1}$ and ~228 $m^3 s^{-1}$, for the 2012 and 2013 field seasons, respectively. Hourly peak discharge is estimated at ~355 $m^3 s^{-1}$ and ~239 $m^3 s^{-1}$, for the 2012 and 2013 field seasons, respectively. However, no discharge measurements were conducted in Valdez Glacier Stream at flows above 157 cms. Therefore, discharge estimates above 157 cms come with large uncertainty and should only be seen as a rough estimation.
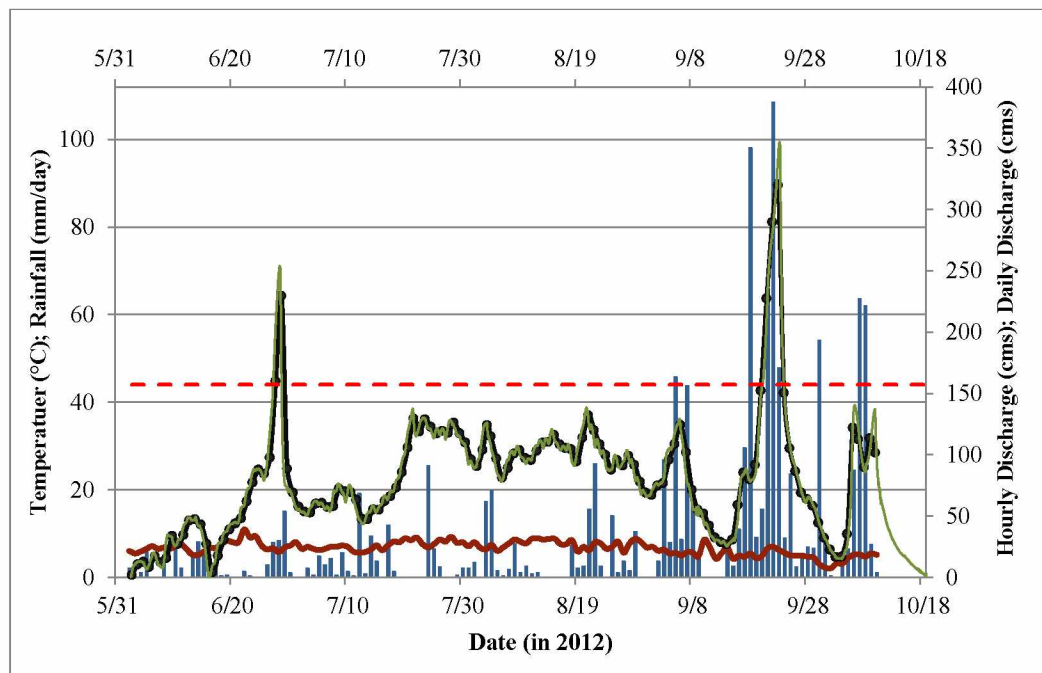
Figure 2.17: Hourly discharge (green line, right axis), daily discharge (black line with black dots, right axis), air temperature from Valdez Glacier Lake (77 m asl; red line, left axis), and precipitation from Valdez WSO (11 m asl; blue bars, left axis) during 2012. Dashed red line indicates discharge value (i.e. 157 cms) above which discharge is considered a rough estimate due to lack of high-flow measurements.
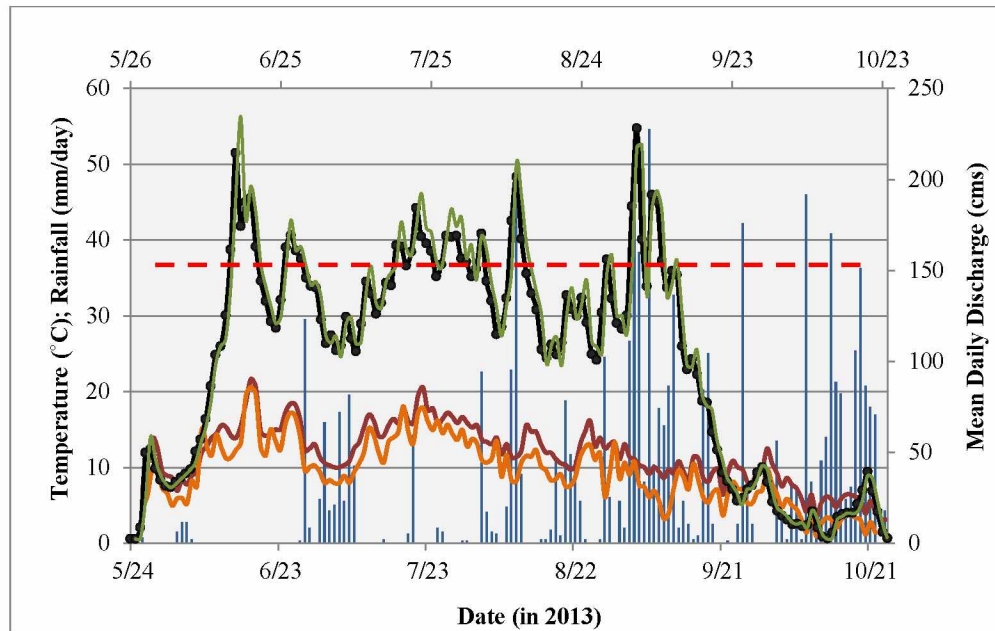
Figure 2.18: Hourly discharge (green line, right axis), daily discharge (black line with black dots, right axis), air temperature from Valdez Glacier Lake (77 m asl; red line, left axis), synthetic air temperature from S-G02 (821 m asl; orange line; left axis) calculated using 2012 daily lapse rates, and precipitation from Valdez WSO (11 m asl; blue bars, left axis) during 2013. Dashed red line indicates discharge value (i.e. 157 cms) above which discharge is considered a rough estimate due to lack of high-flow measurements.

The total specific runoff between September 13 and October 11, 2012 was 644 mm. The hydrograph covering this period shows a peak flow event on September 23 (Figure 2.17). The peak flow event is likely a response of the system to different factors, including a brief temperature increase that precedes the peak flow, as well as two heavy rainfall events, on September 17 and September 21 of 98 mm and 109 mm, respectively (Figure 2.17). The rainfall events were observed near sea level at the Valdez WSO (11 m asl). The September 17 and September 21 rainfall events equate to 182 mm and 193 mm at 1011 m asl, based on the PRISM-derived precipitation gradient (8.4 mm/100 m; Table 2.3).

The total specific runoff during 2013 was 3914 mm (May 26 – October 24, 2013). The five largest peak flow events occurred on June 16 (~237 cms), July 22 (~197 cms), August 11 (~210 cms), September 4 (~239 cms), and September 7 (~197 cms; Figure 2.18). Air temperature throughout the measurement period remained above freezing at the 11 m asl (Valdez WSO) and on-glacier at 821 m asl (location of S-G02; calculated using 2012 daily air temperature lapse rates), suggesting that glacier melt is a contributor to runoff throughout the study period. Rainfall and air temperature data give an idea about the most influential factors contributing to peak flow

events observed in the hydrograph. Based on climate data, it appears that the June 16 event is most likely a result of rapid increases in air temperature on the glacier, which produced a melt event, increasing discharge to ~237 cms (Figure 2.18). The peak on July 22 coincides with a spike in air temperature, as well as a rainfall event that occurred on July 20. The August 11 peak flow event was preceded by a rainfall event that spanned from August 9 – 11. Maximum rainfall during the event occurred on August 10 and amounted to 50.3 mm at 11 m asl, or 134.3 mm at 1011 m asl based on the PRISM-derived precipitation gradient. The peak flow events that occurred on September 4 and September 7 occur in the midst of a period of rainfall spanning August 31 - September 18. The two largest rainfall events during this time period occurred on September 3 and September 6, indicating that each of the peak flow events that occurred on September 4 and September 7 are likely a result of rainfall. The September 4 peak flow event is the largest observed in the hydrograph, and is calculated at ~228 cms.

Diurnal variation, defined as the difference between the maximum and minimum discharge measurement in a given day, varied throughout the 2012 and 2013 measurement periods (Figures 2.17 and 2.18). Diurnal streamflow variations during 2012 and 2013 were greatest at the beginning of the melt season (June) and also at the end of the melt season (September). The high early-season diurnal variations are likely attributable to increases in temperatures resulting in snowmelt. The high late-season diurnal variations are likely attributable to high rainfall. In 2012, the largest diurnal variations were observed during the peak flow event, on September 21, 22, 23, and 24, suggesting that the diurnal flow variations during the summer were highly influenced by rainfall events. Disregarding flow events above 157 cms, diurnal variation in streamflow ranged between ~0.4 and 75 cms throughout the 2012 study period. Disregarding flow events above 157 in 2013, diurnal variations ranged between 3 cms and 49 cms in June and between 1 cms and 68 cms in late-August and September. Diurnal flow variations become lowest in late September and into October, with the exception of heavy rainfall events that can occur during this time period, causing rapid stream response.

Chapter 3

Temperature-Index Modeling of Valdez Glacier Catchment

Introduction:

Models are commonly used to integrate field measurements such as glacier mass balance, meteorology and runoff in order to learn more about snowmelt, glacier melt, and rainfall runoff, and to simulate conditions outside of the existing window of field observations. Here we used the Distributed Enhanced Temperature Index Model, or DETIM, to assess glacier melt and runoff in the Valdez Glacier catchment. DETIM is a fully-distributed glacier mass balance model with the ability to a) analyze systems using a physically-based approach, and b) account for spatial and temporal variability in climate, glacier melt and storage (Hock and Tijm-Reijmer, 2012). DETIM calculates glacier ablation using a temperature-index method, which uses air temperature as a proxy for melt energetics, by summing melt over the glacier area at each timestep. DETIM calculates melt according to the following equation:

$$M = \left(MF + r_{\frac{snow}{ice}} \times DIRECT\right) \times T, \qquad (3.1)$$

where M is melt, MF is melt factor, $r_{\frac{snow}{ice}}$ is radiation coefficient for snow or ice, DIRECT is direct radiation, and T is temperature.

The model estimates glacier runoff using a linear reservoir approach, which assigns storage parameters to each of four units: rock, snow, ice and firn. The rock unit is defined as non-glacierized areas containing bare rock at the surface. Non-glacierized regions that become snow-covered are part of the snow unit. The snow unit incudes regions on- or off-glacier that are snow-covered and located outside of the firn area. The firn unit includes regions within the firn area. The ice unit includes areas of exposed ice located outside of the firn region (Hock and Tijm-Reijmer, 2012). Runoff from each unit includes direct rainfall runoff from the unit. We defined glacier runoff to include water derived from glacier meltwater (snow, ice and firn), and rainfall runoff from within the glacier boundary. Runoff from non-glacierized portions of the watershed are routed through the rock reservoir or snow reservoir, depending upon snow coverage. Calculated total discharge is the sum of runoff derived from all four units, and includes runoff from both glacierized and non-glacierized regions. Runoff is calculated for each reservoir (snow, ice, firn and rock) at each time step (one day; Hock and Tijm-Reijmer, 2012). The model is equipped with batch processing capabilities that enable multiple simulations to run consecutively,

while altering multiple input parameters, thereby allowing for efficient calibration of both the glacier melt and runoff routines.

DETIM requires inputs that include: 1) a digital elevation model (DEM), which allows for calculation of slope, aspect and radiation; 2) glacier coverage, including a distinction between firn and ice; 3) watershed boundary; 4) air temperature and precipitation data and the associated lapse rates; 5) a map of snow depth for model initialization; and 6) glacier mass balance and mean daily discharge for calibration. We first calibrated the glacier melt model to glacier melt data from ablation stakes on Valdez Glacier (Table 2.6; Figure 2.10), according to methods described by Young (2013), to obtain a total summer 2012 glacier mass balance. We calibrated the model using measured glacier mass balance by varying three parameters: a) melt factor, which describes the amount of melt at the glacier surface per day per degree Kelvin; b) snow radiation coefficient, which describes the volume of melt at the snow surface per Watt of direct radiation received per day per degree Kelvin; and, c) ice radiation coefficient, which describes the volume of melt occurring at the ice surface per Watt of direct radiation received per day per degree Kelvin. We began our melt parameter calibration by varying melt factor and radiation coefficients for snow and ice over a broad range of values using the batch routine. Next, we selected parameter sets that produced melt values with the highest R^2 and lowest root mean square error (RMSE) when compared to our ablation stake measurements. We then fine-tuned the selected parameter sets. We ranked our fine-tuning results based first on lowest RMSE, followed by highest R^2. Once calibrated to 2012 stake data, we used the modeled summer glacier-wide mass balance and estimated winter glacier mass balance (Section 2.2.1) to calculate annual glacier mass balance. In addition, we used the best parameter set determined from the 2012 calibration to model summer 2013 glacier mass balance, which we added to our winter 2013 glacier mass balance (Section 2.2.1) to obtain annual 2013 glacier mass balance. We then validated our annual 2013 glacier mass balance estimate on laser altimetry measurements.

After the melt model was calibrated, we used the batch routine to calibrate the runoff model to measured daily streamflow in Valdez Glacier Stream by varying storage constants for snow, firn and ice. Storage constants for snow, firn and ice represent a holding time that controls the speed at which runoff flows through each reservoir. The results were used to select the best runoff parameter sets (i.e. storage constants for snow, firn and ice) for the Valdez Glacier catchment, based on calculations of Nashe-Sutcliffe efficiency (E), as well as modified Nashe-Sutcliffe efficiency (lnE; Krause et al., 2005).

3.1 Elevation Data, Watershed Delineation, and Glacier Outlines

We used a SPOT 2007 digital elevation model (DEM) at a 30 m resolution (Korona et al., 2009) for all data formatting and melt and runoff modeling with DETIM. We delineated the drainage area contributing to the outlet of Valdez Glacier Lake by loading the SPOT 2007 DEM into ArcGIS and calculating the watershed using tools from the ArcGIS hydrology toolbox. The pour point for the watershed delineation was placed at the Valdez Glacier Lake outlet, where ADCP measurements were performed in 2013, in order to compare modeled runoff to measured streamflow.

We used the delineated watershed outline to select glacier outlines from the Randolph Glacier Inventory. The RGI is a collection of digital glacier outlines created using imagery acquired on July 3, 2009 by Landsat 7 ETM+ to create outlines (Pfeffer et al., 2014). Glaciers within the watershed include Valdez Glacier (147 km^2) and several other small, hanging glaciers (52 km^2 in total), including an unnamed former tributary to Valdez Glacier and Camicia Glacier.

3.2 Forcing Datasets: Valdez WSO Air Temperature & Precipitation

The model calculates melt of snow, firn and ice based on air temperature. We used input air temperature and precipitation data from the Valdez WSO (11 m asl) to force model simulations. However, we first created a synthetic air temperature time-series by correcting WSO air temperatures to the Valdez Glacier Lake air temperature sensor location (77 m asl).

3.2.1 Air Temperature Corrections

Air temperature from the Valdez WSO does not represent conditions in the watershed. The WSO, located less than a mile inland and at 11 m asl, is likely more significantly influenced by PWS than are sensors we installed within the watershed boundary (S-G01-03, Prospector, Schrader and VGL), which are located a minimum of seven miles from PWS (the distance to Valdez Glacier Lake) and at 77 m asl (Table 2.1; Figure 2.1). It is also likely that down-glacier winds create an air temperature regime that is considerably different in the proglacial valley than in the town of Valdez, where the WSO is located. We investigated these potential biases by comparing air temperature data measured at VGL to the WSO data. The VGL sensor recorded air temperature from July 4 until October 10, 2012 (Table 2.1), whereas the model calibration period extends from the date of GPR measurement to the date of ablation stake measurement (March 29 to October 11, 2012). We conducted a linear regression analysis of air temperature data from the

Valdez WSO and VGL (Figure 3.1). We then used the linear relationship to extend the VGL series to cover the entire 2012 model calibration period (Figure 3.2).
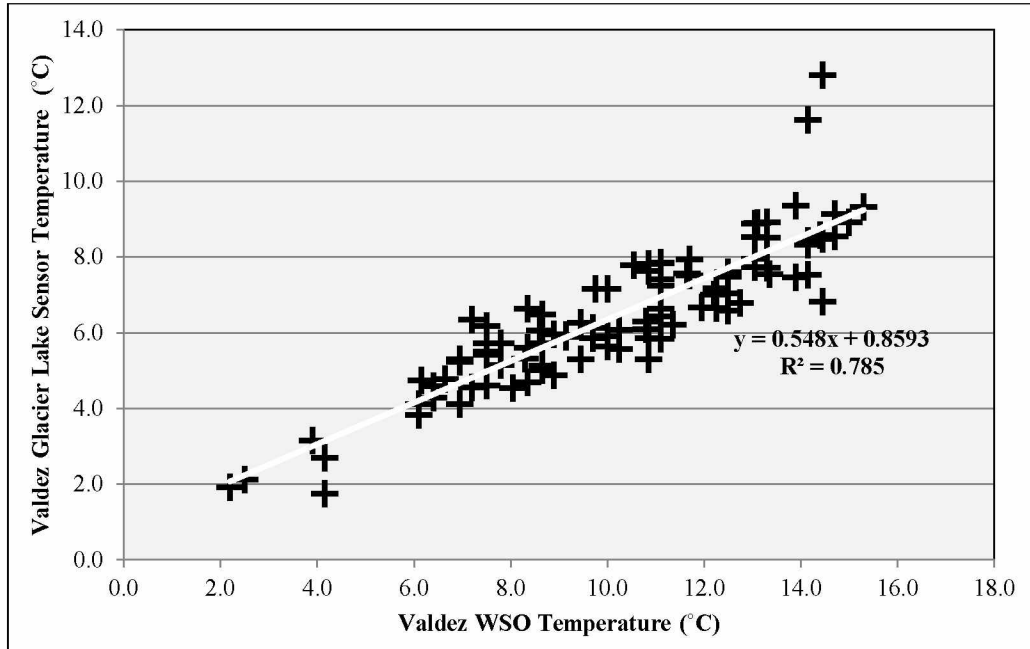
Figure 3.1: Linear regression of VGL (77 m asl) and Valdez WSO (11 m asl) air temperature.
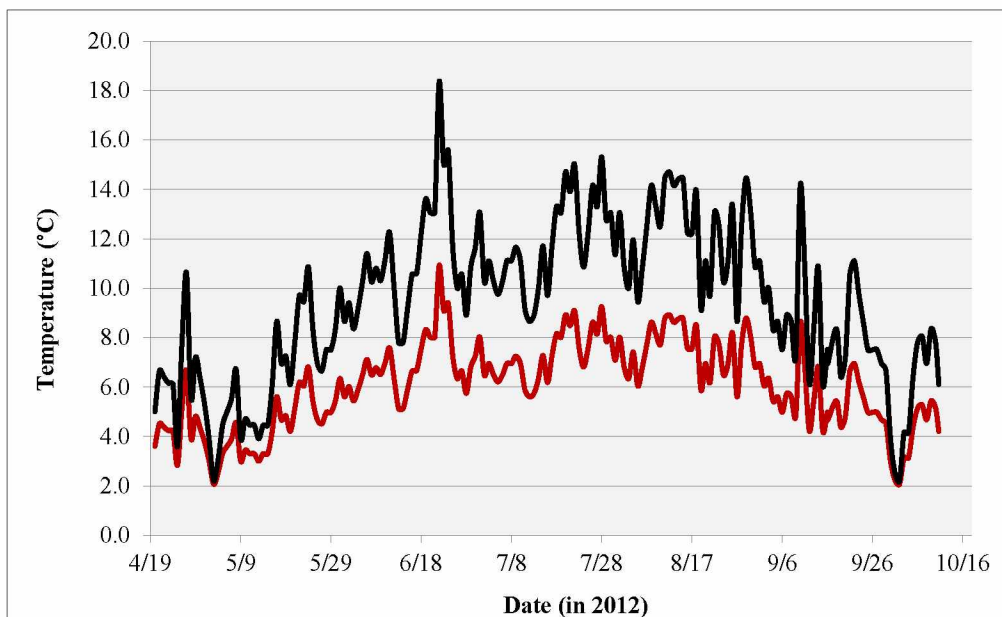
Figure 3.2: Valdez WSO (11 m asl; black line) and VGL(77 m asl) daily air temperature measurements during summer 2012. The VGL daily air temperature time series was used in 2012 model simulations.

We assumed that the same linear regression equation produced by the 2012 air temperature data at VGL and Valdez WSO was applicable to the 2013 simulation period. We used the linear regression equation to create a synthetic daily air temperature times series at Valdez Glacier Lake (77 m asl), which spanned from January 1, 2013 to December 16, 2013 (Figure 3.3). We then used the synthetic daily air temperature time series to force model simulations.
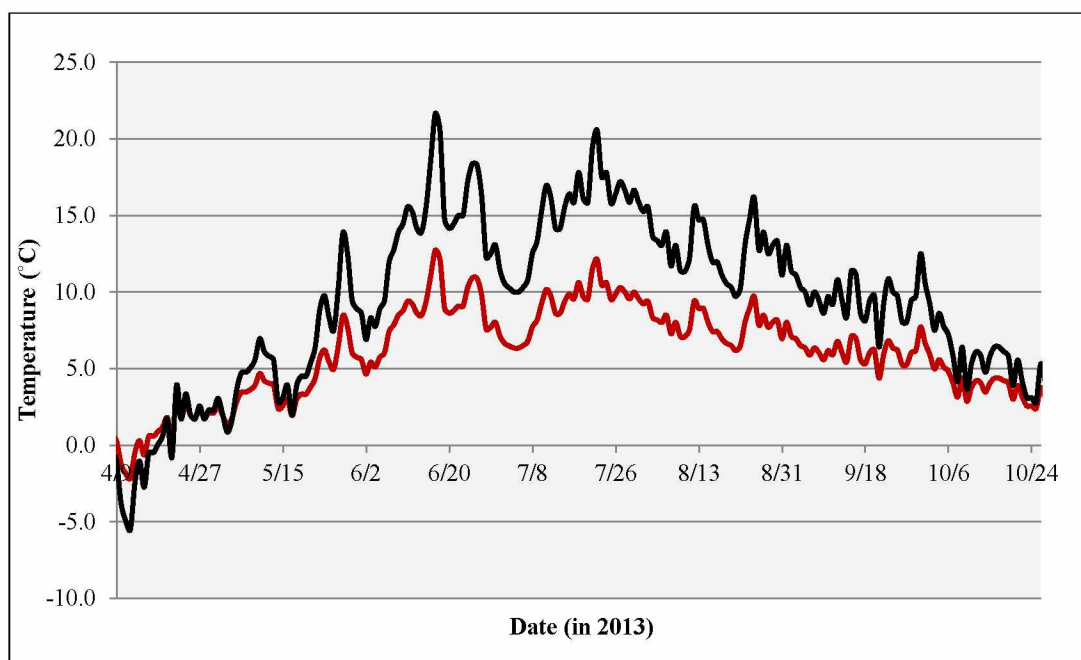
Figure 3.3: Valdez WSO (11 m asl; black line) daily air temperature measurements during summer 2013 and synthetic daily air temperature (77 m asl; red line). The synthetic air temperature dataset was re-calculated using a linear regression equation from 2012 Valdez Glacier Lake (77 m asl) and Valdez WSO (11 m asl) air temperature data (Figure 3.1).

Air temperature lapse rates on the glacier were calculated using S-G01 (278 m asl) and S-G03 (1248 m asl) sensors. Therefore, corrections to forcing temperature datasets from the WSO did not affect lapse rate calculations. We tested the sensitivity of the model to lapse rate by first using average monthly lapse rates derived from on-glacier air temperature data (Table 2.2), then using average daily lapse rates derived from the same on-glacier air temperature data (Figure 2.3). The model proved sensitive to the temporal resolution of air temperature lapse rates. We therefore used daily lapse rates in order to capture the day-to-day variations of modeled glacier melt. Average monthly lapse rates from PRISM were used to fill gaps in our observed air

temperature data (March 29 - April 19, 2012 and September 16 - October 11, 2012) to produce a time series spanning the entire simulation period (March 29 – October 11, 2012 and April 9 – October 24, 2013).

3.2.2 Precipitation Time Series

Prospector and Schrader stations provided poor precipitation information. Therefore, we relied on Valdez WSO daily snowfall and rainfall data for the daily precipitation time series, and on PRISM for the precipitation gradient. The model accepts one average precipitation gradient for the simulation period, which we calculated to 8.4 mm/100 m from the PRISM monthly normal data. We assess the error associated with the adoption of the average precipitation lapse rate in section 4.1.2.

3.3 Glacier Melt Modeling

3.3.1 Glacier Melt Model Calibration to 2012 Data & Results

The model was first calibrated on glacier mass balance only. The first round of batch simulations consisted of 567 simulations where the MF varied from 2 to 8 and $r_{\frac{snow}{ice}}$ varied between 0.1 and 1.0 (Figure 3.4). The initial calibration step suggested that the model performed best (i.e. RMSE was lowest) with a MF between 1 and 5. The model performed best when high MFs in this range (i.e. 4.0 to 5.0; Figure 3.4) were paired with low r_{snow} and r_{ice} values (0.1 to 0.5; Figure 3.4), or when low MFs (1.0 to 3.0) were paired with high r_{snow}- and r_{ice}- values (0.6 to 0.9; Figure 3.4).
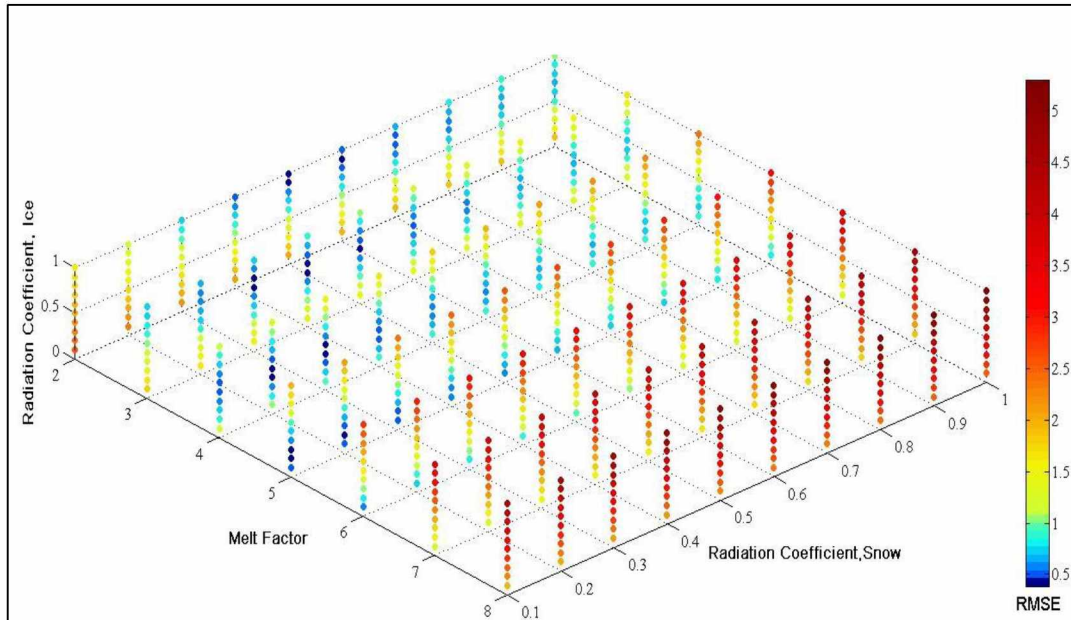
Figure 3.4: RMSE associated with glacier melt model parameter sets as determined from initial step in melt model calibration. Radiation coefficients (r_{snow}, r_{ice}) and melt factors (MF) are independent variables in the parameter space. Dark blue dots indicate lowest (i.e. best) RMSE values. The best parameter set for this the glacier melt model, based on 2012 data, included an MF of 4.0 mm d^{-1} K^{-1}, r_{ice} of 0.50 mm m^2 W^{-1}d^{-1}, and r_{snow} of 0.20 mm m^2 W^{-1}d^{-1}.

The second step in the calibration included selecting more constrained parameter values, e.g. those that produced RMSE <0.40. We more narrowly focused on parameter sets by varying MF between 4.0 and 4.9, r_{ice} between 0.50 and 0.59, and r_{snow} between 0.20 and 0.29. The second round of more narrowly-focused model simulations produced five parameter sets with an R^2 of 0.95 and RMSE within one percent of the best parameter set (Table 3.1).

Table 3.1: The top five best parameter sets, based on lowest RMSE and highest R^2, from the 2012 glacier melt model calibration are observed. The top five best sets all produced the same R^2 and also produced RMSE within 1% of the lowest observed.

	RMSE	R^2	Melt Factor	r_{ICE}	r_{SNOW}
1	0.3865	0.95	4.0	0.50	0.20
2	0.3877	0.95	4.0	0.50	0.21
3	0.3893	0.95	4.0	0.51	0.20
4	0.3894	0.95	4.0	0.50	0.22
5	0.3913	0.95	4.0	0.51	0.21

The best parameter set included a melt factor of 4.0 mm d^{-1} K^{-1}, and radiation coefficients of 0.50 and 0.20 mm m^2 W^{-1}d^{-1} K^{-1}, for ice and snow, respectively (Table 3.1). This parameter set resulted in a modeled summer glacier mass balance (B_s) equal to -0.64 m. w.eq., which combined with our winter glacier mass balance estimate (B_w = 1.90 m. w.eq.) yields an annual glacier mass balance (B_a) equal to 1.26 ± 0.49 m w.eq. for the 2012 balance year (Table 3.2).

Table 3.2: Summary of melt model summer glacier mass balances, GPR winter glacier mass balances, and altimetry-derived annual glacier mass balances. [Column 1: mass balance period name; Column 2: time frame over which the modeled/measured glacier mass balance is applicable. ("Onset" refers to date within year at which air temperatures were consistently below 0°C for most of the catchment, which varies from year to year); Column 3: method of glacier mass balance estimation; Column 4: glacier mass balance.]

2012			
	Time Frame	Measurement Method	Mass Balance (m w. eq.)
Summer Balance	March 29, 2012 – October 11, 2012	Modeled	-0.64
	March 29, 2012 – August 29, 2012	Modeled	-1.85
Winter Balance	Onset winter, 2011 – March 29, 2012	GPR	1.90
Annual Balance	Onset winter 2011 – October 11, 2012	Modeled melt + GPR snow accumulation	1.26 ± 0.49
	Onset winter 2011 – August 29, 2012	Modeled melt + GPR snow accumulation	0.05 ± 0.49
	August 29, 2011 – August 29, 2012	Laser Altimetry	0.20 ± 0.6
2013*			
	Time Frame	Measurement Method	Mass Balance (m w. eq.)
Summer Balance	April 9, 2013 – October 24, 2013	Modeled	-2.08
	April 9, 2013 – August 29, 2013	Modeled	-2.72
Winter Balance	Onset winter, 2012 – March 15, 2013	GPR	1.62
Annual Balance	Onset winter 2012 – October 24, 2013	Modeled melt + GPR snow accumulation	-0.46 ± 0.49
	Onset winter 2012 – August 29, 2013	Modeled melt + GPR snow accumulation	-1.10 ± 0.49
	August 29, 2012 – August 29, 2013	Laser Altimetry	-1.15+0.29/-0.30

*Note: 2013 balance summary portion of the table is based on a melt factor of 7.0 mm d^{-1} K^{-1}.

3.3.2 Glacier Mass Balance in 2013

No glacier mass balance stake measurements were available for 2013. We therefore used altimetry and GPR measurements to validate the model on the 2013 melt season. We adjusted our model simulation dates to the April 9 to August 29, 2013 period in order to test the 2013 glacier mass balance simulations to altimetry measurements. The glacier-wide summer mass balance for 2013 (B_s = -1.07 m w.eq) was then added to the calculated 2012-2013 winter glacier mass balance (B_w = 1.62 m w.eq.; Section 2.2.1), resulting in an annual glacier mass balance of (B_a) 0.55 ± 0.49 m w.eq for hydrologic year 2012-2013. Our annual glacier mass balance estimate for the 2012-2013 hydrologic year fell outside the margin of error of the laser altimetry estimate (B_a = -1.15 +0.29/-0.30). The results suggest that either: 1) the winter balance calculation using our linear extrapolation method overestimated snow depth, 2) altimetry measurements contained a systematic error that is overestimating melt, 3) and/or the melt model parameters calibrated to 2012 data do not apply to 2013.

Our method for calculating SWE may have overestimated winter glacier balance in 2013. We tested the effect of SWE overestimation on annual glacier mass balance by re-calculating winter glacier mass balance using snow density and SWE up-scaling factors from McGrath et al. (in preparation). First, we re-calculated winter glacier mass balance by increasing SWE by 32% (as in McGrath et al. (in preparation)), and using our measured snow pit-derived density from 2012 (ρ = 0.36 g cm^{-3}). We estimated B_w = 1.44 m w.eq. and B_s = -1.07 m w.eq., yielding B_a = 0.37 ± 0.49 m. w.eq. using the McGrath up-scaling factor (Table 3.3, row 1).

Table 3.3: Winter glacier mass balance estimates calculated by varying snow densities and 2013 end-of-season scaling factor. [Column 1: 2013 adjustment type (density and/or correction factor of GPR SWE to end-of-season SWE); Column 2: snow density used in SWE calculations; Column 3: correction factor used to up-scale GPR-derived SWE to end-of-season maximum SWE; Column 4: adjusted winter glacier mass balance; Column 5: 2013 modeled-summer glacier mass balance using a melt factor of 4.0; Column 6: modeled annual glacier mass balance using adjusted winter balances.]

Winter Balance Adjustment Type	Density (g cm^{-3})	Up-Scaling Factor	B_w (m w.eq.)	B_s (m w.eq.)	B_a (m w.eq.)
Up-scaling Factor	0.36	32%	1.44	-1.07	0.37± 0.49
Snow Density	0.33	61%	1.40	-1.07	0.33 ± 0.49
Up-scaling Factor & Density	0.33	32%	1.15	-1.07	0.08 ± 0.49
McGrath et al. (IFSAR DEM, 5 m resolution; multivariate regression)	0.33	32%	2.60	-1.07	1.53 ± 0.49

We calculated winter glacier mass balance at B_w = 1.40 m w.eq. and B_s = -1.07 m w.eq., yielding B_a = 0.33 ± 0.49 w.eq. using snow density reported by McGrath et al. (ρ = 0.33 g cm^{-3}) and maintaining our SWE scaling factor (61% increase; Table 3.3, row 2). Finally, we calculated B_w = 1.15 m w.eq. and B_s = -1.07 m w.eq., yielding B_a = 0.08 ± 0.49 w.eq. using both density and up-scaling factor from McGrath et al. (in preparation) with the SPOT 2007 DEM (Table 3.3, row 3).

McGrath et al. used an IFSAR DEM at a 5-meter resolution to calculate winter glacier mass balance. Therefore, the McGrath et al. 2013 winter glacier mass balance differed from our calculation using the same density (ρ = 0.33 g cm^{-3}) and up-scaling factor (increase by 32%) with the SPOT 2007 DEM at a 30-meter resolution. Assuming that and multivariate regression analysis method using the IFSAR DEM more accurately depicts winter glacier mass balance in 2013, we find that by adopting the McGrath et al. winter balance (B_w = 2.60 m w. eq.), the 2012-2013 annual glacier mass balance is still positive (B_a = 1.53 m w.eq.; Table 3.3, row 4). The results indicate that the parameter set from the 2012 glacier melt model calibration does not calculate enough melt in 2013 to arrive at a realistic (i.e. negative) mass balance for the year.

3.4 Model Validation & Adjustment using Laser Altimetry

3.4.1 Laser Altimetry

Annual balance estimations calculated from our modeled summer and winter balance estimates are validated against annual balances observed by airborne laser altimetry

measurements. Laser altimetry is a method often used in geodetic glacier mass balance calculations (Echelmeyer et al., 1996; Arendt et al., 2002; Johnson et al., 2011), and is conducted by attaching a single-track (profiler) or sweeping laser (scanner) to an aircraft, which sends pulses to points along the glacier centerline, or within a swath area (in the case of the scanner), returning a measured distance to the ice surface from the aircraft (Johnson et al., 2011). By tracking the motion of the aircraft, the glacier surface elevation is then calculated. By performing the airborne laser altimetry measurements on the same day in two consecutive years, elevation changes can be calculated from the two datasets. Using a simple calculation with estimations of ice and snow density estimations, the annual glacier mass balance is calculated based on the measured difference in glacier thickness. The UAF altimetry group conducted measurements on Valdez Glacier, which extend from August 29 to August 29 of each year, for the years 2000, 2001, 2004, 2011, 2012 and 2013. To validate our model simulations for 2012 and 2013, we aligned our simulation period with these altimetry measurement periods.

3.4.2 Model Validation for 2012

We used the best parameter sets determined by our 2012 model calibration, and adjusted the simulation period to overlap with laser altimetry, to produce a B_s = -1.85 m w.eq, which with the GPR-derived winter glacier mass balance (B_w = 1.90 m. w.eq.), yields B_a = 0.05 m. w.eq for hydrologic year 2011-2012. The UAF laser altimetry group estimated annual mass balance for Valdez Glacier at 0.20 ± 0.6 m w.eq. (Table 3.2). Thus, we find that by using the best parameter set from the 2012 calibration results, our modeled glacier-wide annual balance falls within the margin of error of the altimetry-derived annual glacier mass balance estimates for Valdez Glacier.

3.4.3 Melt Factor Adjustment for 2013

The laser altimetry measurements for Valdez Glacier assume a constant vertical density profile (i.e. density of ice, 0.90 g cm^{-3}) on the glacier (Johnson et al., 2011), which can lead to a large error in glacier mass balance estimations on short time scales. Moreover, Sorge's Law, which governs the assumption of constant density, is least valid during high accumulation years when new snow and firn layers have a lower density than ice (Bader, 1954). Therefore, we used the laser altimetry annual glacier mass balance estimates to calibrate the model.

We calibrated the MF parameter in an attempt to minimize misfit between our modeled 2013 annual glacier mass balance (B_a = 0.55 m w.eq.) and the altimetry estimate (B_a = -1.15

+0.29/-0.30 m w.eq.). We assumed that r_{snow} and r_{ice} do not significantly change from one year to the next, and therefore, we only calibrated the melt factor (Table 3.4). Results of the melt factor adjustment indicated that a melt factor of 6.0 or 7.0 mm d^{-1} K^{-1} produces the closest fit to altimetry data, producing B$_a$ = -0.54 m w.eq. and B$_a$ = -1.10 m w.eq., respectively (Table 3.4).

Table 3.4: Modeled annual glacier mass balance extending from October 11, 2012 until August 29, 2013 for comparison with altimetry data. By adjusting melt factor in the 2013 model simulations, glacier-wide annual mass balance becomes closer to the laser altimetry-derived mass balance. At a melt factor of 7.0, the glacier-wide annual mass balance generated by the model is within the margin of error determined by altimetry. The winter glacier mass balance used in all annual glacier mass balance calculations is calculated from the GPR-derived SWE (i.e. 1.62 m w.eq.; Section 2.2.1)

DETIM ANNUAL GLACIER MASS BALANCE (October 11, 2012 – August 29, 2013)				
Melt Factor (mm d^{-1} K^{-1})	4.0	5.0	6.0	7.0
Summer Mass Balance from DETIM (m. w.eq.)	-1.07	-1.61	-2.16	-2.72
Annual Balance (m w.eq.)	0.55 ± 0.49	0.01 ± 0.49	-0.54 ± 0.49	-1.10 ± 0.49
ALTIMETRY ANNUAL BALANCE (August 29, 2012 – August 29, 2013)				
UAF Altimetry Group Measurements (m. w. eq.)	-1.15 +0.29/-0.30			

Melt factor influences runoff calculations. Therefore, results of the melt factor calibration were considered when we calibrated storage constants in the runoff model. We calibrated the storage constants, first with MF set to 4.0, then with MF set to 7.0. The fit of the modeled-hydrographs to measured streamflow using the two MFs allowed us to investigate the most appropriate melt factor to use for 2013 melt simulation (Section 3.5.2).

3.5 Glacier Runoff Model Calibration

DETIM calculates runoff by summing rainfall and melt generation at all grid cells at each time step over the defined drainage area. Grid cells are assigned to one of four reservoirs (snow, firn, ice and rock). Each reservoir is assigned its own storage constant, which represents the flow of water from the reservoir to the basin outlet. The melt and rainfall from each grid cell is summed for each of the four reservoirs, and the totals are combined to produce discharge per timestep.

The runoff sub-model requires optimization of storage constants for the ice, firn, and snow by comparing modeled to measured mean daily discharge. To optimize the runoff parameters to 2012 and 2013 discharge measurements, we set the glacier melt model parameters (MF, r_{snow} and r_{ice}) to those obtained in the 2012 calibration. We then used the batch routine to run 729 different simulations for each year, varying snow-, firn-, and ice- storage constants (k_s, k_f, and k_i) between 100 and 900 in increments of 100. We compared the simulated mean daily runoff to the measured discharge by calculating the Nash-Sutcliffe Efficiency (E) and the modified Nash-Sutcliffe efficiency (lnE) (Krause et al., 2005). The Nash-Sutcliffe efficiency is calculated using the following equation:

$$E = 1 - \frac{\sum_{i=1}^{n}(O_i - P_i)^2}{\sum_{i=1}^{n}(O_i - \bar{O})^2},\qquad (3.2)$$

where O and P are observed and predicted mean daily streamflow values. Nash-Sutcliffe efficiency is a similar calculation to R^2, but is more commonly used to evaluate simulated and measured-hydrographs. The major issue associated with the sole use of E to evaluate model accuracy to measured flow is that E does not account for systematic error in model output. Instead, it is most sensitive to closeness of modeled peak flow to measured peak flow (Krause et. al, 2005).

The modified Nash-Sutcliffe efficiency is calculated using the following equation:

$$lnE = 1 - \frac{\sum_{i=1}^{n}(ln(O_i) - ln(P_i))^2}{\sum_{i=1}^{n}(ln(O_i) - ln(\bar{O}))^2},\qquad (3.3)$$

where, again, O and P are observed and predicted discharge. The modified form of the Nash-Sutcliffe efficiency equation effectively reduces the influence of peak flows on overall model efficiency, thereby placing more emphasis on the influence of base flows and low flows, and accounting for systematic error associated with model output (Krause et. al, 2005). We performed the Nash-Sutcliffe and modified Nash-Sutcliffe calculations using flows between 1 and 157 cms, because calculated flows above 157 cms are considered rough estimates. It is beneficial to utilize a statistical analysis that minimizes the influence of peak flows on how well modeled discharge fits to measured discharge curves. Therefore, the modified Nash-Sutcliffe equation is used as one of our primary metrics for model performance. In addition, because this project aims to assess the potential for hazards associated with peak discharge events, we also consider E as a measure of the model's ability to simulate peak flow.

3.5.1 Runoff Modeling, 2012

The runoff parameter set with the highest lnE was that in which the k_s, k_f, and k_i were 100, 100, and 100, respectively (Figure 3.5; Table 3.5), while the parameter set producing the highest E was that in which the k_s, k_f, and k_i were 100, 200 and 900, respectively (Figure 3.5; Table 3.5). The greatest lnE and E-values for the 2012 runoff simulations were 0.76 and 0.54 (Table 3.5). The hydrograph with the highest E indicates the best fit of modeled to measured peak flows, while the hydrograph with the highest lnE indicates the best fit of the modeled to measured low-flows.

Figure 3.5: Comparison of two simulations of mean daily discharge obtained by varying storage constants for snow, firn and ice (k_s, k_f, k_i), against measured discharge (red line) in 2012. Solid blue line is discharge from simulation with best E (k_s, k_f, and k_i = 100, 200 and 900) and dashed blue line is discharge from simulation with best lnE (k_s, k_f, and k_i = 100, 100, and 100).

Table 3.5: Summary of best storage constant parameter sets from each batch simulation in 2012 and 2013. [Column 1: batch simulation ID; Column 2: storage constants for snow, firn and ice (k_s, k_f, and k_i); Column 3: lnE associated with the simulation; Column 4: E associated with each simulation. Highest lnE and E values are highlighted in bold font.]

Batch Simulation	k_s, k_f, k_i	*lnE*	*E*
2012 (Melt Factor = 4.0)	100, 100, 100	*0.76*	0.38
	100, 200, 900	0.64	*0.54*
2013 (Melt Factor = 4.0)	200, 100, 100	*0.70*	0.74
	200, 400, 200	0.64	*0.79*
2013 (Melt Factor = 7.0)	400, 100, 100	*0.54*	0.17
	900, 100, 900	0.39	*0.44*

Specific runoff from model simulations matched well to measured runoff. Using runoff parameters from the simulation with the best E (k_s, k_f, k_i = 100, 200, 900), total specific runoff was calculated at 630 mm (September 15 – October 11, 2012), which was an underestimate of measured specific runoff (644 mm) by 2.2% (Table 3.6, line 1). Using runoff parameters from the simulation with the best lnE (k_s, k_f, k_i = 100, 100, 100), modeled specific runoff was calculated at 645 mm, which was an overestimate of total measured specific runoff by 0.11% (Table 3.6; line 2).

Table 3.6: Summary of measured versus modeled specific runoff calculated from 2012 and 2013 simulations. [Column 1: batch simulation ID; Column 2: storage constants for snow, firn and ice (k_s, k_f, and k_i); Column 3: modeled specific runoff associated with each parameter set; Column 4: measured specific runoff; Column 5: percent error of modeled to measured specific runoff.]

Batch Simulation	Best k_s, k_f, k_i	Modeled Specific Runoff (mm)	Measured Specific Runoff (mm)	% Error from Measured Runoff
2012 (Melt Factor = 4.0)	100, 200, 900	630	644	-2.2%
	100, 100, 100	645		0.11%
2013 (Melt Factor = 4.0)	200, 100, 100	4076	3914	4.1%
	200, 400, 200	4058		3.7%
2013 (Melt Factor = 7.0)	400, 100, 100	5131		31%
	900, 100, 900	4789		22%

We analyzed the hydrograph resulting from the simulation producing the closest total modeled specific runoff to measured specific runoff (best *lnE*; k_s, k_f, k_i = 100, 100, 100) to determine which linear reservoir type generated the greatest total discharge volume. We observed that runoff from the snow reservoir was the largest contributor to total runoff over the entire 2012 simulation period, contributing 57% (359 mm) of the total specific runoff (Figure 3.6; Table 3.7). Runoff from snow dominated during the peak flow event in 2012, producing 52% (207 mm) of the total runoff (395 mm) from September 18 to September 26. The other reservoir units, including runoff from areas of firn, ice and rock, contributed 12%, 17% and 19%, respectively, of the total specific runoff to the peak flow event (Table 3.7).
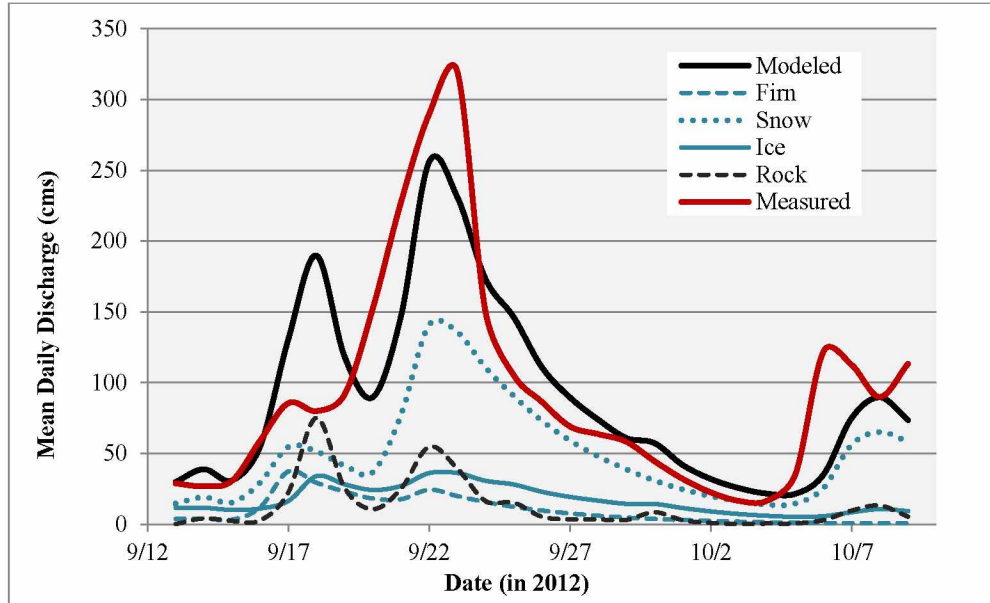
Figure 3.6: Modeled daily discharge from runoff model reservoirs (i.e. snow, firn, ice, and rock; blue and black lines) and measured discharge (red line) during 2012. Solid black line is modeled discharge from all reservoirs; dashed blue line is runoff from the firn reservoir; dotted blue line is runoff from the snow reservoir; solid blue line is runoff from the ice reservoir; and dashed black line is runoff from the rock reservoir.

Table 3.7: Total modeled specific runoff from runoff model reservoirs (i.e. snow, firn, ice and rock) during fall 2012. [Column 1: reservoir unit; Column 2: total modeled specific runoff; Column 3: percent of total modeled specific runoff from reservoir; Column 4: percent of modeled specific runoff from each unit during the peak flow event (September 23), which generated total runoff of 395 mm.]

Reservoir	Total Specific Runoff from Unit, 2012 (mm)	% of Total Modeled Specific Runoff	% of Total Specific Runoff from Peak Flow Event
Snow	346	55%	52%
Firn	69	10%	12%
Ice	120	19%	17%
Rock	88	14%	19%

3.5.2 Runoff Modeling, 2013

The 2013 runoff modeling portion of the study was aimed at determining if the best runoff storage constants for snow, firn and ice identified for 2012 can be applied in 2013 simulations to produce the most statistically accurate hydrographs. We also aimed to determine if runoff can be used to calibrate melt factor. The study was broken into two different steps: 1) calibrating the runoff sub-model by tuning the snow, firn and ice storage constants (k_s, k_f, and k_i) to measured 2013 discharge data, using glacier melt parameters from the 2012 melt model calibration (MF, r_{snow} and r_{ice} = 4.0, 0.20, and 0.50); and 2) calibrating the runoff sub-model to 2013 discharge data using a MF of 7.0. The purpose of the first step was to determine if the best runoff parameter sets for 2013 were the same as those obtained in the 2012 runoff model calibration. The purpose of the second step was to determine if using an MF of 7.0 would produce the same best runoff parameter set and give a better fit to 2013 discharge.

3.5.2.1 Calibration of Runoff Parameters to 2013 Data using 2012 Melt Parameters

We used the 2012-calibrated glacier mass balance parameters (MF, r_{snow} and r_{ice} = 4.0, 0.20, and 0.50) to perform the first part of the 2013 runoff analysis, while varying k_s, k_f, and k_i between 100 and 900 in intervals of 100. Even though applying the calibrated melt parameters from the 2012 to 2013 produced a glacier-wide mass balance outside the margin of error of laser altimetry estimates, we still ran a batch simulation using the calibrated 2012 melt parameters in order to determine if they could produce a runoff hydrograph similar to the observed 2013

discharge. Results showed that the highest values of *lnE* (0.70) and *E* (0.79) were those with k_s, k_f, and k_i of 200-100-100 and 200-400-200, respectively (Figure 3.7; Table 3.5).
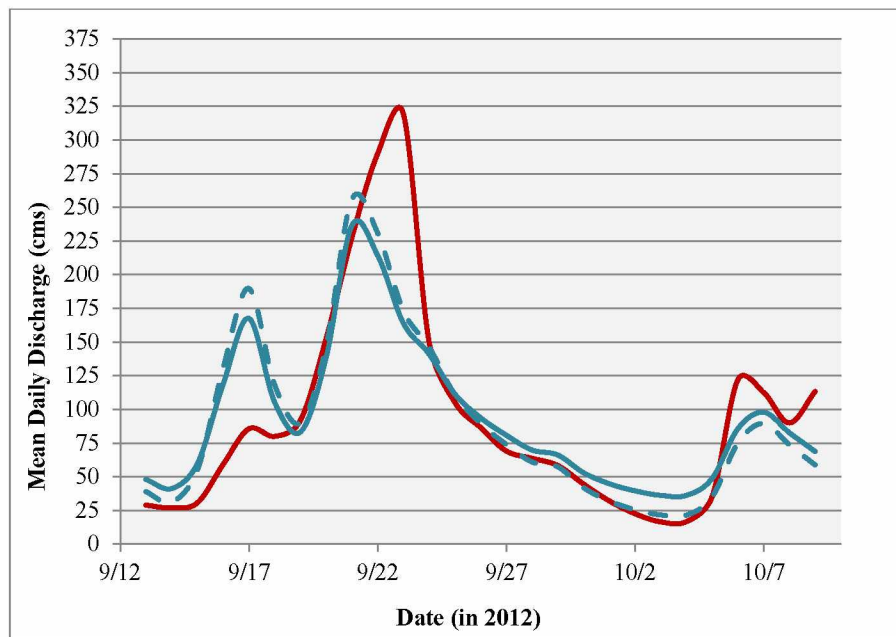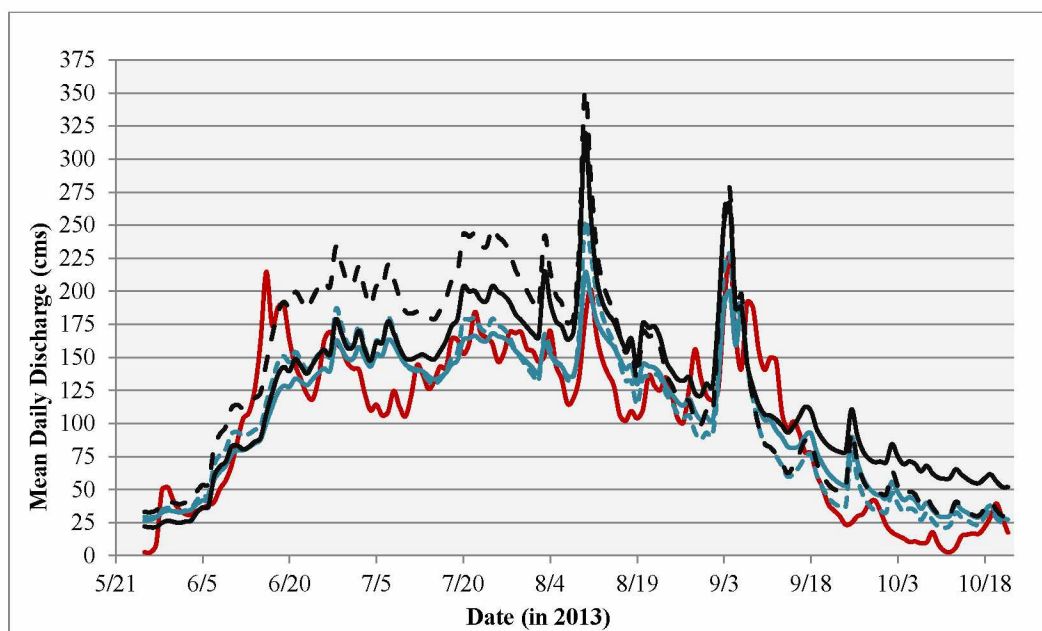

Figure 3.7: Comparison of best 2013 simulations of mean daily discharge (cms), obtained by varying storage constants for snow, firn and ice (k_s, k_f, k_i), and melt factor (MF; Table 3.6, rows 3-6). Results are plotted with measured discharge in 2013 (solid red line). Simulations with highest *lnE* are plotted with dashed lines, while highest *E* are plotted with solid lines (blue for MF = 4.0 and black for MF = 7.0).

The best parameter sets for 2012 did not match those for 2013, indicating that storage constants associated with snow, firn and ice vary from year to year (Table 3.5). The highest *E*-value for 2012 was 0.54, while the highest *E*-value for 2013 was 0.79 (Table 3.5). The highest *lnE*-value for 2012 was 0.76, whereas the highest *lnE*-value for 2013 was 0.70 (Table 3.5). The *E*-values were higher in 2013 than in 2012. Therefore, we concluded that at a melt factor of 4.0, the model produces a better fit to measured high flows in 2013. On the other hand, *lnE*-values in 2012 were greater than in 2013; therefore, the model simulated 2012 low-flows better than 2013 low-flows.

The differences in model accuracy of 2012 versus 2013 runoff could be a result of having more data points to which we compared modeled-discharge to the 2013 dataset. The differences could also have resulted from using a melt factor of 4.0 for the 2013 simulations instead of using a melt factor that resulted in a more comparable glacier-wide annual mass balance to laser altimetry

measurements for 2013. An increased melt factor means that more melt is being added to the system at any given time, which implies that runoff storage constants for snow, firn and ice will need to adjust in order to accommodate the increased runoff from snow-, firn- and ice-melt.

3.5.2.2 Calibration of Runoff Parameters to 2013 Data using a Melt Factor of 7.0

The parameter sets producing the highest values of *lnE* and *E* were those with k_s, k_f, and k_i of 400-100-100 and 900-100-900, respectively (Figure 3.7; Table 3.5). Results of this sensitivity analysis indicated that at a higher melt factor (MF = 7.0), the both *E* and *lnE* decrease. The greatest *E*- and *lnE*-values observed in the melt factor-adjusted batch simulation were 0.44 and 0.54, respectively (Table 3.5). The results suggested that runoff storage parameters for snow, firn, and ice likely change temporally and perhaps spatially.

3.5.2.3 Modeled and Measured Specific Runoff, 2013

Total specific runoff was calculated from modeled streamflow, which represented the best performing simulations, both with a melt factor of 4.0 and 7.0. At a melt factor of 4.0, the parameter set with the highest *E* (k_s, k_f, and k_i = 200, 400 and 200) produced the best match to measured specific runoff (3914 mm), at 4058 mm (Table 3.6). The results indicate that the model overestimated total runoff by roughly 3.7%. At melt factor of 7.0, the parameter set with the highest *E* (k_s, k_f, and k_i = 900, 100, and 900) produced the best match to measured specific runoff, at 4789 mm. The results indicate that the model overestimated runoff by 22% (Table 3.6). Again, as was discovered by comparing calculated values of *E* and *lnE*, runoff hydrographs for 2013 appear to have a better fit to measured hydrographs when a melt factor of 4.0 is used, while glacier-wide annual mass balance has a better fit to altimetry when using a melt factor of 7.0. The reason for the poorer fit when using a MF of 7.0 is that the model generated too much melt, thereby overestimating discharge.

3.5.2.4 Modeled Runoff Partitioning, 2013

We used the 2013 hydrograph from the model simulation producing total specific runoff closest to total measured specific runoff (melt factor = 4.0, best *E*, k_s, k_f, k_i = 200, 400, 200) over the simulation period in order to evaluate the contribution of discharge from individual reservoir units to total specific runoff (Figure 3.8).
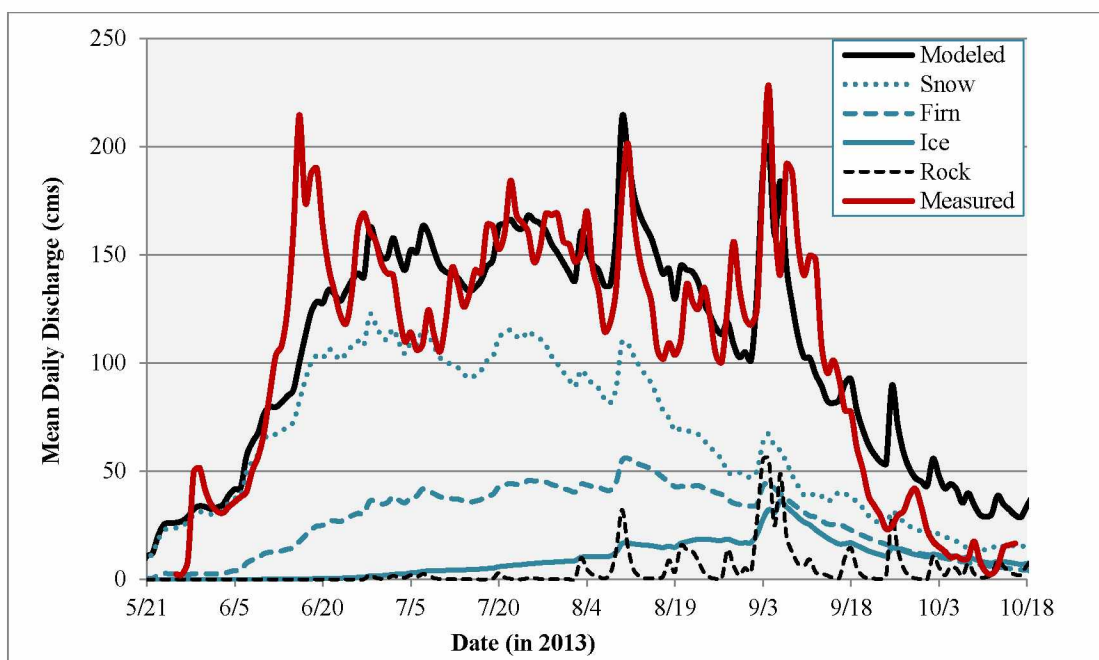
Figure 3.8: Modeled daily discharge from each runoff reservoir (blue and black lines) along with measured discharge (red line) during 2013. Solid black line is modeled discharge from all reservoirs; dashed blue line is runoff from the firn reservoir; dotted blue line is runoff from the snow reservoir; solid blue line is runoff from the ice reservoir; and dashed black line is runoff from the rock reservoir.

Discharge from snow melt dominated contributions to the hydrograph throughout the season (2486 mm, 61%), with the greatest contributions occurring during the spring, and slowly decreasing toward late summer (Figure 3.8; Table 3.8).

Table 3.8: Total modeled specific runoff from runoff model reservoirs during 2013. [Column 1: reservoir unit; Column 2: total modeled specific runoff; Column 3: percent of total modeled specific runoff from the unit; Column 4: percent of total modeled specific runoff from unit during peak flow event on August 10, which generated total runoff of 458 mm; Column 5: percent of total modeled specific runoff from unit during peak flow event on September 4, which generated total runoff of 485 mm.

Reservoir	Total Specific Runoff from Unit, 2013 (mm)	% of Total Modeled Annual Specific Runoff	% of Total Specific Runoff from Peak Flow Event, August 10	% of Total Specific Runoff from Peak Flow Event, September 4
Snow	2486	61%	58%	38%
Firn	1041	26%	30%	27%
Ice	362	9%	8%	20%
Rock	169	4%	4%	15%

Firn contributions were elevated starting in late June and extending through mid-September, comprising 1041 mm (26%) of total specific runoff (Figure 3.8; Table 3.8). Discharge from ice peaks in early September, with the total contribution to specific runoff calculated at 362 mm (9%) (Figure 3.8; Table 3.8). Runoff from the rock reservoir contributed a total of 169 mm (4%) to total specific runoff (Table 3.8). Peak contributions from the rock-covered areas appeared to mimic peak flows on August 11, September 3, and September 8 (Figure 3.8), which corresponded to peak rainfall events (Figure 2.18). On June 8, a peak in the measured discharge was observed (Figure 3.8), which corresponds to a drastic increase in temperature (Figure 2.18). The modeled total runoff (from all reservoirs) did not reflect the peak flow event shown by the measured-hydrograph (Figure 3.8), even though modeled discharge from snow- and firn-runoff increase in response to the increase in temperature.

We were interested in percent contributions of runoff from Valdez Glacier and individual reservoirs to total runoff, because this information provides insight about the potential for increases in discharge if we assume that climate will continue to warm. Total annual runoff contributions from Valdez Glacier (i.e. snow, firn, and ice from within the glacier outline) is equal to the summer glacier mass balance (-2.72 m w.eq., or 9.23×10^8 m^3, with MF = 7.0). The summer glacier mass balance is approximately 69% of the total annual measured runoff (3.91 m, or 1.33×10^9 m^3), or 57% of the total annual modeled runoff (4.79 m, or 1.62×10^9 m^3) from the best runoff simulation using MF = 7.0.

We focused on the largest modeled and measured peak flow events (on August 10 and September 4 according to modeled hydrograph, and on August 11 and September 4 according to measured hydrograph) to evaluate contributions of runoff from the individual reservoirs to total modeled specific runoff. The August 10 modeled-peak flow event preceded the measured hydrograph by one day, while the September 4 modeled-peak flow event occurred on the same day indicated by the measured hydrograph (Figure 3.8). The August peak flow event is defined by the interval from August 5, when discharge begins to increase after reaching a minimum in the hydrograph, to August 15, when discharge reaches the next minimum in the hydrograph. The September peak flow event spans from September 1 to September 15. Total specific runoff from the August event was 458 mm, and was comprised of runoff from the snow, firn, ice and rock reservoirs, at 264 mm (58%), 136 mm (30%), 39 mm (8%), and 19 mm (4%), respectively (Table 3.8). Total contribution of runoff from the glacier was 38% during the August peak flow event, not including runoff from snow-covered portions of the glacier. Total specific runoff from the

September event was 485 mm, and was comprised of runoff from the snow, firn, ice and rock reservoirs, at 184 (38%), 130 mm (27%), 99 mm (20%), and 71 mm (15%), respectively (Table 3.8). The total contribution from the glacier during the September event was 47%, not including runoff from snow-covered portions of the glacier. The results suggest that by early September, contributions to total runoff from ice and rock increase, while contributions from snow and firn decrease.

Chapter 4

Error Analysis of Glacier Mass Balance & Runoff

Introduction:

We evaluated the margin of error associated with our mass balance and runoff estimations by running sensitivity analyses. The errors associated with our estimations are presented in two sections, including Glacier Mass Balance in section 4.1 and Runoff in section 4.2.

4.1 Glacier Mass Balance

The model is reliant on air temperature and precipitation datasets to produce the best fit to glacier mass balance measurements. Therefore, it is important to consider the possibility of error associated with each forcing dataset, and how it might impact our simulations.

4.1.1 Air Temperature Lapse Rates

Error in our glacier mass balance estimates associated with air temperature lapse rates can be a result of a random error due to a single faulty sensor. Error can also be a result of a systematic shift, in which both sensors used in lapse rate calculations are reading inaccurate air temperatures. According to HOBO air temperature sensor specifications, the margin of error for air temperatures above $0°C$ is $±0.21°C$ (*Hobo Pro v2 User's Manual*, 2010). In the case of random error in temperature data, one faulty sensor would mean that the temperature gradient from lower elevations to higher elevations would need to change in order to correct the data. To investigate the sensitivity of the model to random error in air temperature data, we increased temperature lapse rate by $0.2°C$ km^{-1} and decreased temperature lapse rate by $0.2°C$ km^{-1} in our model inputs.

The results show an increase in summer glacier mass balance from -0.65 m w. eq. to -1.05 m. w. eq. (62%) when lapse rate is increased by $0.2°C$ km^{-1} for each timestep, and a decrease in summer glacier mass balance from -0.65 m w. eq. to -0.58 m. w. eq. (11%), when lapse rate is decreased by $0.2°C$ for each time step. The results suggest that, while the model is sensitive to changes in temperature lapse rates in general, the model is most sensitive to increases in lapse rates. In a maritime climate, where air temperatures typically hover around the threshold temperature for rain and snow, changes in air temperatures along the glacier profile can significantly affect the distribution of snow versus rain and the prevalence of melt. More

specifically, a more negative lapse rate would create more snow at lower elevations, thereby reducing the amount of glacier surface directly vulnerable to melt. On the other hand, a less negative or positive lapse rate means warmer temperatures at higher elevations, which translates to less snow and more exposure of firn and ice to melt.

4.1.2 Precipitation Gradient

Precipitation gradient was derived from PRISM monthly averages, as mentioned previously. We altered precipitation gradient by $\pm 5\%$, or by ± 0.42 mm km^{-1}, in order to assess the sensitivity of the model to changes in precipitation gradient. We found that by increasing the precipitation gradient from 8.4 to 8.82 mm km^{-1}, annual glacier mass balance over the simulation period (March 29 to October 11, 2012), increases from -0.65 to -0.61 m w.eq. We found that by decreasing the precipitation gradient to 7.98 mm km^{-1}, summer glacier mass balance decreases to -0.71 m w.eq. The margin of error for a 5% increase or decrease in precipitation gradient is +0.04 /-0.06 m w. eq. Results can be explained by the negative temperature lapse rate, which translates to increased snowfall at higher elevations in the catchment. Therefore, a lower precipitation gradient means that less snowfall is generated at higher elevations. Correspondingly, less melt is required in order to expose ice surfaces as these same elevations. On the other hand, an increase in precipitation gradient translates to more snow on the glacier at higher elevations, and thus more melt is necessary in order to expose the glacier surface.

4.1.3 Debris Cover

Dark bands of color, especially near the terminus, constitute debris-covered areas. Debris layers measuring in thickness above approximately 5 cm have been shown to reduce melt of ice over which it resides, by effectively serving as a radiation insulator (Kayastha et al., 2000; Bozhinskiy et al., 1986). Thus, the amount of debris cover can become an important factor in modeling glacier melt, especially on those glaciers that have a large quantity of debris below the equilibrium line altitude. The model can account for reduction of melt in debris-covered glaciated grid cells in input files by introducing a debris factor, which is a multiplier in the range of 0.0 to 1.0. The model reduces melt in grid cells containing debris-cover by multiplying calculated values of melt by the debris factor.

We ran all model simulations using a debris factor of 0.4, but tested the sensitivity of the model to debris factor by varying debris factor by ± 0.2. Results of the debris factor sensitivity

analysis indicate that by increasing the debris factor by 0.2, the overall summer glacier mass balance for the simulation period (March 29 to October 11, 2012) decreased from -0.65 to -0.69 m w. eq. Similarly, by decreasing the debris factor by 0.2, the summer glacier mass balance increased from -0.65 to -0.61 m w.eq. Therefore, changing the debris factor by ±0.2 effectively changes the summer glacier mass balance by ±0.04 m w. eq. The results were expected, because the debris factor is a scalar quantity intended to adjust melt in debris-covered grid cells only.

4.1.4 Snow Density

As we found in section 3.3.2, by adjusting the density of snow by -0.03 g cm^{-3}, from 0.36 to 0.33 g cm^{-3}, the winter glacier mass balance decreased by 0.15 m. w. eq., which also decreased annual balance by 0.15 m. w. eq. The same magnitude of change in annual glacier mass balance results from increasing snow density by 0.03 g cm^{-3}. Thus, we find that by adjusting density by ±0.03 g cm^{-3}, the annual balance increases or decreases by ±0.15 m w. eq.

4.1.5 Estimated Total Error on Glacier Mass Balance

Once error was calculated for each sensitivity analysis, we combined them in quadrature to produce an overall margin of error associated with our modeling approach. We included RMSE in our total estimated error because it is a measure of error in the model's calculations of melt compared to measured mass balance at ablation stakes. For those sensitivity analyses that did not produce an error with maxima and minima centered on the best estimate, we took the average offset. For example, the error associated with precipitation gradient was calculated at +0.04/-0.06 m w. eq. Thus, the average offset was ±0.05 m w. eq. (Table 4.1). The total error (±0.49 m w. eq., Table 4.1) represents the margin of error associated with our modeled glacier mass balances.

Table 4.1: Error associated with glacier mass balance modeling approach is summarized. [Column 1: error element; Column 2: range of error associated with element; Column 3: average error.] Note: RMSE is taken from best melt model parameter set from the 2012 calibration and therefore does not have an error range.

Error Element	Error Range	Value (m w. eq.)
RMSE	--	±0.39
Temperature Lapse Rate Sensitivity	+0.07/-0.40	±0.24
Precipitation Gradient Sensitivity	+0.04/-0.06	±0.05
Debris Factor Sensitivity	±0.04	±0.04
Snow Density Sensitivity	±0.15	±0.15
Total Error		**±0.49**

We recognize that there are other potential errors associated with our modeling approach that are not easily quantified by the sensitivity approach presented herein. For example, by extrapolating precipitation and temperature data from a point source to the entire extent of Valdez Glacier, we introduce error that is not quantifiable without installing additional temperature and precipitation sensors.

An additional potential source of error can be attributed to ablation stake measurements, to which the model was calibrated over the 2012 study period. At any given elevation band, the surface of the glacier may differ in roughness, shading, and even channelization, each of which has an effect on melt at a given point. By installing three ablation stakes at approximately the same elevation at 584, 586, and 590 m asl (within 6 m elevation), we determined that ablation might vary up to 0.97 m w. eq., or ±0.6 m w. eq. on average. Even knowing this, we were unable to say that this particular average error in ablation is applicable to all elevation bands. While errors such as these are acknowledged to exist, they were not included in our overall glacier melt modeling error equation because we were unable to quantify them.

4.2 Runoff Modeling

Factors such as instrument accuracy, melt parameters, and storage coefficient calibration all influence how well the system is represented by modeled streamflow data. The purpose of this study was to calibrate runoff storage coefficients in order to obtain modeled-hydrographs that would best match those observed through field investigations. As we observed in Chapter 4,

runoff model accuracy to low flows and high flows is performed using the Nash-Sutcliffe values. Another way to quantify error associated with modeled discharge, is to compare modeled and measured specific runoff, and to assess sensitivity of the modeled-specific runoff to changing parameter values. In a similar fashion as was performed in the melt model error analysis, we use the runoff parameter set with the highest $(E+lnE)$-value with our 2013 data to examine the runoff model sensitivity to changes in melt factor, debris factor, temperature lapse rates, and precipitation gradient. We calculate the total specific runoff associated with each simulation, and compare this value to the specific runoff produced by our best-fit hydrograph from Chapter 4, using a melt factor of 7.0 in order to align glacier mass balance of Valdez Glacier with laser altimetry measurements.

4.2.1 Air Temperature Lapse Rate

By increasing temperature lapse rate by $0.20°C$ km^{-1}, we observed an increase in total specific runoff by 1.91 m (i.e. from 3.91 m to 5.82 m). By decreasing temperature lapse rates by the same value, we observed a decrease in total specific runoff by 2.02 m (i.e. from 3.91 to 7.89 m). The results imply that the runoff model is more sensitive to decreases in air temperature lapse rate for this catchment, than to increased air temperature lapse rate. Air temperature in the region typically hovers at the threshold temperature for rain and snow, especially at higher elevations. Therefore, increases or decreases in lapse rates can result in more snow, or less snow, depending on the direction of temperature change. The albedo of snow is generally higher than the albedo of ice or firn (Hock, 2003). Therefore, decreases in air temperature lapse rate mean that more precipitation is held in storage as snow for longer periods of time, due to the increased reflection of radiation at the snow surface.

4.2.2 Precipitation Gradient

We assessed the effect on the simulated runoff by adjusting the precipitation gradient by $\pm5\%$, or 0.42 mm km^{-1}. We used a melt factor of 7.0, and the best runoff parameter set from Chapter 4 for 2013, for this analysis. By increasing the precipitation gradient by 5%, we observed an increase in total specific runoff by 0.04 m (i.e. from 3.91 to 3.96 m). By decreasing precipitation gradient by 5%, we observe a decrease in specific runoff by 0.04 m, implying that the runoff model is equally sensitive to increases and decreases in precipitation gradient. A decrease in precipitation gradient by 5% results in less rainfall and snowfall. Therefore, less rain

and snowmelt are available as runoff. On the contrary, an increase in precipitation gradient results in more rainfall and snowfall. The result is an increase in availability of snowmelt and rainfall runoff.

4.2.3 Debris Factor

We adjusted the debris factor by ±0.2 from the original value of 0.4, and examine the effect on specific runoff over the 2013 simulation period in order to assess the sensitivity of the runoff model to debris factor. By increasing the debris factor by 0.2, total specific runoff over the simulation period increases by 0.02 m from our best estimate, whereas decreasing the debris factor by 0.2 decreases specific runoff by 0.02 m. , An increase in debris factor equates to an increase in melt at each grid cell on the glacier containing debris-cover, while a decrease in debris factor equates to decreased melt at these same grid cells. Therefore, the results of this analysis are expected.

4.2.4 Melt Factor

We assessed the runoff model sensitivity to melt factor by adjusting melt factor by ±1.0 and calculating changes to specific runoff. By increasing the melt factor by 1.0, we find that the specific runoff is increased by 0.29 m, (i.e. from 3.91 to 4.2 m). By decreasing the melt factor by 1.0, we find that the specific runoff is decreased by 0.31 m (i.e. from 3.91 to 3.60 m).

4.2.5 Lake Stage & Discharge Measurements

In addition to the error associated with the modeling, there are also errors associated with sensors used to measure both discharge and water levels. We used the accuracy measure provided by the HOBO pressure transducer manufacturer specifications to estimate error in specific runoff calculations resulting from lake stage sensor error. The manufacturer's specification for the HOBO pressure transducer is within ±0.005 m (*HOBO U20 Water Level Logger*, 2012). To assess error associated with the pressure transducer sensor, we adjusted all lake stage measurements by ±0.005 m. We then re-calculated our rating curve and discharge measurements for the 2013 season, since the bulk over the calibration period was in 2013. The results showed that by increasing stage measurements by 0.005, specific runoff increased by 0.02 m (i.e. from 3.91 to 3.93 m). By decreasing stage measurements by 0.005, specific runoff decreased by 0.02 m (i.e. from 3.91 to 3.89 m).

We assessed error associated with StreamPro and RiverRay ADCP measurements using standard deviations from discharge measurements in 2013. Each discharge measurement was determined from multiple transect measurements, as described in Section 2.4.1. We calculated the standard deviation associated with each discharge measurement to obtain an estimated margin of error per discharge measurement (Table 2.9). To assess the overall error associated with all discharge measurements, we calculated average standard deviation (2.27 m^3 s^{-1}). We then adjusted discharge over the entire simulation period by ± 2.27 $m^3 s^{-1}$ and re-calculated specific runoff. An increase in discharge measurements by 2.27 m^3 s^{-1} results in an increase in specific runoff by 0.09 m (i.e. from 3.91 to 4.00 m). A decrease in discharge measurements by 2.27 m^3 s^{-1} results in a decrease in specific runoff by 0.09 m (i.e. from 3.91 to 3.83 m).

4.2.6 Estimated Total Error

We calculated total error associated with modeled specific runoff by combing the error from the sensitivity analyses in quadrature (Table 4.2). Similarly, we calculated total error associated with specific runoff measurements by combining the streamflow and lake stage margins of error in quadrature. The total error was calculated to ± 0.09 m for measured runoff and to ± 2.0 for modeled runoff.

Table 4.2: Error associated with glacier runoff modeling approach is summarized. Measured runoff error values were calculated based on 2013 measurements only. The modeled runoff error values represent error over the runoff model simulation period (i.e. September 13 – October 11, 2012 and May 26 – October 24, 2013). Error values are normalized to the watershed area. [Column 1: specific runoff type; Column 2: error element; Column 4: error value; Column 4: estimated total error for specific runoff type.]

Runoff Type	Error Element	Value (m)	Total Error (m)
Measured Runoff (2013)	ADCP Accuracy	±0.09	±0.09
	HOBO Pressure Transducer Accuracy	±0.02	
Modeled Runoff (2012 & 2013)	Temperature Lapse Rate Sensitivity	±1.97	±2.0
	Precipitation Gradient Sensitivity	±0.04	
	Debris Factor Sensitivity	±0.02	
	Melt Factor Sensitivity	±0.30	

In addition to error associated with instrument accuracy, we recognize that other sources of error existed that were difficult to quantify formally and include in our error analysis. Examples of these sources include operator error or difficult measuring conditions during ADCP measurement. Such errors may result from standing waves causing loss of sensor contact with the water surface, directional bias, inaccurate calculation of blanking distance along stream banks, and even errors associated with satellite motion and receipt of signal by the instrument. Each of the items mentioned in this discussion, while often observed and corrected for during the data quality evaluation of transect data, can be a source of error not easily quantified. As a result, these types of errors were not accounted for in our overall runoff modeling error calculation.

Runoff modeling error can result during calibration of the model storage constants, which may change on short timescales as the glacier's hydrologic network evolves throughout the simulation period. Therefore, the best approach for modeling runoff might be to perform model validations and calibrations over shorter periods, e.g. individual seasons. However, even by calibrating over shorter timescales, error may still occur as a result of glacier lake outbursts, which may result in random instantaneous changes in storage constants. Further, the model does not take into account groundwater recharge, nor contributions from sub-aqueous melting of the calving front of Valdez Glacier or icebergs in Valdez Glacier Lake. We assumed that those errors were relatively low in comparison to total flux of water moving through the catchment.

Chapter 5

Discussion & Conclusions

Our goals were to: 1) determine the limitations associated with calibrating a temperature-index model to ablation data from only a single year; 2) investigate how well temperature-index modeling can depict runoff in the Valdez Glacier catchment; and, 3) to determine the main controls of glacier mass balance and runoff on Valdez Glacier. In this chapter, we discuss each of these main topics and the evidence provided by our study that leads us to each of our conclusions.

5.1 Limitations to Melt Modeling Methods

We modeled glacier mass balance over two consecutive years (2012 & 2013) and runoff in the Valdez Glacier catchment in fall of 2012 (September 13 – October 11, 2012) and the 2013 hydrologic year. We calibrated the glacier melt model on 2012 data and 2013 laser altimetry data. In 2012, the best parameter set as determined from the glacier mass balance calibration produced an annual glacier mass balance (B_a = 0.05 ± 0.49 m w.eq.) that fell within the margin of error determined by laser altimetry measurements for 2012 (B_a = 0.20 ± 0.6 m w.eq; Johnson et al., 2011). The 2012 modeled-hydrograph fit well to the measured-hydrograph (i.e. within 0.11% of measured runoff). Next, we used the 2012 parameter set to evaluate the model on melt and runoff in 2013. Our modeled annual glacier mass balance for 2013 resulted in a positive annual glacier mass balance (B_a = 0.55 ± 0.49 m w.eq.), whereas the UAF altimetry group estimated a negative annual glacier mass balance (B_a = -1.15 ± 0.30 m.w.eq; Johnson et al., 2011). Interestingly, the modeled-runoff hydrograph from the 2013 simulation fit well to the measured-hydrograph, with the best *lnE* and *E* calculated at 0.70 and 0.79, respectively. Increasing the melt factor in 2013 resulted in a better fit of modeled 2013 annual mass balance of Valdez Glacier to altimetry estimates, but worsened the fit to the measured discharge.

The 2013 model simulations were calibrated to laser altimetry. However, because laser altimetry uses a bulk density assumption (ρ = 0.90 g cm^{-3}) to extrapolate changes in glacier thickness, according to Sorge's law (Bader, 1954), estimations can be inaccurate over short time scales due to annual or seasonal variations in firn and snow density (Johnson et al., 2011). The bulk density assumption is least accurate when estimating positive glacier mass balance years (Bader, 1954) because the additional snow and firn have a lower density than is assumed by Sorge's Law. Given that 2012 was a positive mass balance year for Valdez Glacier, the resulting altimetry balances likely overestimate mass gain in 2012, and overestimate mass loss in 2013.

Therefore, calibrating the model based on altimetry carries the error associated with the constant density assumption into our model simulations.

Weather patterns in Valdez during 2012 were much different than in 2013, according to meteorological data from the Valdez WSO. Temperatures in 2013 were, on average, 0.61 °C above temperatures in 2012 throughout the simulation periods. According to the Alaska Science Research Center, record high total precipitation occurred during the month of September 2012 (66.4 cm) was observed at Valdez WSO), which is typically a month when heavy precipitation is observed. No extremes in temperature were observed during 2012. On the other hand, climate in 2013 produced a record high daily maximum temperature on June 17, 2013 (32.2°C) at Valdez WSO, record high mean daily temperatures in July (14.9°C), record high total monthly precipitation in May (27.2 cm) and October (45.3 cm), and record high total snowfall for the month of May (69.3 cm). Perhaps most important of these climate records is the record snowfall observed in May, which likely changed the melt factor over a short time-span within the simulation period due to changes in surface albedo, insolation and energy flux (Shea et al., 2009). In addition, SWE gradients observed in 2012 and 2013 differed significantly (i.e. 0.0012 m w. eq/m in 2012, and 0.0005 m w. eq./m in 2013; Section 2.2.1). Therefore, for every one meter increase in elevation, nearly twice as much snow was accumulated in 2012 versus 2013.

Temperature-index models assume a constant melt factor throughout a simulation period, and thus do not account for melt parameter changes that occur as a result of surface changes, such as the late-season snowfall observed in 2013. Therefore, the assumption of constant melt factor throughout the entire simulation period, and moreover, the assumption of constant melt factor from year to year is a likely source of error when using a temperature-index model to estimate glacier mass balance (Shea et al., 2009; Matthews et al., 2014). By changing the melt factor in 2013 by 1.0 mm d^{-1} K^{-1}, or 25% (Table 3.3), melt increased by approximately 0.55 m w.eq. Considering that melt factor may change over the course of a season, the magnitude of error may be significant over short-term simulations.

At different sites, typical melt factors for snow and ice range from 2.5 to 11.6 mm K^{-1} d^{-1}, and from 6.6 to 10.0 mm K^{-1} d^{-1}, respectively, with snow melt factors typically lower due to the higher snow albedo when compared to ice (Hock, 2005). A recent study by Shea et al. (2009), suggests that inter-annual variance of snow- and ice- melt factors at a single site can range from 17 to 18% for snow, and from 14% to 25% percent for ice. On Valdez Glacier, an increase of melt factor from 4.0 to 7.0 mm K^{-1} d^{-1} (75%) was required in order to force annual balance to

align with altimetry measurements. While the melt factors observed in our study agree with degree day factors used in other studies (Hock, 2003; Hock, 2005), the inter-annual variability that we observed is outside literature values. Again, the requirement for extreme adjustment to melt factor can be explained by the significant climatic differences observed between 2012 and 2013, and more specifically the late-season snowfall observed in 2013.

Results of our study indicate that the anomalous weather pattern (i.e. record high spring season snowfalls) in 2013 resulted in a poor estimation of annual glacier mass balance when using parameters calibrated to melt conditions and ablation data in 2012. This suggests that having ablation data is essential in order to accurately estimate glacier mass balance using a temperature-index model because weather patterns differ significantly from year to year. Recent studies have proposed that temperature-index models are best employed by calibrating degree-day factors to synoptic long-term "average" weather types (Lang & Braun, 1990), or by explicitly tying specific weather patterns to specific model parameters, in a weather-type-dependent temperature-index model (Matthews et al., 2014). Based on simulations of melt and runoff in the Valdez Glacier catchment, our findings agree, suggesting that variability of weather patterns from year to year greatly diminishes the inter-annual transferability of temperature-index model parameters.

The strong agreement of modeled- versus measured- runoff hydrographs in 2013 using the melt factor determined from 2012 model calibrations suggests that a lower melt factor of 4.0 best depicted runoff in the basin. In order to accurately depict glacier mass balance in the Valdez Glacier catchment, we had to sacrifice the fit between modeled and measured runoff. However, by varying the melt factor, radiation coefficients, and runoff storage constants throughout the simulation period, it may be possible to achieve an improved statistical fit of modeled-runoff while still effectively representing glacier mass balance.

5.2 Runoff Modeling using a Temperature-Index Model

We calibrated the runoff model by tuning storage constants of linear reservoir units (i.e. residence time of water in snow, firn, ice and rock). In the real world, melt water is stored in the snowpack and flows downward and down-gradient through pore spaces in the snow profile, often re-freezing and re-melting along the way (Dingman, 1994). A similar phenomenon occurs in firn, which captures and stores water in a layer above the impenetrable ice surface, before discharging it to the glacier via crevasses or other openings. Water that flows into glacier ice is stored in

interconnected pores and cavities that develop into larger distributed networks of channels as the melt season progresses (Kamb, 1987; Jansson et al., 2003). By calibrating the model to storage constants, we tried to force the model to mimic the rates and volumes at which runoff from precipitation and melt flow into and out of each reservoir.

The storage constants generating the best-fitting modeled hydrographs differed between 2012 and 2013, suggesting that parameters should vary from year to year. Results of the runoff calibration in 2012 and 2013 suggest that the average seasonal storage constants needed to be greater in 2013 in order to most accurately predict runoff. This may be explained by the englacial hydrologic network as it evolves over time and the inter-annual variability of the rate of evolution. Further, the weather patterns in Valdez, which saw late season snowfall and elevated temperatures in 2013 compared to 2012, may have complicated the calibration of the storage constant parameters.

In general, the runoff model produced hydrographs that matched well to measured hydrographs in both 2012 and 2013, using a melt factor of 4.0. Modeled total runoff in 2012 and 2013 was calculated to within 5% of the measured runoff. However, the modeled runoff in 2012, calibrated from the 2012 field measurements, had a better fit to measured runoff, falling within 0.11%. The better performance of the model in 2012 is likely a result of the shorter streamflow calibration period (23 days in total), whereas the 2013 dataset included 128 calibration days between May 26 and October 24. It is likely that changes in 2012 storage constants were small, thereby allowing the model to more accurately simulate runoff without needing to alter runoff storage constants. The variation in storage constants was likely much greater in 2013 due to the span of the simulation period. The 2013 simulations began when the hydrologic network within the glacier was comprised of a less-developed hydrological system (i.e. linked-cavity system), and ended when the glacier hydrologic network was better developed (i.e. distributed channel network). Therefore, water was able to flow more rapidly through the glacier hydrologic system by the end of the 2013 simulation period than it was at the beginning (Kamb, 1987; Fountain and Walder, 1998; Jansson et al., 2003).

For heavily glaciated catchments, special consideration must be given to glacier-hydrologic features like ice-dammed lakes, such as the marginal lake in the Valdez Glacier catchment (Figures 1.1 & 2.1). Ice-dammed lakes can outburst and instantaneously change the hydrology in the catchment (Neal, 2007). Even by varying storage constants seasonally, it is difficult to capture changes in storage associated with outbursts of ice-dammed lakes, due to the

extreme variations in magnitude and frequency of outbursts, which depend upon weather patterns and the drainage networks within the glacier. Calibrating a runoff model to short periods containing anomalous events such as glacial lake outbursts can result in calibrated parameters that are specific only to the measurement period containing the anomaly. Therefore, it is important to consider the effect of runoff anomalies on calibration results. The influence of runoff anomalies on model calibration can be minimized by either excluding anomalous runoff events from statistical analysis of the hydrographs or by lengthening the calibration period.

5.3 Main Controls of Melt and Runoff in the Valdez Glacier Catchment

Data from weather stations and modeled- and measured-hydrographs from Valdez Glacier Stream aid in determining specific climatologic influences that most greatly contribute to melt and runoff in the Valdez Glacier catchment. More specifically, by comparing peak flow events in the measured- hydrograph to the timing of increases in temperature and precipitation events, and the modeled-runoff contributions of each reservoir component (i.e. runoff from areas of snow, firn, ice or rock), we determined which factors are likely responsible for melt and runoff.

Two peaks occurred in the measured-hydrograph from 2012: one on September 17-18 (P1), which precedes the largest peak flow event, and the second during September 22-23 (P2; Figure 2.17). Event P1 occurs during a period of significant rainfall and a small increase (~1°C) in the temperature time-series (Figure 2.17). The P1 modeled-runoff contributions from all reservoirs together (Figure 3.6) were larger than the measured-hydrograph, and suggested that the runoff from the rock reservoir is the greatest contributor. Thus, the model agrees with our interpretation that the largest contributor to runoff during P1 is derived from rainfall. Runoff from the snow, firn, and ice components also peak during P1, suggesting that advective heat also contributed to melt of all three units, thereby generating additional runoff.

The largest peak flow in 2012, or P2, coincided with an increase in temperature (~4 °C) and a precipitation event (~270 mm; Figure 2.17), with snowmelt and rainfall-derived runoff being the largest contributors (Figure 3.6). The magnitude of P2 is not observed in the modeled-hydrograph. The modeled-hydrograph overestimated P1, suggesting that a large portion of the runoff generated during P1, in reality, was routed and stored elsewhere within the watershed prior to P2 (e.g. in the marginal ice-dammed lake, snow reservoir, firn reservoir, or ice reservoir). From this information, we deduced that both temperature and precipitation are drivers of melt and runoff in 2012 and also that the snow, firn and ice reservoirs, and perhaps even the marginal ice-

dammed lake, serve as significant storage units and major sources of runoff given the right conditions.

Peak flows in 2013 were generally lower in runoff volume than those observed in the 2012 hydrograph. Peak flows at the beginning of the melt season correlated to sharp increases in air temperature, suggesting that the first event is a result of heavy snow melt (Figure 2.18). This corresponded to the climatic record for 2013, which included a record-breaking month of late-season snowfall amounts in May, followed by record-breaking high air temperatures in June. In general, from May to late August, the hydrograph mimicked the air temperature time series, peaking when temperature peaks (Figure 2.18). The data suggest that air temperature was the main driver to melt throughout the late-spring and early-summer period. In early August, heavy rainfall events recorded at the Valdez WSO (11 m asl) were major contributors to runoff (Figure 2.18). By late October, air temperature began a downward trend and precipitation increased at the Valdez WSO (Figure 2.18), suggesting that rainfall-derived runoff was the main source of runoff throughout the fall season. Snowmelt dominated the hydrograph from May to early-September, based on the modeled-hydrograph (Figure 3.8). By early September, peaks in the modeled-hydrographs for the rock- and ice-reservoirs indicated that the major contributor to runoff is rainfall-derived runoff and melt of glacier ice (Figure 3.8).

5.4 Conclusions

Our preliminary assessment of Valdez Glacier catchment suggests that temperature-index models are an appropriate tool for investigating temporal patterns in discharge from the Valdez Glacier Lake, provided that ground observations are available for model calibration. From comparisons of simulation results in 2012 and 2013, we determined that because weather is variable from year to year, parameters calibrated to one year of ablation data may be non-transferable to other years. For this reason, we find that more ablation data must be collected for several years of different weather patterns, and propose using a synoptic average weather-type approach, similar to what Lang and Braun (1990) proposed for temperature-index glacier mass balance modeling in other regions. By performing more model calibrations to multiple years, which naturally include a larger spectrum of weather types, we are more likely to hone in on a single "average" weather-type model parameter set that might allow for more accurate long-term temperature-index modeling. In addition, we may also be able to assign a parameter set to a

particular year based on weather type, by pulling from the pool of pre-calibrated parameter sets without having to re-calibrate.

We found that precipitation is a primary control on glacier mass balance in this maritime region. Although our study benefited from the detailed GPR snow measurements, large precipitation events can occur after radar surveys, which makes initializing the model difficult. Unfortunately, the lack of high elevation weather station data in the Valdez Glacier catchment may limit our ability to include early season snowfall events in our meteorological forcing datasets. Future modeling efforts should investigate improved methods to account for summer season snowfall events. Possible approaches include examining high temporal resolution satellite imagery to assess the impact of large low-elevation precipitation events on the location of the summer snowline. The location of the summer snowline can then be used to track the accuracy of modeled snow distribution. In addition, deployment of on-glacier precipitation monitoring equipment at high elevations would provide direct observations that could be used to drive the model.

The temperature-index model depicts runoff in Valdez Glacier Stream well, estimating specific runoff within 5% of measured specific runoff in both fall of 2012 (September 13 – October 11, 2012) and throughout the 2013 hydrologic year. Similar to our findings regarding melt model parameters, however, we found that runoff model parameters (i.e. storage constants) are non-transferrable inter-annually, and perhaps not even sub-annually, due to the seasonal evolution of the hydrologic system in snow, firn and ice. Importantly, the limited timeframe over which we calibrated the runoff model impedes our ability to hone in on storage constants that are appropriate for longer simulation periods. Maintaining a constant set of storage values over multiple years with varying weather patterns will likely result in highly erroneous modeled discharges, unless the model were calibrated over several years. We recommend the same synoptic weather-type modeling approach as we suggested for the melt parameters (Lang & Braun, 1990) in order to avoid the necessity of re-calibrating to streamflow during every year of simulation. Finally, we find that while the model can accurately depict runoff hydrographs in a maritime climate, it is limited in its ability to account for outbursts of ice-dammed lakes. Therefore, calibrating a runoff model to anomalous runoff resulting from lake outbursts can result in parameters that are heavily influenced by the anomaly and can be non-transferable to time periods outside the calibration period. It is important to restrict calibration of runoff parameters to periods that do not present anomalous data for this reason.

The marginal ice-dammed lake in the Valdez Glacier catchment formed, presumably within the same timeframe as Valdez Glacier Lake (i.e. early to mid-1900's), as a glacier tributary began to retreat and disconnect from the main trunk of Valdez Glacier. The retreat of the tributary created an area into which meltwater from both the tributary and main trunk of Valdez Glacier collects. The lake is dammed by the main trunk of Valdez Glacier, which could fail seasonally once the lake reaches a critical volume, creating outburst flows. Many alpine glaciers in Alaska are characterized by similar retreating tributaries and the resulting marginal ice-dammed lakes, which also seasonally outburst. Examples of seasonally draining ice-dammed lakes include lakes along the Mendenhall Glacier, in Juneau, Alaska, which drain to Mendenhall Lake and then to Mendenhall River, and two lakes along the Tulsequah Glacier in British Columbia, which ultimately drain to the Taku River. Many more ice-dammed and moraine-dammed lakes are expected to form along other glaciers in alpine regions as climate changes and glaciers and their tributaries begin to recede, thereby posing a risk of outburst flooding in communities located in close proximity. For this reason, and because glacial lake outbursts are so difficult to predict and model, monitoring changes in glaciers and their glacial lakes becomes essential to mitigating the hazards they pose on communities.

References Cited

Alaska Division of Geological & Geophysical Surveys. *Ground-penetrating radar snow depth measurements on Valdez Glacier in 2012 and 2013.* Unpublished raw data. In press.

Arendt, A., K. Echelmeyer, W. Harrison, C. Lingle, and V. Valentine. "Rapid wastage of Alaska glaciers and their contribution to rising sea level." *Science* 297 (2002): 382-386.

Arendt, A., K. Echelmeyer, W. Harrison, C. Lingle, S. Zirnheld, V. Valentine, B. Ritchie, and M. Druckenmiller. "Updated estimates of glacier volume changes in the western Chugach Mountains, Alaska, and a comparison of regional extrapolation methods." *Journal of Geophysical Research* 111 (2006): 1-12.

Bader, H. "Sorge's Law of Densification of Snow on High Polar Glaciers." *Journal of Glaciology.* 2 (1954): 319-323.

Berenbrock, C. and A.W. Tranmer. U.S. Geological Survey. "Simulation of flow, sediment transport, and sediment mobility of the Lower Coeur d'Alene River, Idaho". *Scientific Investigations Report* 2008-5093 (2008):1-164.

Bliss, A., R. Hock, Radic, V. "Global response of glacier runoff to twenty-first century climate change." *Journal of Geophysical Research: Earth Surface.* 119 (2014): 1-14.

Bozhinskiy, A. N., M. S. Krass, and V. V. Popovnin. "Role of debris cover in the thermal physics of glaciers." *Journal of Glaciology* 32.111 (1986): 255-266.

Braithwaite, R. J and Y. Zhang. "Sensitivity of mass balance of five Swiss glaciers to temperature changes assessed by tuning a degree-day model." *Journal of Glaciology.* 47 (2000): 7-14.

Carenzo, M. F. Pellicciotti, S. Rimkus, and P. Bulando. "Assessing the transferability and robustness of an enhances temperature-index glacier-melt model." *Journal of Glaciology.* 55 (2009): 258-274.

Case, J. E., D. F. Barnes, G. Plafker, and S.L. Robbins. U.S. Geological Survey. "Gravity Survey and Regional Geology of the Prince William Sound Epicentral Region, Alaska." *Geological Survey Professional Paper* 543-C. (1966): C1-7.

Clague, J.J., and S.G. Evans. "A Review of Catastrophic Drainage of Moraine-Dammed Lakes in British Columbia." *Quaternary Sciences Review* 19 (2000): 1763-83.

Clague, J. J., and S. G. Evans. "Formation and failure of natural dams." *Geological Survey of Canada, Bulletin* 464 (1994): 35.

Cogley, J.G. A.A. Arendt, A. Bauder, R.J. Braithewaite, R. Hock, P. Jansson, and G. Kaser. "Glossary of glacier mass balance and related terms, IHP-VII technical documents in hydrology No. 86, IACS Contribution No. 2." *International Hydrological Program, UNESCO, Paris* (2011).

Daly, C., R.P. Neilson, and D.L. Phillips. "A statistical-topographic model for mapping climatological precipitation over mountainous terrain." *Journal of Applied Meteorology*. 33 (1994): 140-158.

Dingman, S. L. *Physical Hydrology*. 2nd Edition. New Jersey: Prentice Hall, 1994. Print.

Dorava, J.M. and A.M. Milner. "Role of lake regulation on glacier-fed rivers enhancing salmon productivity: the Cook Inlet watershed, south-central Alaska, USA." *Hydrological Processes* 14 (2000): 3149-59.

Echelmeyer, K.A, W.D. Harrison, C. F. Larsen, J. Sapiano, J.E. Mitchell, J. DeMallie, B. Rabus, G. Adalgeirsdottir, and L. Sombardier. "Airborne surface profiling of glaciers: A case-study in Alaska." *Journal of Glaciology* 42 (1996): 538-47.

Field, W.O. Jr. "The Glaciers of the Northern Part of Prince William Sound, Alaska." *Geographical Review* 22 (1932): 361-388.

Field, W.O. Jr. "Observations on Alaskan Coastal Glaciers." *Geographical Review* 27 (1937): 63-81.

Fountain, A.G. and W.V. Tangborn. "The effect of glaciers on streamflow variations." *Water Resources Research* 21 (1985): 579-86.

Fountain, A.G. and J.S. Walder. "Water flow through temperate glaciers." *Reviews of Geophysics*. 36 (1998): 299–328.

Gardner, A.S. G. Moholdt, J.G. Cogley, B. Wouters, A.A. Arendt, J. Wahr, E. Berthier, R. Hock, W. T. Pfeffer, G. Kaser, S. R. M. Ligtenberg, T. Bolch, M. J. Sharp, J. O. Hagen, M. R. van den Broeke, and F. Paul. "A reconciled estimate of glacier contributions to sea level rise: 2003 to 2009." *Science*. 340 (2013): 852-57.

Grant, U.S. and D.F. Higgins. "Glaciers of Prince William Sound and the Southern Part of the Kenai Peninsula, Alaska Part I. Glaciers of the Northern Part of Prince William Sound." *American Geographical Society*. 42 (1910): 721-738.

Groisman, P.Y. and D.R. Legates. "The Accuracy of United States Precipitation Data." *Bulletin of the American Meteorological Society* 75.2 (1994): 215-227.

Gusmeroli A., G.J. Wolken and A.A. Arendt. "Snow accumulation in valley glaciers with compound basins. An example from Valdez Glacier, Alaska, U.S.A." Manuscript in preparation. (2014).

Heidemann, H. K.. U.S. Geological Survey. *Lidar base specification version 1.0: U.S. Geological Survey Techniques and Methods*. Book 11, Chap. B4 (2012): 1-63.

HOBO Pro v2 User's Manual. Onset Computer Corporation (2010).

HOBO U20 Water Level Logger (U20-001-0x and U20-001-0x-Ti) Manual. Onset Computer Corporation (2012).

Hock, R. "Temperature index modeling in mountain areas." *Journal of Hydrology* 282 (2003): 104-115.

Hock, R. "Glacier melt: a review of processes and their modelling." *Progress in Physical Geography.* 29 (2005): 362-91.

Hock, Regine, Peter Jansson, and Ludwig N. Braun. "Modelling the response of mountain glacier discharge to climate warming." *Global Change and Mountain Regions*. Springer Netherlands, 2005. 243-252.

Hock R. and Tijm-Reijmer. *A Mass Balance, Glacier Runoff and Multi-Layer Snow Model: DEBAM and DETIM*. 27 (2012).

Hulth, John. "Instruments and Methods Using a draw-wire sensor to continuously monitor glacier melt". *Journal of Glaciology*. 56 (2010): 922-24.

Huss, M. A. Bauder, M. Funk, and R. Hock. "Determination of seasonal mass balance of four Alpine glaciers since 1865." *Journal of Geophysical Research*. 113 (2008): 1-11.

Jansson, P., R. Hock, T. Schneider. "The concept of glacier storage: a review." *Journal of Hydrology*. 282 (2003): 116-129.

Johnson, A.J., C.F. Larsen, N. Murphy, A. A. Arendt, S.L. Zirnheld. "Mass balance in the Glacier Bay area of Alaska, USA, and British Columbia, Canada, 1995-2011, using airborne laser altimetry". *Journal of Glaciology*. 59 (2011): 632-48.

Juen, I., G. Kaser, and C. Georges. "Modelling observed and future runoff from a glacierized tropical catchment." *Global and Planetary Change*. (2007): 37-48.

Kamb, B. "Glacier surge mechanism based on linked cavity configuration of basal water conduit system." *Journal of Geophysical Research: Solid Earth*. 92 (1987): 9083-9100.

Kayastha, R. B., Y. Takeuchi, M. Nakawo and Y. Ageta. "Practical prediction of ice melting beneath various thickness of debris cover on Kliumbu Glacier, Nepal, using a positive degree-day factor." *Debris-covered Glaciers: Proceedings of an International Workshop Held at the University of Washington in Seattle, Washington, USA, 13-15 September 2000*. No. 264. IAHS, 2000.

Keinholz, C. *Shrinkage of Selected South-Central Alaskan Glaciers AD 1900-2012*. MS Thesis. Bern University, 2010.

Kennedy, E.J. U. S. Geological Survey. *Discharge ratings at gaging stations: U.S. Geological Survey Techniques of Water Resources Investigations*. United States Government Printing Office, Washington: 1984.

Korona J., E. Berthier, M. Bernard, F. Remy, E. Thouvenot. "SPIRIT. SPOT 5 stereoscopic survey of Polar Ice: Reference Images and Topographies during the fourth International Polar Year (2007-2009)." *ISPRS Journal of Photogrammetry and Remote Sensing* 64 (2009): 204-12.

Krause, P., D.P. Boyle, and F. Base. "Comparison of different efficiency criteria for hydrological model assessment."*Advances in Geosciences* 5 (2005): 89-97.

Lang, H. and L. Braun. "On the information content of air temperature in the context of snow melt estimation." *Hydrology of Mountainous Areas*. 190 (1990): 347-54.

Lorang, M.S. and F.R. Hauer. "Flow competence and streambed stability: an evaluation of technique and application." *Journal of North American Benthological Society* 22 (2003): 475-91.

Martin, Lawrence. "Alaskan Glaciers in Relation to Life." *Bulletin of the American Geographical Society* 45 (1913): 801-818.

Matthews, T., R. Hodgkins, R. L. Wilby, S. Gudmundsson, F. Palsson, H. Bjornsson, and S. Carr. "Conditioning temperature-index model parameters on synoptic weather types for glacier melt simulations." *Hydrological Processes*. (2014).

McGrath, D., A.A. Arendt, G. Wolken, A. Gusmeroli, C. Keinholz, C. McNeil, S. O'Neel, and L. Sass. "End-of-winter snow water equivalent variability across a range of Alaskan glaciers." Manuscript in preparation. (2015).

Mernild, S.H., G.E. Liston, and B. Hasholt. "Snow-distribution and melt modeling for glaciers in Zackenberg river drainage basin, north-eastern Greenland." *Hydrological Processes* 21 (2007): 3249-63.

Mueller, D. S. and C. R. Wagner. U.S. Geological Survey. "Measuring Discharge with Acoustic Doppler Current Profilers from a Moving Boat." *U.S. Geological Survey Techniques and Methods* 3A-22 (2009): 1-72.

Neal, E.G. U.S. Geological Survey. "Hydrology and Glacier-Lake-Outburst Floods (1987-2004) and Water Quality (1998-2003) of the Taku River near Juneau, Alaska." *U.S. Geological Survey Scientific Investigations Report*. 2007-502 (2007).

Neal, E.G. and R.H. Host. U.S. Geological Survey. "Hydrology, Geomorphology, and Flood Profiles of the Mendenhall River, Juneau, Alaska." *Water-Resources Investigations Report* 99-4151 (1999):1-41.

Oerlemans, J., B. Anderson, A. Hubbard, and P. Huybrechts. "Modelling the response of glaciers to climate warming." *Climate Dynamics* 14 (1998): 267-274.

O'Neel, S., E. Hood, A. Arendt, and L. Sass. "Assessing streamflow sensitivity to variations in glacier mass balance." *Climatic* Change. 123 (2014): 329-41.

Pellicciotti, F., B. Brock, U. Strasser, P. Burlando, M. Funk, and J. Corripio. "An enhanced temperature-index glacier melt model including the shortwave radiation balance: development and testing for Haut Glacier d'Arolla, Switzerland." *Journal of Glaciology* 51.175 (2005): 573-587.

Pfeffer, W.T., A.A. Arendt, A. Bliss, T. Bolch, J.G. Cogley, A.S. Gardner, and J. Hagen. "The Randolph Glacier Inventory: a globally complete inventory of glaciers." *Journal of Glaciology* 60.221 (2014): 537.

Post, A. & L. R. Mayo. U.S. Geological Survey. *Glacier Dammed Lakes and Outburst Floods of Alaska* [map], 1971.

Radic, V. A. Bliss, A. C. Beedlow, R. Hock, E. Miles, and J.G. Cogley. "Regional and global projections of twenty-first century glacier mass changes in response to climate scenarios from global climate models." *Climate* Dynamics. 42 (2014): 37-58.

Radic, V. and R. Hock. "Modeling future glacier mass balance and volume changes using ERA-40 reanalysis and climate models: A sensitivity study at Storglaciaren, Sweden." *Journal of Geophysical Research* 111 (2006): 1-12.

Shea J. M., R. D. Moore, and K. Stahl. "Derivation of melt factors from glacier mass-balance records in western Canada." *Journal of Glaciology*. 55 (2009): 123-130.

Shulski, M. and G. Wendler. *The Climate of Alaska*. Fairbanks: University of Alaska Press, 2007.

Stahl, K., R.D. Moore, J.M. Shea, D. Hutchinson, and A.J. Cannon. "Coupled modeling of glacier and streamflow response to future climate scenarios." *Water Resources Research* 44 (2008): 1-13.

U.S. Army Corps of Engineers. *Alaska Baseline Erosion Assessment: Erosion Information Paper – Valdez, Alaska*. Alaska District, U.S. Army Corps of Engineers. 2007.

Yang, D., B.E. Goodison, and J.R. Metcalfe. "Adjustment of daily precipitation data at 10 climate stations in Alaska: Application of World Meteorological Organization intercomparison results." *Water Resources Research* 34.2 (1998): 241-256.

Young, J. C. *Temperature index modeling of the Kahiltna Glacier: Comparison to multiple field and geodetic mass balance datasets*. MS thesis. University of Alaska, Fairbanks, 2013.

Zhang, Y., S. Liu, and J. Xu. "Glacier change and glacier runoff variation in the Tuotuo River basin, the source of Yangtze River in western China." *Environmental Geology*. 56 (2008): 59-68.